Optimization of Centrifugal Slurry Pumps through Computational Fluid Dynamics

by

Timothy Gjernes

B.A.Sc., Simon Fraser University, 2012

Thesis Submitted in Partial Fulfillment of the
Requirements for the Degree of
Master of Applied Science

in the
School of Mechatronic Systems Engineering
Faculty of Applied Sciences

SIMON FRASER UNIVERSITY

Summer 2014

Approval

Name: **Timothy Gjernes**

Degree: **Master of Applied Science**

Title: ***Optimization of Centrifugal Slurry Pumps through Computational Fluid Dynamics***

Examining Committee: **Chair:** Mehrdad Moallem
Professor

Siamak Arzanpour
Co-Supervisor
Associate Professor _____

Gary Wang
Co-Supervisor
Professor _____

Erik Kjeang
Supervisor
Assistant Professor _____

Carolyn Sparrey
Internal Examiner
Assistant Professor
School of Mechatronic Systems
Engineering _____

Date Defended: August 22, 2014

Partial Copyright Licence

Abstract

Centrifugal slurry pumps are a very unique turbomachine that must be able to handle the flow of high concentrations of solid particles which greatly accelerate wear. With Computational Fluid Dynamics (CFD), it is possible to accurately simulate the flow through such pumps to predict performance. A centrifugal slurry pump was simulated using water and results were validated with physical test results which also used water. Validation yielded good correlation where the most efficient flow rate was predicted correctly. With the confirmed CFD model, design changes were made to the pump to incorporate splitter blades which are shorter versions of the main blades. Optimization using the Adaptive Response Surface Method algorithm with an Intelligent Space Exploration Strategy was performed to find the optimum splitter configuration to minimize wear in the pump impeller. The optimum splitter configuration yielded an almost 19% decrease in the wear with a slight increase in efficiency.

Keywords: Centrifugal pumps; slurry; optimization; computational fluid dynamics; metamodeling; splitter blades

Acknowledgements

I would first like to acknowledge God who, through His grace, has blessed me with the opportunity and wisdom to complete this milestone in my education. I would like to especially thank my family who has greatly loved and supported me through my years as a student and has always encouraged me to put my best effort into all I pursue.

I would like to thank my supervisors, Dr. Gary Wang and Dr. Siamak Arzanpour, for presenting me with this project and for their guidance, motivation and support throughout my studies. They have patiently pushed me to grow in academia, helping me learn how to conduct effective research that can truly stand out in my field. They have always had a strong faith in me and have helped me succeed in my research.

I would like to acknowledge Toyo Pumps for providing the possibility of collaborating with them in my research. I'd like to thank them for not only their resources and expertise, but also for treating me as an employee and making my internship enjoyable, meaningful and memorable. I especially want to thank Nick Guenther, Managing Director of Engineering, for patiently providing me with endless help and guidance as I learned about their pumps, their function and how to properly analyze centrifugal pumps.

I would like to acknowledge Simutech Group for their support in my research on the CFD side. I want to especially thank Nathan Bushnell, CFD Consulting Engineer, who went out of his way to be an invaluable mentor in assisting me in my research, giving me guidance, tips and advice to properly and effectively perform my CFD analyses. Learning CFD would have been a much slower and more daunting task without Nathan's willingness to help.

I would also like to acknowledge CMC Microsystems for the provision of ANSYS products and services that facilitated this research. I would like to thank the Natural Sciences and Engineering Research Council of Canada for funding this research. I would also like to acknowledge Mitacs for facilitating the research partnership with Toyo Pumps, providing me with invaluable industry experience.

Table of Contents

List of Tables

List of Figures

List of Acronyms

ARSM	Adaptive Response Surface Model
ARSM-ISES	Adaptive Response Surface Model – Intelligent Space Exploration Strategy
BEP	Best Efficiency Point
CCD	Central Composite Designs
CFD	Computational Fluid Dynamics
EARSM	Enhanced Adaptive Response Surface Model
IARSM	Improved Adaptive Response Surface Model
LE	Leading Edge
LHD	Latin Hypercube Design
MBDO	Metamodel-Based Design Optimization
pARSM	Pseudo-Adaptive Response Surface Model
RSM	Response Surface Model
SDS	Significant Design Space
TE	Trailing Edge

Glossary

Impeller	Rotating portion of a turbomachine consisting of the blades to transfer energy to the fluid
Mesh	Small three dimensional sub-regions to define a geometrical fluid model for flow calculation
Metamodeling	Generating mathematical models to represent the response of a system to inputs
Optimization	The process of finding the optimum set of input parameters to produce the best output
Parameter	An input variable to optimization that is changed within bounds to affect a change in the output
Slurry	A mixture of solids and liquids
Splitter blade	Small blade in an impeller, shorter than a main blade
Turbomachinery	Machines that transfer energy between a rotating component and a fluid
Volute	Stationary portion of a turbomachine to collect and guide the flow towards the outlet

Chapter 1. Introduction

Centrifugal pumps are a very common type of turbomachine used for fluid transport in a wide variety of industries. They operate on the overarching principle of raising a specific volume flow to a specific pressure level using a rotating impeller inside a volute casing [1]. Figure 1.1 shows a simple, labelled diagram of a typical centrifugal pump. Some of the many industries that use centrifugal pumps include mining, sewage and irrigation. One type of centrifugal pump is a slurry pump and this is the focus of the author's research. Slurry is a mixture of liquid and solid particles of a variety of shape and size and is commonly found in the mining industry, among others.

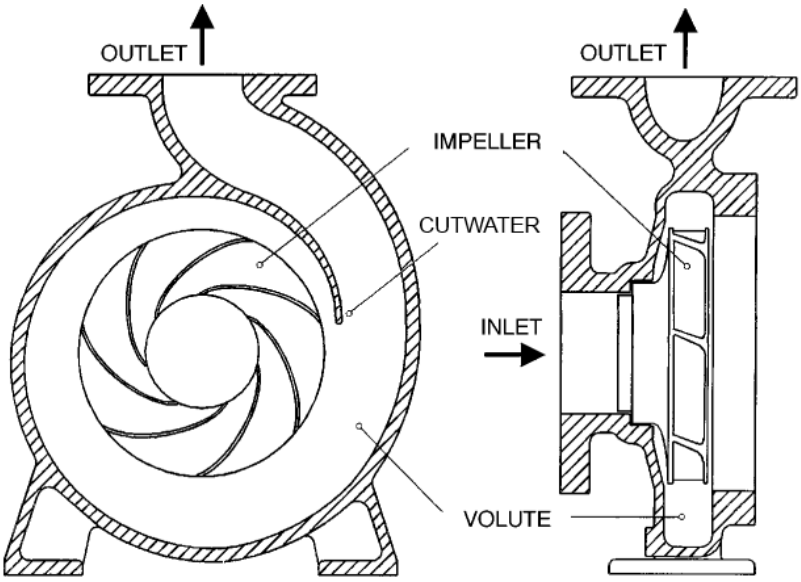

Figure 1.1. Centrifugal pump diagram [2]

Slurry pumps have been used for many decades and are a very specific and unique type of centrifugal pump. While they run on the same principle of operation of clear liquid or gas pumps, there are many differences between the two. It is very important to note that slurry pumps will never reach the same efficiency as a clear liquid pump even if both are pumping water [3]. Decades of research and development have

gone into perfecting and optimizing clear liquid centrifugal pumps. They very commonly have five to ten thin blades that offer minimal flow obstruction. Passageways are thus narrow and effectively guide the liquid through the impeller to the volute. The impeller surfaces are also often machined and polished to make them as smooth as possible [3].

While both clear liquid and slurry pump design are based on science, “with slurry pumps, science is mixed also with a good sprinkling of art and a designer’s know-how” [3]. Basically, since slurry pumps cannot be designed to the same optimum as a clear liquid pump may be, knowledge and experience are more important in determining the trade-off between the ideal objective and what is actually achievable with respect to wear and lifetime costs of the pump. Slurry pump impellers must have thicker blades than clear liquid pumps to withstand wear and prevent them from breaking from the impact of solids. With this extra thickness, there must be fewer blades, not only to minimize obstruction but also to keep the passageways wide enough to allow the largest solid particles to pass through. In the volute a larger distance is required between the impeller and cutwater to ensure passage of solids. Clear liquid pumps usually have a minimal gap to reduce recirculation inside the volute and guide the fluid to the outlet [3]. A typical, preferred volute design type for water pumps and especially compressors is an overhung volute, shown in Figure 1.2. This design is preferred over a symmetric volute as the overhung volute improves performance by increasing velocities in the volute that reduce recirculation of the flow back into the impeller inlet. This design is rarely used for slurry pumps since it causes increased wear from the high, swirling velocities in the overhung volute. Velocities within the hydraulic designs of slurry pumps are limited as much as possible to decrease wear, quite opposite to the designs in any other centrifugal pumps [4].

With these limitations, the fluid through the impeller is not guided as closely as in a clear liquid pump which, in turn, causes a reduction in the performance. Slurry pump impellers are rarely machined or polished, not only because they are cast from very hard materials that are tough to machine, but because they will wear very fast from the slurry, giving very little short-term advantage from a smooth surface [3].

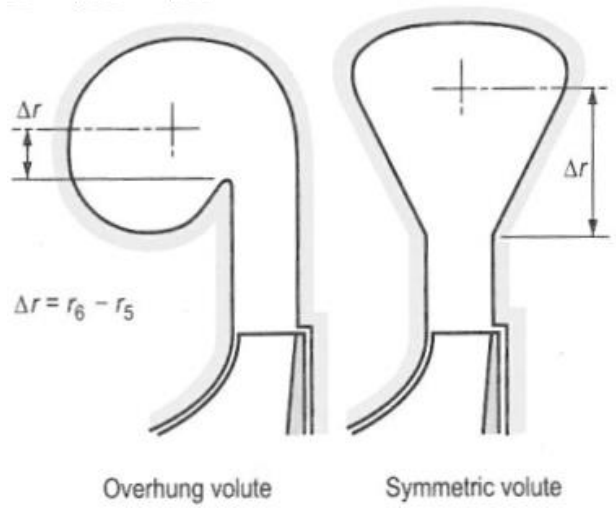

Figure 1.2. Overhung vs symmetric volute design [4]

Development of slurry pumps has mostly been accomplished through physical testing combined with the extensive knowledge of experienced design engineers. Computational Fluid Dynamics (CFD) is a relatively new technology that allows for simulation of fluid flowing through or over bodies. CFD has been used extensively in fields such as aerospace. It has also been used for turbomachinery although its use in centrifugal pumps has been less prominent. Centrifugal pumps are not a symmetrical design because of the volute which makes the simulation much more difficult as there is unsteady interaction between the impeller and volute [5]. There is relatively little literature discussing the use of CFD in slurry pumps, specifically. Most work has involved developing CFD models to validate and predict performance. Predicting efficiency and wear are the most common.

The author's research involved an industry collaboration with Toyo Pumps, a company based in Vancouver, BC, Canada that provides slurry pumping solutions. They design, manufacture and distribute a wide variety of slurry pumps. All of Toyo's pumps have been developed without the use of CFD. In order to stay ahead of competition, Toyo is implementing the use of CFD in the design process to not only test potential designs but also to optimize designs before they are ever manufactured.

Optimization is the process of seeking the best possible solution to a non-trivial problem. It has been applied to many different types of turbomachines, however it has

not been widely applied on slurry pumps. There have been numerous studies on optimizing non-slurry centrifugal pumps. For example, one study involved optimizing efficiency by changing a number of parameters including the blade angles and impeller size [6]. Another study involved improving cavitation characteristics by varying only the shape of the leading edge of an impeller [7]. Since slurry pumps are much different from clear liquid pumps, optimization can be more difficult since the parameters for optimization must comply with the necessary requirements for a slurry pump. One such example is assigning the number of blades to be a parameter. In water or gas pumps, this is a common parameter since increasing the blades often increases the efficiency and reduces pressure pulsation. However, increasing the number of blades in a slurry pump is counterproductive, most significantly because there must be a minimum clearance between blades to allow for the passage of solid matter [8].

In slurry pumps, wear is the most significant plague to performance because of the solid particles contacting the walls of the pump components. Surfaces are worn through erosion due to impact where solids hit the wall at a perpendicular angle and due to friction where solids slide against the wall. Therefore, a major objective in slurry pump design is to decrease the wear in the pump. This will increase the mean time between failures of the pump by effectively slowing down the wearing process inside the pump. It can also reduce the total cost of ownership of the pump, provided that other performance measures such as efficiency remain consistent or improve as wear is reduced. In fact, a small reduction in efficiency is acceptable if it can be proven that the total cost of ownership will still decrease. There are numerous factors that contribute to wear and it can be difficult to automatically determine the wear in a CFD analysis. For example, recirculation within the vanes is a common problem where there is a small vortex of flow swirling in a small area. This will wear that specific area of the pump faster. Additionally, it will decrease the efficiency since that recirculation is basically wasted flow. Recirculation is very hard for the solver to automatically find and quantify. One method of approximating wear is by analyzing the maximum velocity since wear increases fairly linearly with velocity and high velocities are generally known to correspond to greater wear [9–11]. Both the impact force and friction will increase with a higher velocity. The assumption here is that by reducing the maximum velocity, the wear will also be reduced.

The impeller blades are critical components in the pump since they define the flow throughout the pump. They experience high wear due to the high velocities relative to the blade motion and are often the first parts to wear as observed at Toyo, requiring adjustment or replacement. Therefore, to ensure optimal operation, it is beneficial to focus on reducing the wear on the blades which will be the focus in this thesis.

In order to change the velocity and thus the wear, splitter blades will be added to an impeller with wide vanes. Splitter blades are additional blades that are shorter than the main blades, shown in Figure 1.3. They are used especially in situations where a higher blade count may be desired for improved performance but may not be possible because it would cause blockage near the impeller inlet with too many blade leading edges so close together. In an impeller with wide vanes, velocities are fairly high along the blades. The goal is to reduce the high velocities by adding splitter blades to distribute the flow better. There is also a lot of space for recirculation to occur and there is less guidance of the flow from the blades. Adding in splitter blades can help guide the flow, reduce the open area and make recirculation less likely to occur.

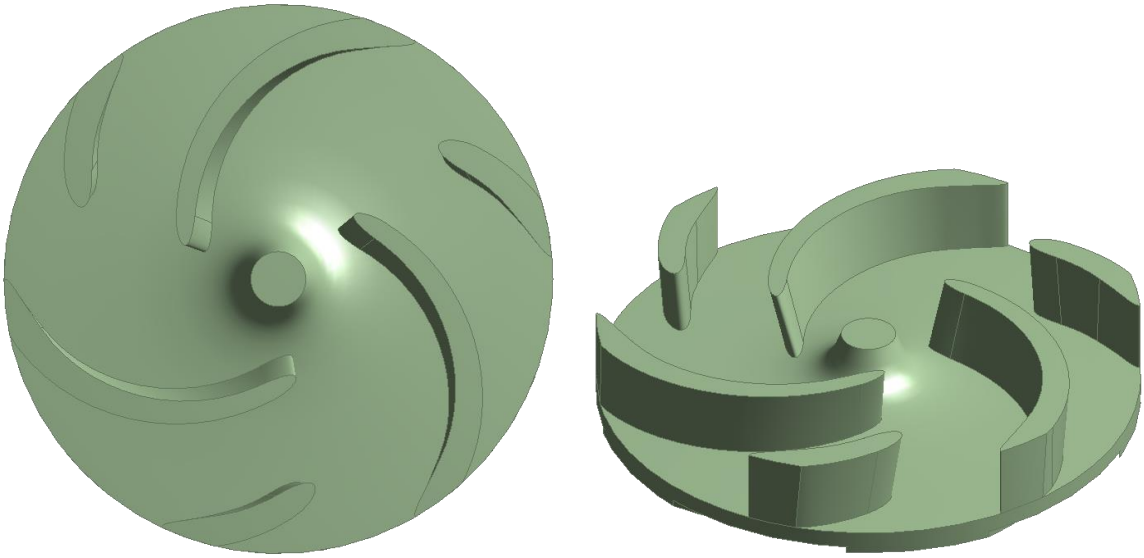

(a) (b)

Figure 1.3. Impeller with splitter blades; (a) top view, (b) 3D view

There has been very limited use of splitter blades in slurry pumps to date. Furthermore, no evidence of optimization on splitter blades in slurry pumps is present.

One patent presents the use of partial splitter blades that do not span the full width of the impeller like the main blades do [8]. Figure 1.4 shows an example of one type of partial splitter blade. Splitter blades can be used to accomplish different objectives such as decreasing wear or increasing efficiency and their location may vary depending on the application. For example, Jang and Choi investigated splitter blades in a blower fan and found two different optimum splitter blade locations to achieve either the maximum pressure or efficiency [12]. For this study, the focus is on reducing wear through reduction of high velocities on the blade surfaces. Since the size and location of the splitter blade can be varied to a great extent, it is not obvious where the best location should be. Three parameters are assigned to these splitter blades to adjust the length and their positioning in the impeller vane passage.

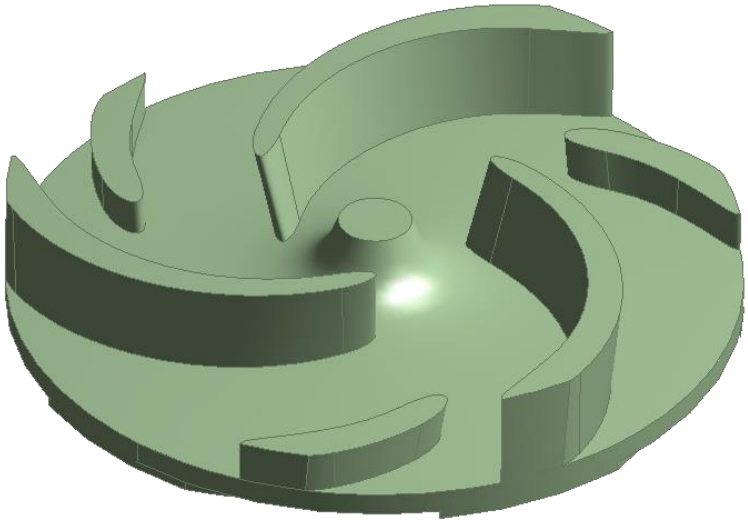

Figure 1.4. Impeller with partial splitter blades

Optimization will be performed using a simplified CFD model of the pump where only one vane and no volute is considered in the analysis. The purpose of using a simplified model is to provide significant time savings in the analysis. The study will show a validation of using the single vane model. The chosen optimization is the Adaptive Response Surface Method using an Intelligent Space Exploration Strategy developed by Long *et al.* [13]. It was chosen especially due to its strength in being used for expensive black box functions.

1.1. Research Objectives

The first objective of the research was to generate a CFD model of an existing pump made by Toyo Pumps to produce results and then validate the results with physical tests. The results must agree to show that the CFD model can make reliable predictions of the performance of the pump. Once validated, a simplified model consisting of only a single vane of the impeller will be simulated and results will be compared and analyzed to ensure similarity between results predictions. If this simplified model corresponds well to the full model, it will be used for optimization. A new impeller will be simulated, consisting of three splitter blades. The splitter blades will be used as optimization parameters to find the best location to reduce the wear in the pumps by minimizing the maximum velocity on the blades and splitter blades. In the end, this research should provide Toyo Pumps with a new impeller design that uses splitter blades to improve the wear characteristics of their pumps while maintaining similar or better performance to similar pumps without splitter blades. This should decrease the total cost of ownership of the pump while increasing the mean time between failures.

1.2. Scope

The scope of this study is to use CFD as a tool to predict the performance of a centrifugal pump. By validating a CFD simulation of an existing pump with physical results, the CFD model will be assumed to be a good predictor of pump performance. Then, CFD will be used to perform an optimization of minimizing the high velocities on the blades in the pump. The simulation will use water as the fluid, not slurry. Water must be used for validation since Toyo only tests their pumps in water. Furthermore, simulating slurry is difficult and needs more work. This work will serve as the foundation for the future work that will focus on the effect of slurry. Another major assumption involves using a lower fidelity single vane model for optimization. Validation will involve simulating the entire pump and replicating physical conditions as closely as possible, but the optimization will use a simple and much less costly model. Results will be different between the models, but it is assumed that if trends are similar between the low- and high-fidelity models, performance improvements will be correctly predicted. For example, a decrease in wear on the single vane model will correspond to a similar decrease in

wear on the full model. Additionally, that improvement should be reflected on the physical pump if it were manufactured and tested.

1.3. Outline

Following the introduction, Chapter 2 presents a literature review. Chapter 3: CFD Modeling, gives a comprehensive description of the CFD model that was developed for this research. Chapter 4: Results Analysis and Validation presents an analysis of the results generated using the CFD model. The results are then validated by comparing to physical tests that were performed at Toyo Pumps. The section also presents results of a single vane analysis of the impeller and compares it to simulations of the full model. Finally, Chapter 5: Optimization presents the optimization of wear by varying the configuration of splitter blades in an impeller. Chapter 6 gives a conclusion of the work presented in this thesis as well as recommendations for future work. Following the conclusion are references and appendices.

Chapter 2. Literature Review

The turbomachinery industry is a prominent user of CFD due to the large amount and variety of products including turbines, fans, compressors and pumps. Most turbomachines handle fluids, therefore most studies consider those types of turbomachines. Based on available literature, turbines and compressors appear to be the types of turbomachines studied most extensively through CFD. Centrifugal pumps seem to be studied much less than other types of turbomachines. This is likely due to their non-symmetrical design which causes unsteady flow between the impeller and volute.

Over the past decades, CFD for turbomachinery has increased in complexity and accuracy as computing power has become more available and software has been further developed. This is very evident in the evolution of CFD on centrifugal pumps. Many earlier studies focused on two dimensional approximations of the flow through these pumps. Wang and Tsukamoto performed a 2D analysis of the interaction between the rotor and stator in a pump to observe the effects of pressure fluctuations [14]. Many recent studies have focused on 3D analyses of centrifugal pumps, however, many still make assumptions to greatly simplify the CFD simulation. Mentzos *et al*. performed a 3D, but simplified, analysis of a centrifugal pump by only considering a single vane of the impeller [15]. This study just focused on CFD and obtaining results to investigate the flow through the impeller. Grapsas *et al*. and Byskov *et al*. presented very similar studies but validated their results or performed further tests to investigate some impeller design changes or different test conditions [16,17].

Shojaeefard *et al*. presented one of many studies of a full pump that used a multiple reference frame method referred to as frozen rotor to simplify analysis [18]. The primary purpose of their study was to validate their simulation and then compare results with simulations of other similar designs. The frozen rotor method performs a steady

approximation of the flow through a turbomachine. It assumes two references frames, stationary and rotating, but only simulates with the two frames at a set position. Therefore, in centrifugal pumps, this can cause inaccuracies since it ignores the unsteady flow features inside the pump. Zhou *et al*. presented a similar analysis on a multistage centrifugal pump, which has a much different design with a symmetrical volute, making the design much more appropriate for a frozen rotor analysis [19]. The study investigated the effect of trimming the rear shroud radius. The results correlated well with physical tests. Asuaje *et al*. also performed a frozen rotor study but went one step further by running nine frozen rotor simulations at different impeller positions to get an idea of the unsteadiness in the results [20].

More recent studies focus on higher fidelity simulations by running fully transient simulations which can accurately take into account the unsteady interactions inside a centrifugal pump. Due to the high computational cost, these transient simulations are used less often for extensive investigations and are usually to examine a specific design or feature. Several studies focused on examining the unsteady interaction between the impeller and volute cutwater which causes pulsations [5,21–23]. Li *et al*. investigated the flow during the starting period of a pump which is another common use of transient simulations [24]. The main purpose of their work was to assess the validity of performing a transient analysis and to validate with physical results where they found good correlation. Lucius and Brenner studied vibrations in an impeller during rotating stall [25]. They used the results, which were successfully validated with physical results, to find the locations of the worst vibration.

Another area of interest in turbomachinery is splitter blades which are generally used to improve performance by increasing efficiency. Golcu *et al*. used CFD to investigate the effect of adding splitter blades to an existing impeller. With a lower blade count, splitter blades yielded a more efficient impeller [26]. Kergourlay *et al*. performed a similar investigation and reported on the pros and cons of adding splitter blades in a liquid pump [27]. The main pros were that pressure fluctuations were reduced, the flow was guided better, and head was increased. The main cons were that efficiency did not improve and radial thrust increased which can worsen vibrations.

CFD analysis is a good platform for optimization of complex problems such as improving the performance of turbomachines. Optimization has proven to be very effective in conjunction with CFD especially in aerodynamics, one of the most prominent fields using CFD. For example, Leifsson and Koziel presented a multi-fidelity design optimization study on wing design to maximize the lift [28]. They developed methodology to combine cheap, but low-fidelity, and expensive, but high-fidelity, models in optimization. This increased the efficiency of the optimization since the expensive CFD model was simulated 90% less, using the lower-fidelity model most of the time instead. The most common optimization in turbomachinery is on the impeller blades with the goal to improve performance. Performance is generally improved by maximizing efficiency or head (a measurement that defines how high a pump can transport fluid in a vertical pipe) or minimizing deterrents to good performance such as cavitation or vibration. In a study by Grapsas *et al*., the leading edge geometry of a blade was considered for optimization to decrease cavitation [7]. This study involved only a 2D simulation of a single blade of the impeller and a stochastic evolutionary algorithm was used for optimization. Derakhshan *et al*. presented another optimization on only the impeller, but in 3D [6]. The goal was to improve the efficiency based on the blade angles and impeller size. The optimization used a metamodel approach which involves generating mathematical models to represent the response of a system to certain input changes. The optimization method used was based on Artificial Neural Networks and Artificial Bee Colony algorithms. Westra, in a thesis, presented an extensive, thorough optimization analysis of a centrifugal water pump, again analyzing only the impeller [29]. The Differential Evolution optimization method was chosen, which is a member of the evolutionary algorithm family. The objective was a more complicated cost function that involved increasing the head of the pump and minimizing boundary-layer losses and cavitation. Thirteen parameters were chosen that defined the number of blades, blade shape and shroud shape. The optimization reduced the cost function from 1.68 to 1.35, almost a 20% decrease.

Optimization using metamodeling, referred to as Metamodel-Based Design Optimization (MBDO), is a very common and effective approach when optimizing expensive function evaluations. Many MBDO algorithms exist and all have different pros and cons. Many algorithms use the Response Surface Method (RSM) as their basis.

RSM involves a set of mathematical and statistical techniques that are used to develop a metamodel relationship between a response of interest and input variables [30]. A very simple and basic MBDO algorithm can use only RSM where sample points are generated on the expensive function to generate an RSM. Optimization is then performed on the RSM to find the best point. A more advanced MBDO algorithm to consider is Mode Pursuing Sampling developed by Wang *et al*. especially for global optimization of expensive black-box functions such as CFD [31]. It is an RSM based algorithm which creates metamodels from random samples. More samples are generated in the neighbourhood of the current optimum based on a cumulative probability estimation. It is an efficient method for expensive functions with good global convergence. However, it relies on the function being continuous near the global optimum, otherwise it may get trapped at a local optimum.

Another MBDO algorithm that uses RSM is Adaptive RSM (ARSM) developed by Wang *et al*. ARSM advances RSM by adaptively updating metamodels during optimization to improve the RSM approximation. It also employs a cutting plane space reduction method to continuously reduce the design space to focus on the current optimum. The Central Composite Designs (CCD) strategy is used for model fitting and plans experimental sample points. Some of ARSM's merits are that it is highly efficient and capable of global optimization. However, a drawback is occasionally missing the global optimum due to the cutting plane approach which reduces the design space and will never again allow exploration of the areas that were cut out. Additionally, the CCD method is not highly efficient [32]. ARSM spawned several modified methods including Improved ARSM (IARSM), pseudo-ARSM (pARSM), Enhanced ARSM (EARSM) and ARSM using an Intelligent Space Exploration Strategy (ISES), termed ARSM-ISES. IARSM was developed by Wang *et al*. to improve the efficiency of ARSM by replacing CCD with Latin Hypercube Design (LHD) to generate design experiments [33]. LHD, which is developed by Mckay *et al*. is a method of generating sample points by ensuring they are spaced evenly within the bounds [34]. It further ensures constrained maximum spacing between the points [35]. Whereas CCD involved generating new sets of data points in each reduced space, LHD data points can be inherited in future iterations, reducing the number of data points to be generated. IARSM has a significantly higher efficiency and is capable of optimization on high-dimensional problems. However,

IARSM still suffers the same notable drawback as ARSM as it uses the cutting plane space reduction approach [33]. pARSM, developed by Panayi *et al*., is an application-specific variation of ARSM for the optimization of piston skirt profiles. It uses LHD from IARSM but does not use space reduction but rather space adjustment [36]. EARSM was another improvement to ARSM and the other ARSM based methods, formulated by Long *et al*. While it uses LHD, the major upgrade in EARSM was changing the design space reduction method to a novel Significant Design Space (SDS) approach. SDS generates a design space that is successively reduced in size around the current optimum for exploitation. It can move with the current optimum as it is updated and thus, in later iterations, the design space may include areas not included in the previous iteration. EARSM achieved much better global convergence capability and higher efficiency than ARSM [37]. ARSM-ISES was developed by Long *et al*. to further improve ARSM beyond the improvements made in EARSM [13]. The most significant enhancement in ARSM-ISES is specifically the ISES feature which uses a new SDS identification algorithm that improves the efficiency of the optimization and the global exploration capability such that the probability of missing the global optimum is reduced. The new SDS fully makes use of previous expensive function evaluations in the current iteration. Similar to the basic SDS, used in EARSM, the new SDS will shrink in size for exploitation, however, when the RSM fit is acceptable, the SDS will be enlarged to promote exploration and help prevent convergence on only a local optimum. A further enhancement is the adaptive penalty function for expensive constraint handling, a feature not present in many other MBDO algorithms. Whereas static penalty function factors are difficult to set for good expensive constraint handling, the adaptive factor is increased based on the amplitude of any constraint violations. Limitations of ARSM-ISES are that it occasionally may still miss a global optimum for some problems and the required number of function evaluations drastically increases with high dimension problems [13].

ARSM-ISES was chosen as the optimization method to use for the research presented as it has been proven to be superior to the other methods presented. ARSM-ISES was proven to be superior to ARSM and IARSM based on a number of benchmark test problems. In general, ARSM-ISES was observed to have better performance in terms of global exploration, efficiency, and robustness. MPS yielded fairly comparable

performance to ARSM-ISES, but ARSM-ISES was still superior. Over several optimization runs, ARSM-ISES had less variance in the optima for most problems and also showed the best global exploration capability. While not as applicable to this study, ARSM-ISES also performs the best for high dimension problems where some of the other methods are not practical. It also has the best expensive constraint handling capability.

Only one study could be found on optimization involving splitter blades which was on a blower fan (basically an air centrifugal pump) [12]. In that study only two design parameters were varied: the length of the splitter and the pitch of the splitter or angle of the splitter with respect to the main blade. The two objectives of the investigations were increasing the pressure and efficiency and optimization was performed by RSM. The full model of the blower including the volute was used to generate the RSM. The two objectives were optimized separately and different designs were found to achieve each optimum with great success. It was found that the success was owed to the splitter blades reducing reverse flow and circulation in the vane passages. Figure 2.1 shows the optimum design result for optimizing efficiency. It is important to note that the splitter blade is very close to the main blade and is hardly shorter than the main blade. This would not be possible to incorporate into a slurry pump due to the requirement to pass relatively large solid particles.

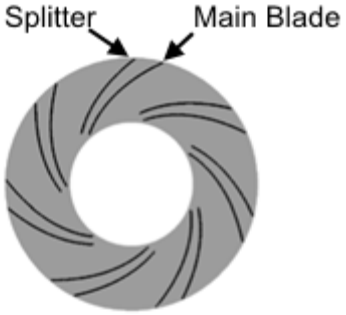

Figure 2.1. Optimized blower pump with splitter vanes [12]

Slurry pump analysis using CFD is a less common topic of study in the literature. Simulating slurry is a more difficult task than simply simulating a liquid since slurry is two-phase, containing liquid and solids. Most slurry studies found are for slurry flow in pipelines or in bubble column reactors. For example, Chen *et al*. studied dense coal and

water slurry flow in a horizontal pipeline using an Eulerian multiphase approach. Their goal was to prove that the approach was effective for very dense flows and to then analyze how the dense slurry behaved [38]. Troshko and Zdravistch simulated a slurry bubble column reactor which synthesizes gas into hydrocarbon liquid fuels. The slurry is very different, but still has similar principles. These reactors consist of three phases: gas bubbles, liquid, and solid catalyst particles that are suspended in the liquid. Their study focused on quantitatively analyzing performance in the reactor [39].

Most slurry pump studies are performed to investigate the wear in a pump to find the critical locations that will wear the most. Pagalthivarthi *et al*. presented two studies of the wear in slurry pumps. They simulated slurry but only considered a 2D model of just the volute. Slurry properties such as the concentration and size of the solids were varied and wear was found to increase as both parameters increased. A few design changes were then made in an attempt to improve wear characteristics. For example, it was found that with a smaller gap between the cutwater and impeller, the impact wear was reduced. Increasing the volute width also decreased the wear [40,41]. One thesis investigated the 3D flow in a full slurry pump using only water. The main purpose was to generate and analyze the pressure and velocity distributions inside the pump [42]. Another thesis showed a similar investigation but also ran some simulations with slurry consisting of water and ash of varying concentrations to compare the performance. It was found that head and efficiency both decreased when slurry was used and they decreased further as the solid concentration of the slurry was increased [43].

The only work found that showed splitter blades being used in slurry pumps was a patent by Weir Minerals [8]. Weir used partial splitter blades that were added to reduce recirculation and improve performance. Wear was also observed to be reduced.

There is a void in current literature for optimization applied to centrifugal slurry pumps. Moreover, there are no optimization studies that have investigated the best configuration for splitter blades to reduce impeller wear. Because of the fundamental differences between slurry and clear liquid pumps, there are different requirements for splitter blades in slurry pumps, which differentiates this work from others. The optimization goals are also different from other studies involving splitter blades since the

primary focus will be to reduce the wear with a much lesser focus on other performance measures such as efficiency. In fact, a small decrease in efficiency is acceptable if wear characteristics can be improved sufficiently enough to still yield a decrease in the total cost of ownership.

Chapter 3. CFD Modeling

3.1. Background

3.1.1. Turbomachinery Theory

The fundamental theory behind all turbomachinery design is Euler's pump and turbine equation. It relates the energy transfer process of an impeller to the geometry of the impeller based on the velocities throughout it. Euler's equation is based on the conservation of angular momentum and conservation of energy. The general formulation of Euler's equation is shown in Equation 3.1

$$\dot{W} = C_{w1}U_1 - C_{w2}U_2 \quad \text{(Eq. 3.1)}$$

where $\dot{W}$ is the rate of energy transfer, C_w refers to the tangential fluid velocity and U refers to the tangential impeller velocity. The subscripts 1 and 2 represent the inlet and outlet of the impeller, respectively [44].

A typical centrifugal pump was shown in Figure 1.1. Fluid to be transported flows through the inlet into the rotating impeller. The impeller, driven by a motor, will transfer kinetic energy to the fluid, causing it to accelerate circumferentially. The velocity of the fluid is diffused into static pressure as it exits the impeller and is decelerated within the volute as it flows towards the outlet and into a pipe for transport. Figure 3.1 shows a labelled meridional section and plan view of a typical centrifugal pump impeller. The arrow labelled ω refers to the rotational velocity. The impeller in Figure 3.1 is called a closed impeller because it has both a hub and shroud. Some impellers do not have a front shroud and are termed semi-open impellers. LE and TE in the figure refer to the Leading Edge and Trailing Edge of the blade. The pressure and suction surfaces of the

blade are so named because the pressure surface experiences the highest pressure at that radial position whereas the suction surface experiences a lower pressure [1].

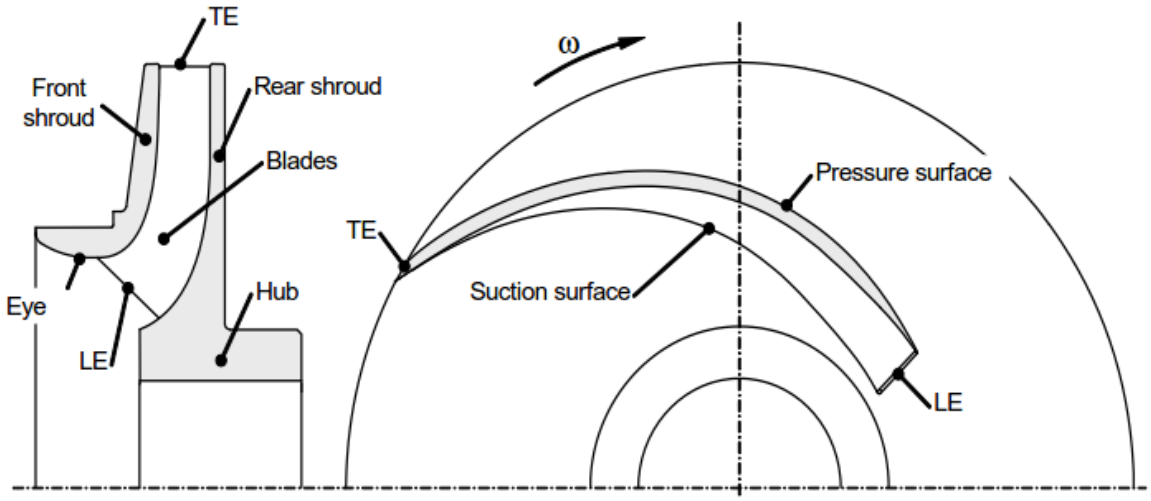

Figure 3.1. Meridional section (left) and plan view (right) of an impeller [1]

3.1.2. Pump Performance

There are three main performance specifications discussed in this thesis. They are the flow rate, head and efficiency. The flow rate is the useful volume that flows through the outlet of the pump [1]. Head is a very important measure of performance in pumps which simply refers to the height in a vertical pipe that a pump can raise fluid to at a specific operating condition. It is therefore expressed as a distance in metres or feet [45]. Referring to Figure 3.2, it is important to note that the total head refers to the vertical distance with respect to the height of the fluid in the existing reservoir, termed the suction head. The head with respect to the height of the pump is called the discharge head. The head is really just a way of expressing the difference between the total pressures at the inlet and outlet of the pump in a way that is often more meaningful to customers.

Total discharge head (different from the discharge head shown in Figure 3.2) is what is measured in Toyo's pump tests. The equation for total discharge head, h_d is shown in Equation 3.2.

$$h_d = h_{g_d} + h_{v_d} + Z_d \qquad \text{(Eq. 3.2)}$$

The first term, h_{g_d}, is the gauge head which is calculated from the pressure measured at the output of the pump. The second term, h_{v_d}, is the velocity head which is calculated based on the flow rate and the outlet pipe diameter. The final term, Z_d, refers to the elevation head which is the height between the pressure gauge and the water [46].

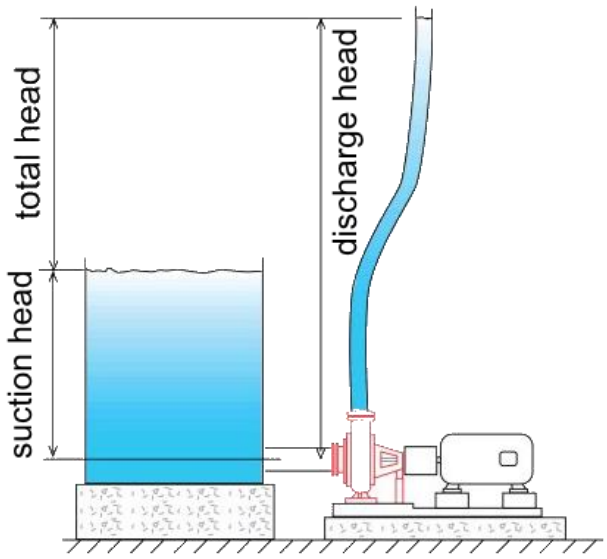

Figure 3.2. Pump head [45]

The efficiency is also an extremely important parameter which is an important focus of research in this thesis. The efficiency, represented as a percentage, is the ratio of the pump output power, also referred to as the liquid horsepower, to the pump input power, also referred to as the brake horsepower. The liquid horsepower is the power provided to the liquid by the pump and is proportional to the product of the flow rate, head and specific gravity of the fluid. The brake horsepower is the power delivered by the driver to the pump input shaft [46].

During regular operation, pumps will not operate at a single flow rate at all times. Therefore, pump specifications are generally presented via pump characteristic curves which display the head and efficiency and sometimes other data over a range of flow rates. Figure 3.3 displays a sample of head and efficiency pump curves generated by simulation. The flow rate, head and efficiency values are not enumerated to maintain confidentiality. There is clearly a certain point on the efficiency curve where the

efficiency is a maximum, indicated by the circle. This is called the Best Efficiency Point (BEP) and is the operating point at which the pump is designed for. The flow rate, head and efficiency at BEP measured on the physical pump are taken as reference values and are referred to as Q_{ref}, H_{ref} and η_{ref}, respectively. All other measured values are displayed relative to the reference values as defined in Equations 3.3 to 3.5

$$Q_{rel} = \frac{Q}{Q_{ref}} \quad \text{(Eq. 3.3)}$$

$$H_{rel} = \frac{H}{H_{ref}} \quad \text{(Eq. 3.4)}$$

$$\eta_{disp} = \frac{\eta}{\eta_{ref}} \quad \text{(Eq. 3.5)}$$

where Q, H and η refer to measured values. For example, the efficiency at 100% flow rate in Figure 3.3 is 88.93% which refers to 88.93% of the actual efficiency on the physical pump at BEP.

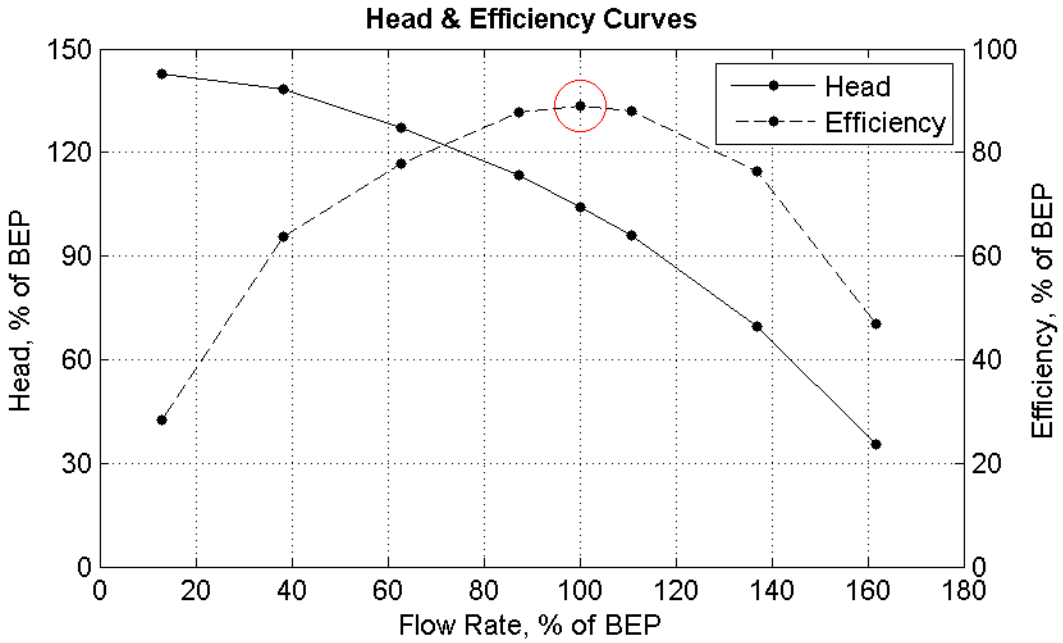

Figure 3.3. Sample pump performance curve data

3.2. CFD Methodology

Computational Fluid Dynamics (CFD) is a quickly growing technology that is being used in academia and increasingly more in the industry as an aid in the design process. It solves equations of fluid flow over or through a region based on conditions specified by the user at the boundaries of the region. The ideal use of CFD is basically to skip physical prototyping steps in the design phase, allowing virtual prototypes to be tested, analyzed and even optimized. CFD can provide major time and cost savings as well as allow engineers to see detailed flow phenomena in their designs [47]. There are currently a number of CFD software providers, but one of the leading products is ANSYS. ANSYS has two major CFD software suites: FLUENT and CFX. CFX was chosen as the CFD software for the author's research. While both software suites are very capable, CFX is generally recommended over FLUENT for turbomachinery. Further advantages that ANSYS provides for turbomachinery include specific software meant for generating and editing turbomachines. One of these is BladeGen which is software meant for designing impellers and quickly and easily generating three dimensional models. Another software incorporated into DesignModeler, the ANSYS CAD software used to import and modify geometry, is BladeEditor. BladeEditor can also be used for impeller generation but also adds powerful and very user-friendly features that allow a user to modify blade geometry directly in the CAD editor. It also allows parameterization of key features of the design such as the blade shape or size. This allows a user to apply design changes by simply changing numerical parameter and further gives the capability of easily automating the design change process.

3.2.1. Basic CFD Theory

CFD is based on the Navier-Stokes differential equations of fluid flow, often referred to as the fluid momentum equations. Named after Claude-Louis Navier and George Gabriel Stokes, they were derived in the early 1800s to describe the process of momentum, heat and mass transfer in a fluid flow [48]. To fully compute fluid flows, there are three major governing equations, one of which is the Navier-Stokes equation in its compact form. They are mathematical representations of fundamental conservation laws

of physics. The names of the three equations and their corresponding laws are listed in Table 3.1 [49].

Table 3.1. CFD governing equations

Equation	**Conservation law explanation**
Continuity or mass conservation equation	A fluid's mass is conserved
Momentum equation	Based on Newton's second law, the rate of change of momentum is equal to the sum of forces on a fluid particle
Energy equation	Based on the first law of thermodynamics, the rate of change of energy is equal to the rate of heat added to a particle plus the rate of work done on a particle

There are four independent and seven dependent variables in the governing equations, shown in Table 3.2, with their accompanying symbolic representations. The dependent variables are the variables to be solved for [48].

Table 3.2. Variables of governing equations

	Variable	**Symbol**
Independent	x coordinate	x
	y coordinate	y
	z coordinate	z
	Time	t
Dependent	Velocity (vector with 3 components)	$\boldsymbol{U}(u, v, w)$
	Pressure	p
	Density	ρ
	Temperature	T
	Internal or thermal energy of fluid	i

The following equations make use of the gradient and divergence operators, both represented by ∇. The notation for the gradient of a function f is ∇f whereas the notation for the divergence of f is $\nabla \cdot f$. The definitions of the gradient and divergence functions in two dimensions are shown in Equations 3.6 and 3.7, respectively.

$$\nabla f(x, y) = \left(\frac{\partial f}{\partial x}, \frac{\partial f}{\partial y}\right) \quad \text{(Eq. 3.6)}$$

$$\nabla \cdot f\big(A(x,y), B(x,y)\big) = \frac{\partial A}{\partial x} + \frac{\partial B}{\partial y} \quad \text{(Eq. 3.7)}$$

The continuity equation is shown in Equation 3.8.

$$\frac{\partial \rho}{\partial t} + \nabla \cdot (\rho \boldsymbol{U}) = 0 \quad \text{(Eq. 3.8)}$$

The first term of the continuity equation represents the rate of change of density over time and the second term, called the convective term, represents the net flow of mass out of the fluid element across its boundaries. In an incompressible fluid, the density does not change. In the work presented in this thesis, the fluid is assumed to be incompressible. With incompressible fluids, the first term of the continuity equation, $\frac{\partial \rho}{\partial t}$, becomes zero and the continuity equation can be reduced to Equation 3.9.

$$\nabla \cdot \boldsymbol{U} = 0 \quad \text{(Eq. 3.9)}$$

The momentum equation consists of an extra dependent variable – the viscous stress components τ_{ij}. In Newtonian fluids, the viscous stresses are proportional to the linear and volumetric deformation rates. There are two constants of proportionality: the first or dynamic viscosity, μ, which relates stress to linear deformations; and the second viscosity which relates stress to the volumetric deformation. The volumetric deformation is given by $\nabla \cdot \boldsymbol{U}$ and for incompressible liquids, the continuity equation shows this is zero. Therefore, there is no volumetric deformation in incompressible fluids, thus the second viscosity is only applicable to compressible flows and observations have shown the effect of it to be small there.

The momentum equation, in its compact vector form is shown in Equation 3.10. It is common to represent the momentum equation by three equations for the x-, y- and z-momentum. Equation 3.11 shows the x-momentum equation, from which the y- and z-momentum equations can also be deduced.

$$\frac{\partial (\rho \mathbf{u})}{\partial t} + \nabla \cdot (\rho \boldsymbol{U} \otimes \boldsymbol{U}) = -\nabla p + \nabla \cdot (\mu \nabla \boldsymbol{U}) + S_M \quad \text{(Eq. 3.10)}$$

$$\frac{\partial(\rho u)}{\partial t} + \nabla \cdot (\rho u \boldsymbol{U}) = -\frac{\partial p}{\partial x} + \nabla \cdot (\mu \nabla u) + S_{M_x} \quad \text{(Eq. 3.11)}$$

Most of the terms represent surface forces such as pressure or viscous forces. The S_M term is a source term which includes effects of body forces such as centrifugal, Coriolis or electromagnetic forces, where applicable. It also includes the effect of the second viscosity in compressible fluids.

The energy equation is shown in Equation 3.12

$$\frac{\partial(\rho i)}{\partial t} + \nabla \cdot (\rho i \boldsymbol{U}) = -p \nabla \cdot \boldsymbol{U} + \nabla \cdot (k \nabla T) + \Phi + S_i \quad \text{(Eq. 3.12)}$$

where k refers to the thermal conductivity, Φ is the dissipation function which takes into account all the effects due to viscous stresses and S_i is a combination of S_M and a source of energy per unit volume per unit time, S_E, as defined in Equation 3.13.

$$S_i = S_E - \boldsymbol{U} \cdot S_M \quad \text{(Eq. 3.13)}$$

Five differential equations have now been introduced: the continuity equation, three momentum equations and energy equation. However, there are still seven unknowns present. Two equations of state are used which relate the four thermodynamic variables, ρ, p, i and T, to each other. Equations of state relate variables to the two state variables which are taken to be the density, ρ, and temperature, T. The equations are obtained by assuming thermodynamic equilibrium. Equations 3.14 and 3.15 show the form of these equations as well as their common definitions in a perfect gas where R is the ideal gas constant and C_v is the specific heat at constant volume [49].

$$p = p(\rho, T) = \rho R T \quad \text{(Eq. 3.14)}$$

$$i = i(\rho, T) = C_v T \quad \text{(Eq. 3.15)}$$

In this study, there will be no thermal analysis. The fluid will be assumed to remain at a constant temperature. Referring to the equations of state, the pressure and energy will thus be constant since both the density and temperature are constant. The

energy equation will not be involved in computations since there will only be four unknowns (three velocity components and pressure) and four differential equations.

The governing equations of flow only have known analytical solutions for extremely simple flows under ideal conditions. This is where the purpose of CFD is realized. To generate solutions for most flows, the equations must be discretized which involves replacing them with algebraic approximations that can be solved numerically [50]. Several techniques exist to do that including finite difference, finite volume, finite element and spectral methods [48]. The finite volume technique is the most common of those and is the method used by ANSYS CFX. In the first step of the finite volume method, the domain to be simulated is broken up into small sub-regions or control volumes. The combination of control volumes forms a mesh of the whole domain. Each control volume is used to conserve mass, momentum and energy. Figure 3.4 shows an example of a portion of a typical mesh in two dimensions. The figure shows one control volume, four mesh elements and six nodes (element vertices). A control volume is formed around every mesh node using the median dual. The medial dual is defined by lines that connect the centres of each element edge and the centres of each element as illustrated in the figure. Once solved, the dependent variables and fluid properties are stored at the nodes.

The equations are discretized and solved iteratively via integration of volume and surface integrals over each control volume. Figure 3.5 shows a single mesh element to help illustrate the discretization process. Volume integrals of a control volume are discretized within each element sector with the results being attributed to the control volume that the sector belongs to. Referring to Figure 3.4, it is clear that the single mesh element shown in Figure 3.5 covers three different control volumes. Surface integrals are discretized at integration points, represented by $ip1, ip2$ and $ip3$ in the figure. The integration points are located at the centre of each surface segment of an element. The results are then attributed to each adjacent control volume. Each control volume adjacent to an integration point will thus have equal but opposite surface integrals which are thus locally conservative.

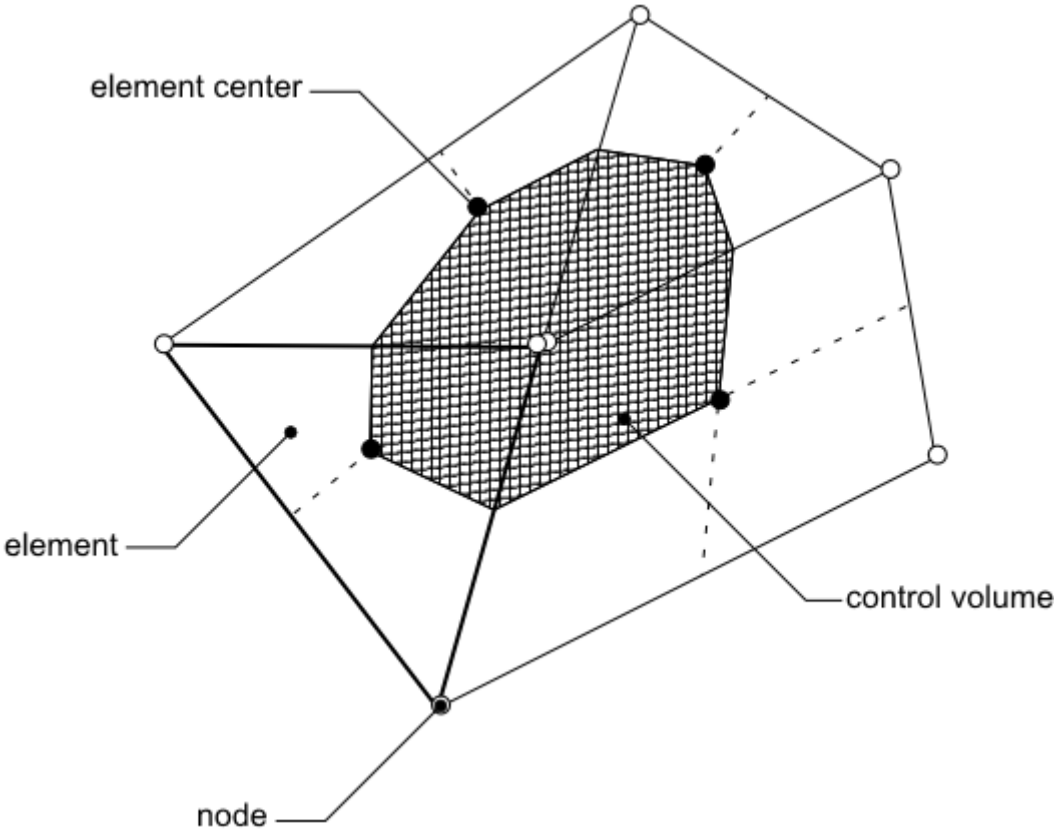

Figure 3.4. 2D control volume [50]

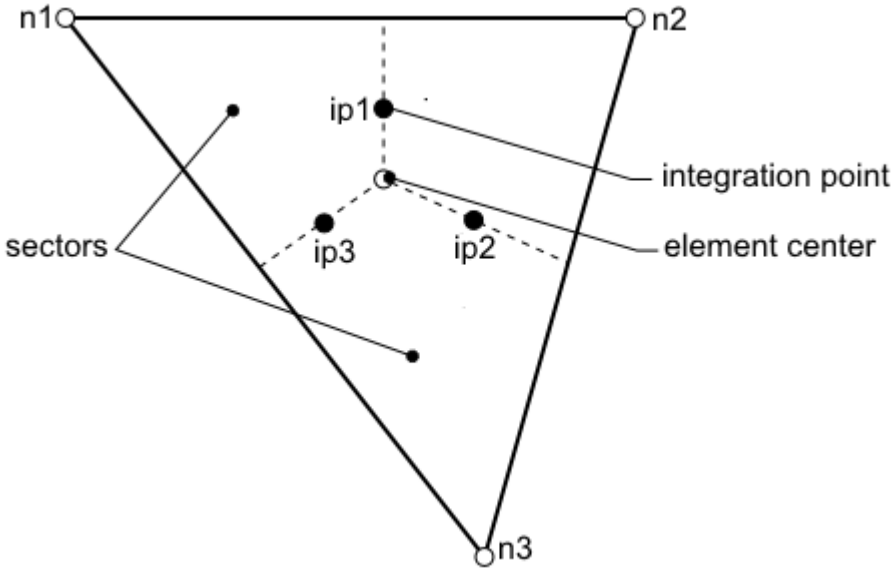

Figure 3.5. Single mesh element [50]

After solving all the discretized equations, the solutions yield approximations for the values of the dependent variables such as pressure and velocity at all nodes throughout the domain. Combined together, these nodal solutions give an overall view of the flow throughout the entire domain [47,50].

3.2.2. Methodology Overview

The learning curve for ANSYS CFX is quite steep for a beginner. Delving into CFD can be quite a daunting task with no training. The author learned to use CFX through tutorials, several ANSYS courses and discussions with several CFD experts that gave great insight into the project. Much of the learning also involved trial and error which is quite common in CFD. It is often necessary to try different methods and experiment with different settings to obtain correct, reliable results. Much time was spent on this project running simulations on various pumps and sequentially adding more complexity to the simulation to more closely model the real scenario. The following sections will outline this process in the order that a complete CFD analysis is performed, starting with the geometry from a Computer Aided Design (CAD) Model, generating a mesh of the model and setting up the simulation parameters, followed by simulation results in the following chapter.

3.2.3. Geometry

The first step of a CFD analysis is to generate and prepare the geometry to be analyzed. Unlike conventional CAD modelling, for CFD, it is the fluid that must be modelled, not the actual pump itself. The easiest and most common way to do this is to generate a negative of the pump to be studied. ANSYS has tools built-in for this purpose that allows the user to ‘fill’ an object with fluid, generating the fluid geometry. Figure 3.6 shows the geometry of the pump designed by Toyo that was investigated in this research. Figure 3.6 shows (a) the volute of the pump with the impeller inside, (b) the impeller from above, and (c) the impeller from below. Exact dimensions of the pump cannot be given due to confidentiality, but to give an estimate, this pump is a medium size pump which has an impeller diameter that will be in the range of 100 to 600 mm.

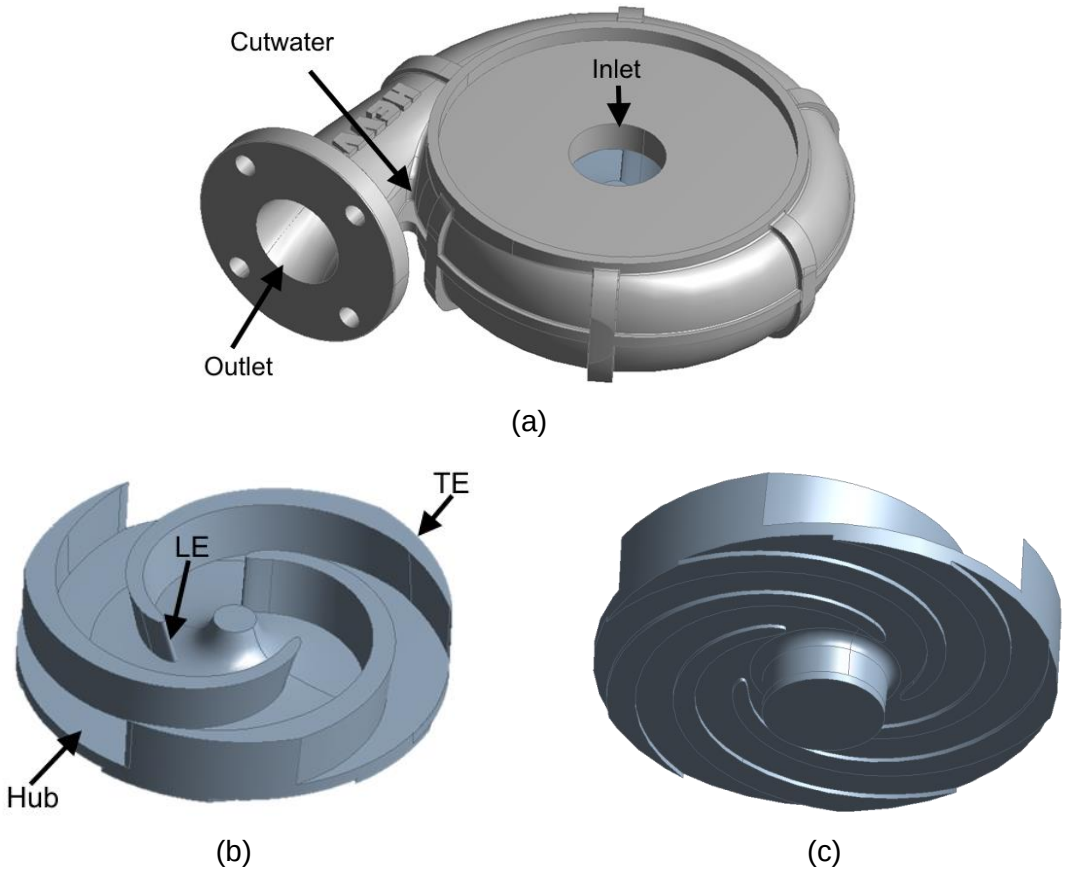

Figure 3.6. Toyo pump geometry: (a) Volute with impeller inside; (b) Impeller view from above; (c) Impeller view from below

The impeller is a semi-open impeller because it does not have a front shroud. The small blades that can be seen on the bottom of the impeller in Figure 3.6 (c) are called expeller vanes. The purpose of expeller vanes is to prevent most solids from entering the gap between the bottom of the impeller and the bottom of the volute, referred to as the lower sidewall gap. The lower sidewall gap areas are shown in the cross-section view of the pump in Figure 3.7 (b), indicated by the black boxes. On this impeller, there are five expeller vanes while there are only three impeller vanes.

Filling the pump geometry generates the fluid domain of Toyo's pump which is shown in Figure 3.8. Once the fluid geometry has been imported, there is still much more work required. Since the fluid domain consists of both rotating and stationary parts, the two must be separated. As for the location to cut the geometry to separate the domains, the commonly recommended location is halfway between the narrowest gap of

the impeller outlet and the volute [51]. This narrowest gap is usually near the tip of the cutwater which is true in the case of this slurry pump. Figure 3.9 shows the separated stationary and rotating domains.

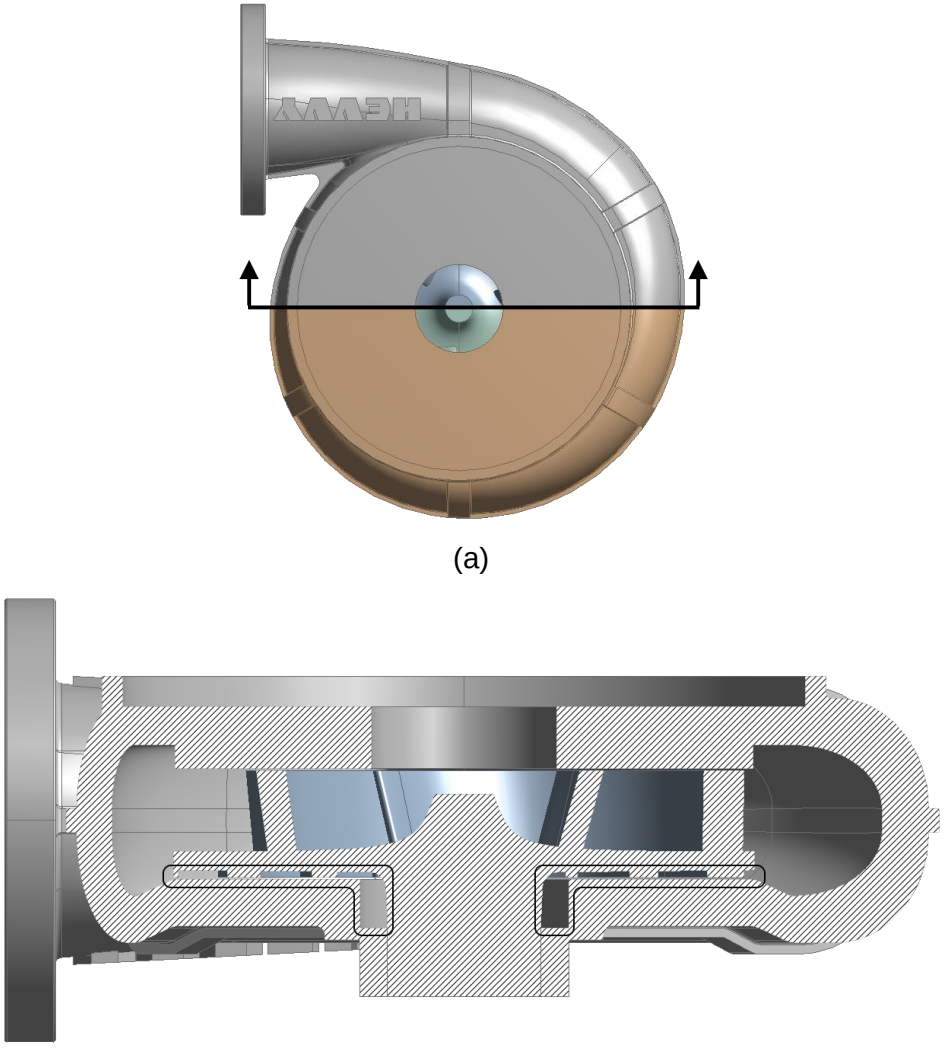

(a)

(b)

Figure 3.7. (a) Cross-section cut location of pump and (b) cross-section view showing sidewall gaps as indicated by black lines

While the separated model could be used for simulation, it is common to cut out only one impeller vane for the meshing step. Later, during preparation for simulation, the one vane will be multiplied to make a full impeller of three vanes again. There are two main advantages of doing this. First, it significantly increases the efficiency and speed of the meshing step. It is mainly because it reduces the meshing required by one third

since only one of three blades will be meshed. Secondly, it ensures the mesh is the same in each vane and prevents any inaccuracies due to the vanes having different meshes. To cut out one impeller vane, the rotating fluid domain portion needs to be separated into two parts, one containing the impeller vanes and one containing the expeller vanes in the lower sidewall gap. This separation is shown in Figure 3.10. The lower sidewall portion must also have one of the five expeller vanes cut out of it.

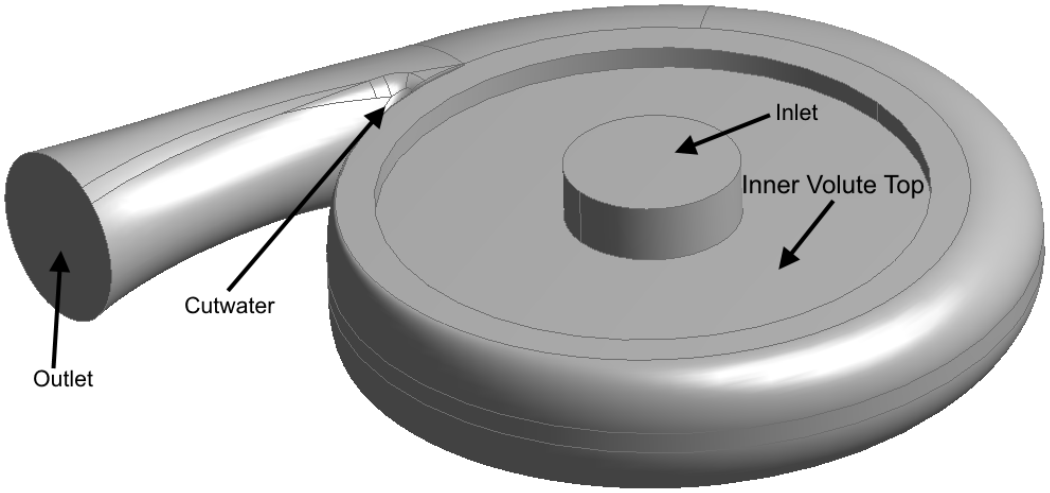

Figure 3.8. Fluid domain of pump

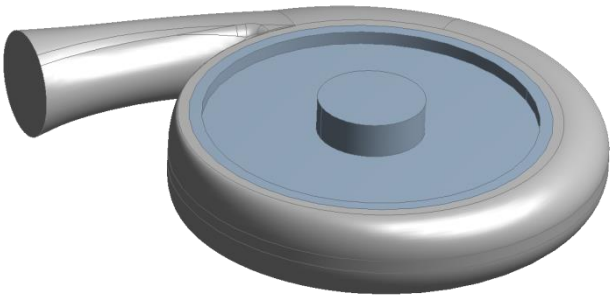

Figure 3.9. Separated stationary and rotating domains

There are a number of ways in which one vane can be cut from the impeller. The easiest method to do this is to simply slice the impeller by two planes with the angle between them being 360° divided by the number of blades. For the impeller shown, that would mean cutting out a 120° portion of the impeller as shown in Figure 3.11. While this is functional, it was found that meshing could be fairly difficult with the vane cut this way since the blade was geometrically broken up.

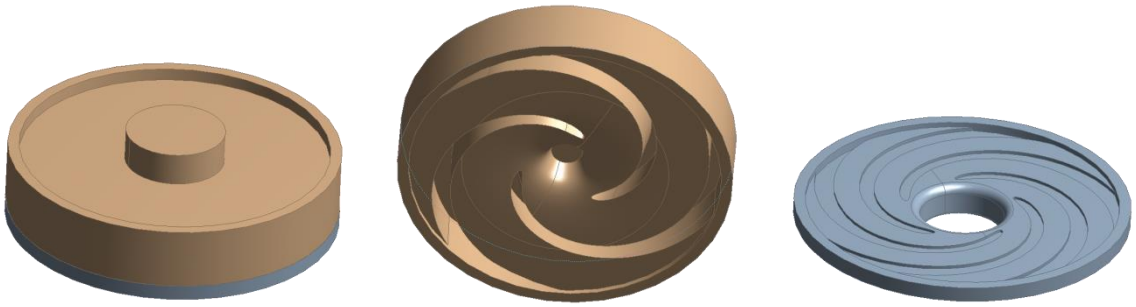

(a) (b) (c)

Figure 3.10. (a) Separated impeller and lower sidewall gap fluid portions; (b) impeller portion from below; (c) lower sidewall portion showing the expeller vanes

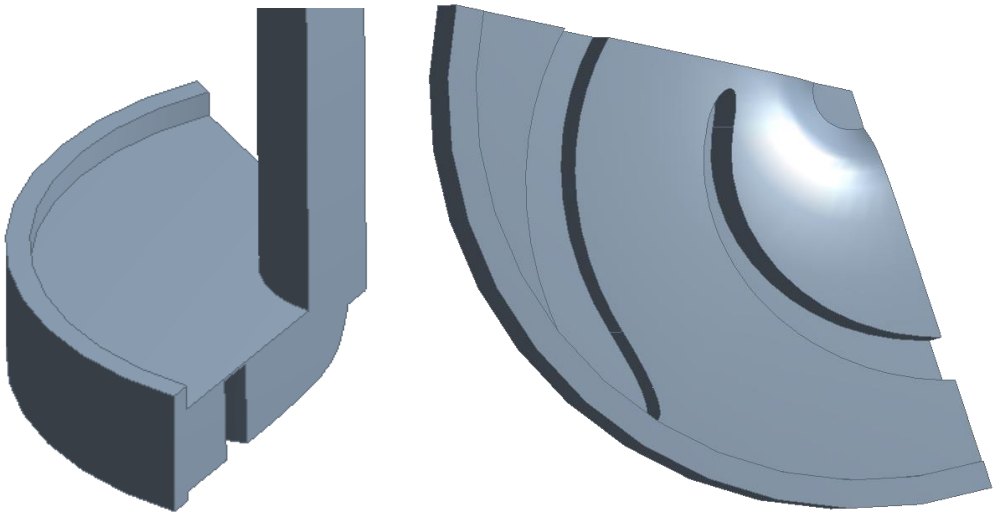

(a) (b)

Figure 3.11. Simple impeller vane cutout viewed from the (a) top and (b) bottom

Another method to cut out the vane is to slice the geometry around the blade by a contour that is more similar to the shape of the blade as shown in Figure 3.12. This method is more common and was used in most of the literature reviewed. It was easier to work with this geometry compared to the geometry shown in Figure 3.11. The same procedure was applied to cut out one expeller vane from the lower sidewall gap section.

Another important step in the geometry model is to extend the inlet and outlet portions as if a pipe was attached to each. At the inlet and outlet locations shown in Figure 3.8, the flow can be fairly unpredictable since it is very close to the impeller at the

inlet and the cutwater at the outlet. There is also a high possibility that there will be recirculation, that is, the flow may not all be going in or out of the domain. It is much better practice to place the inlet and outlet farther away where the flow will be more predictable and uniform. A common recommendation was to extend the inlet and outlet by twice the diameter of the inlet and outlet, respectively [21]. Furthermore, that location is where inlet and outlet pressure are measured on the physical pump when it is tested (for the exact same reasons).

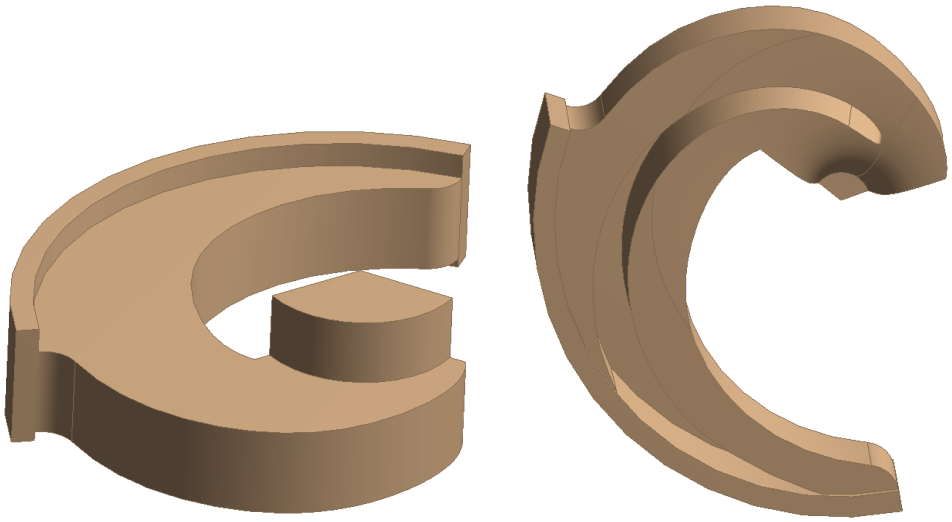

(a) (b)

Figure 3.12. Contour vane cutout viewed from the (a) top and (b) bottom

Ensuring the geometry is ‘clean’ and simplified is extremely important for an efficient and accurate simulation. For example, there are often tiny faces or sharp, narrow corners on faces of the geometry that are often generated upon importing the geometry. These should be removed as part of the cleanup since they force the mesh to be much finer than necessary which can significantly increase the simulation time. Removing other features that are not important and may overcomplicate the mesh and simulation should be based on the engineer’s intuition and knowledge. On the original impeller, there were small diameter fillets at the edges between the blades and rear shroud and also in the center as shown in Figure 3.13. These were removed based on the assumption that they will have very little effect on the flow and will force the mesh to be too fine to accurately define the curve. This assumption was tested and will be discussed later in Section 4.3: Sensitivity Analysis.

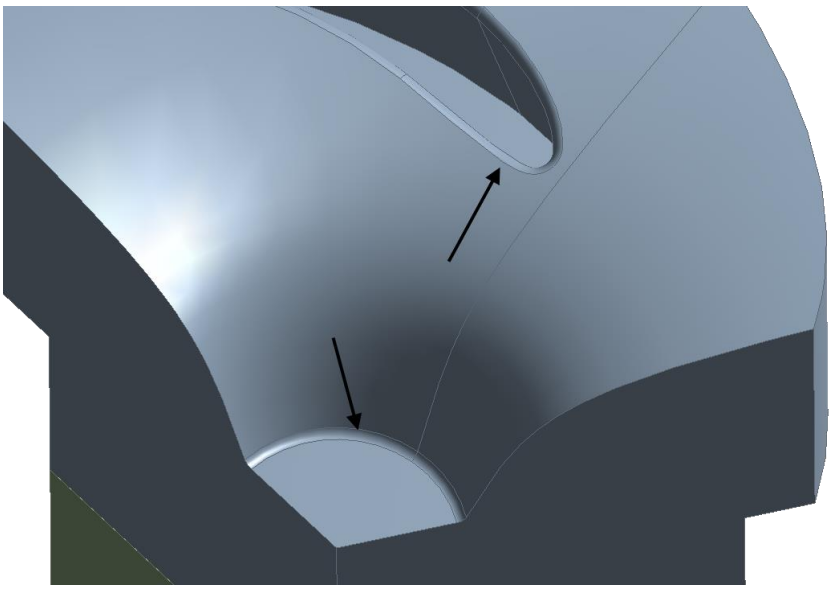

Figure 3.13. Impeller fillets

The final geometry used for simulation is shown in Figure 3.14. As it can be seen, the impeller and lower sidewall gap sections do not line up which will not affect the simulation since, when all vanes are added to form the full impeller again, they will line up. More diagrams showing all the steps of the geometry generation can be found in the Appendix.

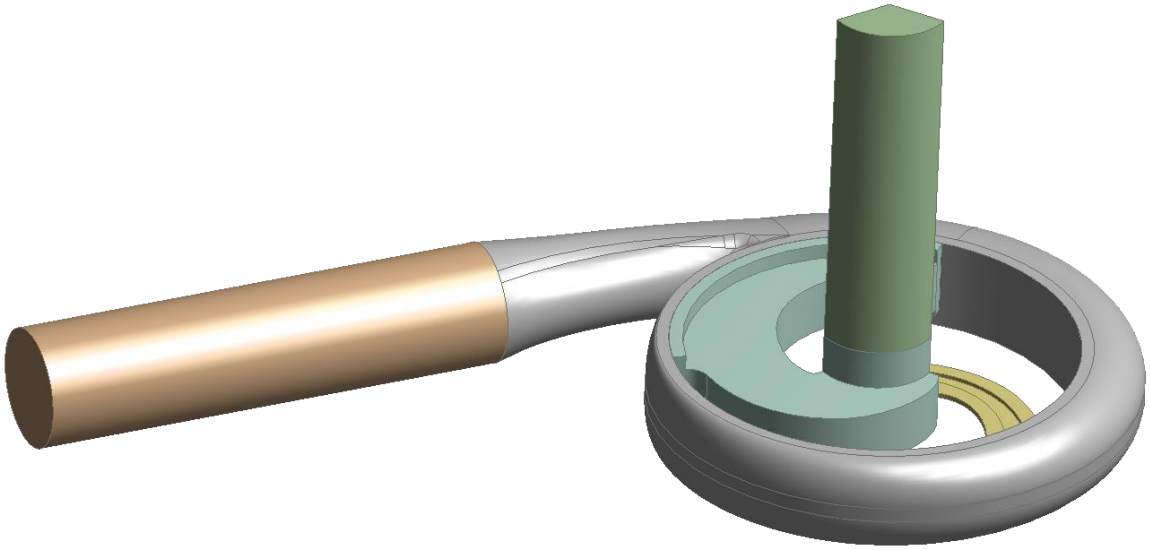

Figure 3.14. Final fluid domain geometry

Single Vane Model

The geometry shown in Figure 3.14 will be used to simulate the entire pump model which can be referred to as a high-fidelity model. Simulations were very time consuming and expensive with that model, usually taking around 20 hours, depending on the conditions. Therefore, a goal for this research was to generate a simplified or low-fidelity model that could run in about an hour or less and be used to predict the performance of the full model. CFD analyses of many types of turbomachines commonly only consist of a simulation of the flow through the impeller over just one or two blades rather than through the entire machine [15]. This is possible using symmetry settings in ANSYS CFX which is explained further in Section 3.2.5: CFD Setup. While no literature was found performing a single vane analysis on slurry pump impeller vanes, there were several studies performed on simulating a single vane of a clear liquid centrifugal pump. For example, in [6], a single vane was considered for analysis and optimization and the results were further validated on the high-fidelity model.

A single vane model of the pump was shown in Figure 3.12. The same model is shown in Figure 3.15 (a) but with two sections circled. Those sections above and below the vane are part of the volute and are present in the impeller model because of where the rotating domain was cut as displayed in Figure 3.9. To further simplify the single vane model, those parts are removed as it can be seen in Figure 3.15 (b).

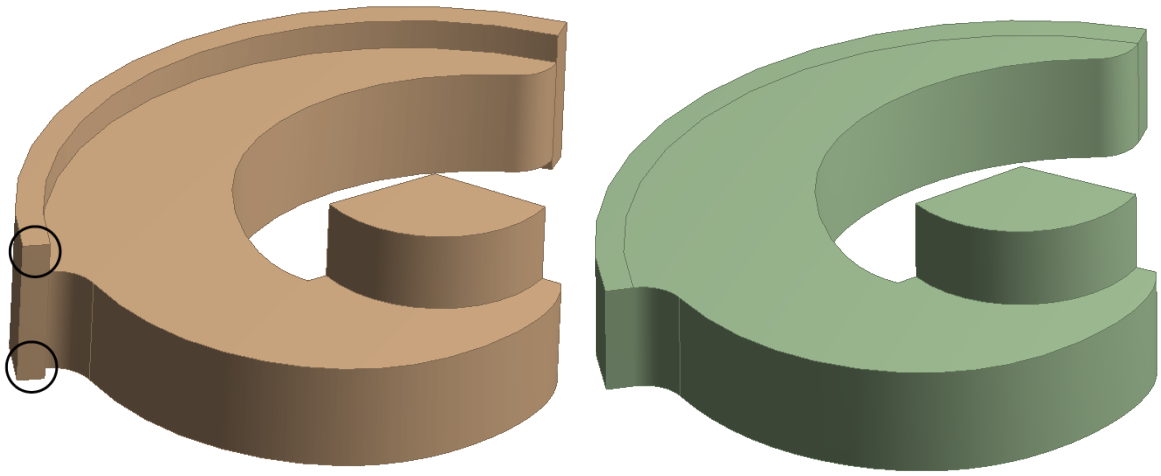

(a) (b)

Figure 3.15. (a) Full model impeller; (b) Single vane model impeller

3.2.4. Meshing

Overview

Meshing is the process of breaking up the geometrically-defined fluid domain into many small sub-regions for simulation. This step is often the most difficult and time-consuming part of a CFD analysis since a high quality simulation requires a high quality mesh. More importantly, meshing requires validation that the assumed high-quality mesh is, in fact, sufficient for accurate and reliable results [1]. ANSYS has built-in software called Meshing that has become increasingly automatic. However, assuming that the initial, automatic mesh generated is sufficient would be very poor practice for any simulation. The theory behind meshing is very extensive and complex and is far beyond the scope of the author's research. Only the important basics that were considered and studied for this research are presented.

Two of the most important aspects of meshing are the size and shape of the mesh elements. A fine mesh refers to one where the elements are smaller for the size of the domain whereas a coarse mesh has larger elements and thus fewer for the same domain. A fine mesh is generally a better mesh to a certain extent. Going beyond a certain point can over-complicate the simulation and make it take much longer than is required. However, having too coarse of a mesh can yield false results. False results may also be yielded if the element shape is not appropriate [1].

Considering shape, there are two major types of meshes: structured and unstructured. Each mesh type has its advantages and disadvantages. Figure 3.16 demonstrates the difference between a structured and unstructured mesh on a cube. A structured mesh is composed of rectangular, six-sided elements. The main advantage is that the mesh covers the domain in a uniform manner due to the simple data structure. The disadvantages are that it is not very flexible and can be harder to implement. An unstructured mesh fills the domain with tetrahedrons (four-sided triangular elements) and does not have continuous grid lines. This type of mesh is much easier to implement and is more flexible, meaning it can be used in a variety of cases. The disadvantage is the increase in calculation time [1]. There are many cases where a structured mesh will not provide good results. A structured mesh can be an excellent choice if the flow

direction is known and will be fairly uniform and predictable. The mesh must then be oriented in that direction. However, for more complex flows without a dominating flow direction, such as those that would occur in a slurry pump, the structured mesh loses its advantage [52].

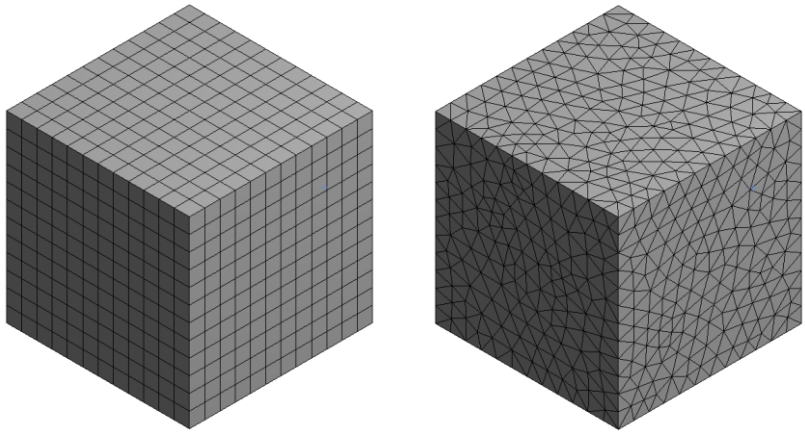

(a) (b)

Figure 3.16. Cube with (a) a structured mesh and (b) an unstructured mesh

Procedure

The meshing for most of the pumps studied was broken up into three parts so that three separate meshes were generated: one for the impeller and inlet extension; one for the lower sidewall gap; and one for the volute and outlet extension. This made it easier to independently control each mesh. With separate meshes, it is possible to have a conformal mesh, meaning the two meshes will have matching nodes at the interface between the two. For the interface between the stationary and rotating region, it is clear that conformal meshing will not be possible. Since the meshes will be moving with respect to each other, the mesh will be at many different locations as the impeller rotates. ANSYS CFX provides a general grid interface feature to take care of this and connect the two non-conformal meshes. For connecting the impeller and lower sidewall conformal meshing is possible, since the two meshes will not move with respect to each other. However, splitting up the meshes does not make this possible. While the meshing could be done together on the two parts, conformal meshing only provides a small benefit of making an easier grid connection. Therefore, it is often easier to forgo the conformal mesh to make the rest of the meshing process simpler. As for cutting the

impeller into a single vane, the sides of symmetry can have conformal meshing assigned which makes the mesh lined up when the parts are multiplied prior to simulation.

Sizing

Choosing the correct mesh sizing is not a simple task in the process of mesh generation. The mesh size depends on many factors including the size of the object itself, the complexity of the geometry and the type of flow occurring at a location. The process used for the pumps studied was to first assign an appropriate global maximum mesh size and then further refine the mesh as required. Assigning the global maximum mesh sizing was initially accomplished largely through intuition and comparison to meshes observed in literature. The final chosen maximum size was 6.0 mm. That size appeared to be fine enough to provide enough elements to capture sufficient detail of the flow through the domain. The sizing was further confirmed through sensitivity analysis which can be found in Section 4.3: Sensitivity Analysis.

The ANSYS meshing software can automatically perform meshing refinement based on the geometry. This feature is called an Advanced Size Function and can be turned on by the user. The sizing can be based on proximity and/or curvature. Both were turned on which means that at more complex features such as curves and in narrow passages, the geometry will be refined. Sometimes it is necessary to refine further or reduce the refinement. For proximity sizing (sizing in narrow passages), the default setting is to have a minimum of three cells across a gap. For the impeller fluid domain model, there is a very small gap of one mm between the top of the blade and the top of the volute as it can be seen in Figure 3.17. Since the impeller is an important part of the analysis, it is important to ensure all parts of the impeller will be accurately simulated. For that reason, the minimum number of cells across a gap was set manually to four for the impeller. For the volute, it was left at the default since there were no narrow gaps.

As for the sidewall gap, there are some very comparably narrow sections along the blade faces as it can be seen in Figure 3.18. However, the lower sidewall is not important for the focus of the simulations presented here so the default value for the number of cells across a gap is kept. Additionally some local sizing was added to the lower sidewall on the blade faces to set a larger minimum size than the default. The

default mesh size was too small near the narrow gaps which would cause the simulation to take significantly longer to run.

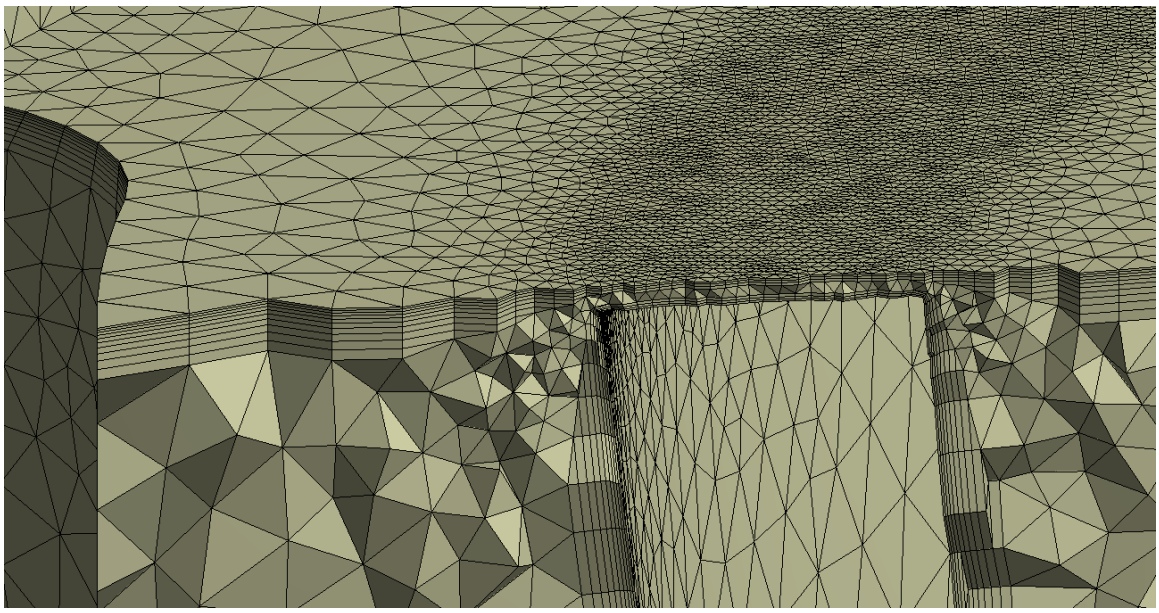

Figure 3.17. Impeller mesh cross-section showing narrow gap

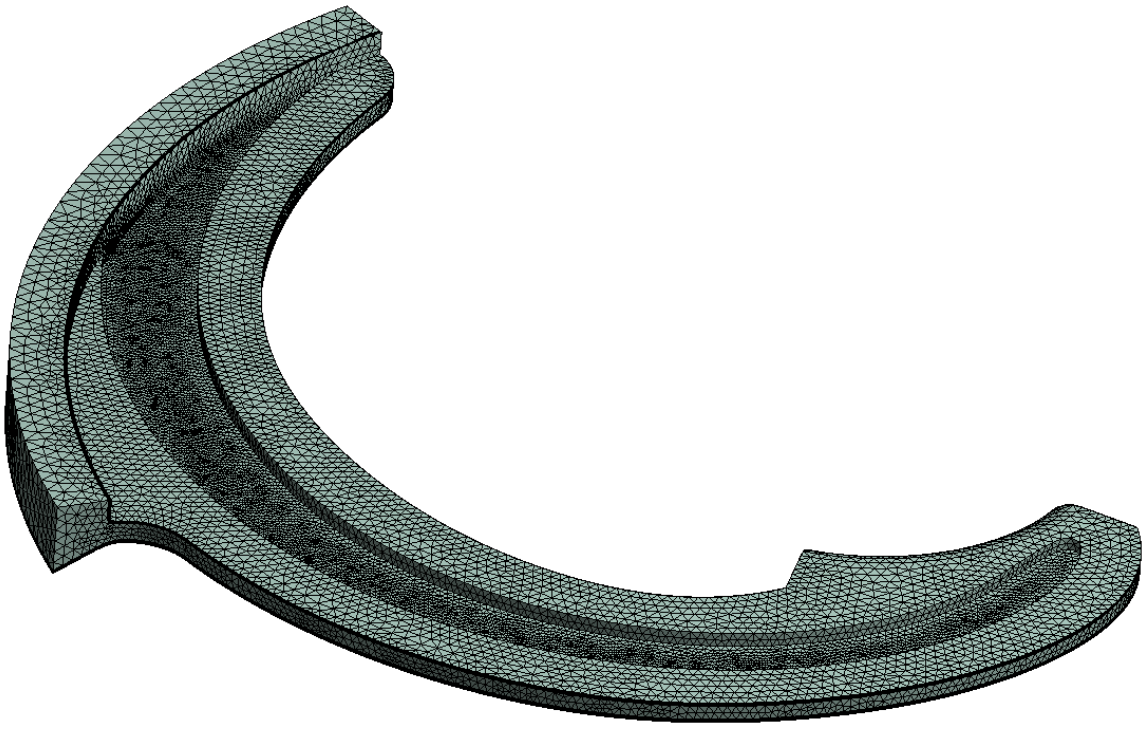

Figure 3.18. Lower sidewall mesh

Shape

Unstructured elements were used for all components of the pump. As mentioned above, structured components can be very good if the flow direction is known. The flow will more or less follow the contours of the blade. Therefore, a structured mesh was examined first and it was found to be very difficult to generate. This had a lot to do with the shape of the vane passages being quite wide to handle slurry. It was also determined that unstructured meshes would be more appropriate after running initial simulations. Especially when simulations at flow rates away from BEP were run, the flow often did not follow the contours of the blades which makes an unstructured mesh seem more appropriate. As for the volute, the shape is not appropriate for a structured mesh. There were many examples in literature where unstructured meshes were used for centrifugal pump simulation. Furthermore, [5] stated that unstructured meshes will provide better convergence than structured ones in centrifugal pumps.

Inflation

In CFD analyses, it is necessary to put inflation layers at all wall boundaries. Inflation refers to increasingly smaller, narrower elements near to the walls as illustrated in Figure 3.19.

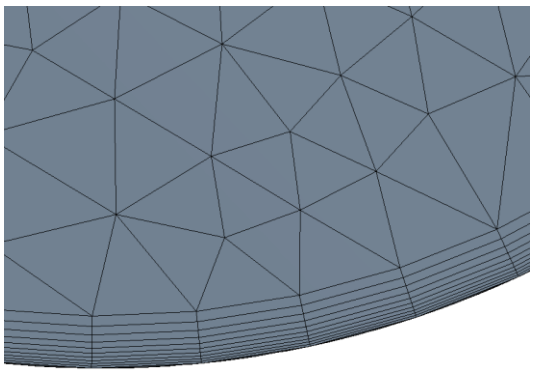

Figure 3.19. Inflation layers

From basic fluid dynamics knowledge, the velocity of a moving fluid right at a wall boundary will be 0 with respect to the wall. Moving away from the wall, the velocity of the fluid will increase non-linearly. This velocity profile is referred to as the boundary layer and is very important in a CFD analysis. The most intuitive way to capture this boundary layer is to ensure that there are sufficient mesh elements of a small enough size to

accurately define it. This can add significant cost to the simulation. Instead of fully resolving the boundary layer, a number of empirical wall functions have been developed that can help determine the boundary layer flow and thus reduce the number of inflation layers required [53]. Figure 3.20 shows an example of how this works. The curved line in the figure is the boundary layer velocity profile. The arrow labelled y is the distance away from the wall. As the boundary layer gets farther from the wall, the velocity increases as shown by the magnitude of u.

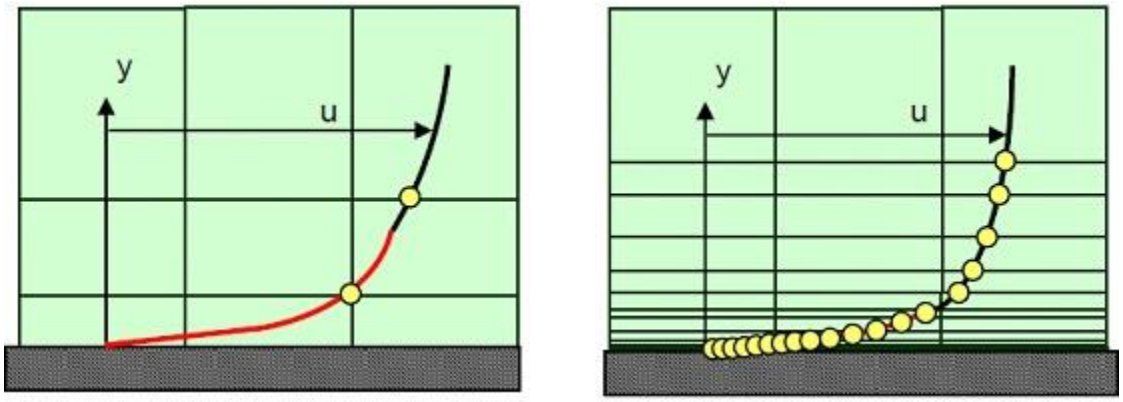

(a) (b)

Figure 3.20. Boundary layer defined (a) with and (b) without the use of wall functions [53]

The number of inflation layers depends heavily on the turbulence model used. Shear Stress Transport (SST) was the chosen turbulence model which will be described in more detail in Section 3.2.5: CFD Setup. With SST, a minimum of 10 inflation layers is strongly recommended [54]. One of the easiest ways to define the inflation size is by defining the thickness of the first layer at the wall. To determine that, there is a non-dimensional distance term, y^+, which describes the distance from the wall to the first node based on the velocity in the cell. The value of y^+ should be within a certain range. When using a wall function, a recommended range was $20 < y^+ < 100$. While y^+ was not commonly mentioned in most literature, several sources used values within that range [55].

The inflation settings used for the pump mesh are outlined in Table 3.3. The inflation in Figure 3.19 uses those settings. The growth rate refers to how much each

layer grows compared to the previous one. Each layer will be approximately 1.2x thicker than the previous layer. The lower sidewall has one exception to the inflation settings as it has only five inflation layers. Since the lower sidewall is a small and narrow part, there is less room for all the inflation layers plus it would make the mesh count very large and make the simulation take too long. Again, the reason for using a mesh that may be less accurate was justified by the fact that the flow in the lower sidewall region is not very important to the present analysis.

Table 3.3. Inflation settings

Setting	Value
First Layer Thickness	0.08 mm
Number of Layers	10
Growth Rate	1.2

Since y^+ is based on the cell velocity, it cannot be easily estimated before simulation, especially in a pump flow where the velocity will be very different everywhere throughout the pump. While initial estimates can be made, the best way is to simply run a simulation and then obtain y^+ results from CFX and adjust the mesh accordingly. These y^+ results can be viewed graphically to see exactly what the value is on all the walls. This can be helpful to determine where the mesh may need refining. The average and maximum y^+ can also be reported.

As it will be discussed in more detail in Section 3.2.5: CFD Setup, the walls of all parts of the pumps were assigned a roughness value to more closely represent the true case. Roughness was specified by an equivalent sand-grain roughness of 0.26 mm. This adds complication since the roughness scale is larger than the thickness of the first inflation layer of 0.08 mm. However, there was very little discussion of how to deal with this in any ANSYS documentation or other literature. It is not something that appears to have been used or researched much. With a rough wall, single vane simulations revealed average dimensionless y^+ values of around 130 and a maximum of above 200 which are outside the desired target range. Following a sensitivity analysis approach, the mesh was refined to have smaller elements and the inflation was changed to have a first layer thickness of 0.05 mm with 12 layers. This yielded almost no change in the values.

Since y^+ is expected to change as inflation changes, the same simulations were run again with no roughness, that is, the walls were smooth. With the original mesh, the average y^+ was found to be about 45 with a maximum of 110 at only a few limited locations. With the more refined mesh, the average and maximum were only 28 and 55. This shows that roughness definitely affects the y^+ values but that the y^+ value is probably as good as possible with roughness turned on. This was further tested with coarser inflation as well. The results are summarized in Figure 3.21. It is clear that even as the mesh coarsens beyond 0.08 mm, the y^+ values hardly change for the rough wall setting until a much coarser mesh is used (0.2 mm). On the other hand, y^+ appears to change almost linearly with the first layer thickness when the walls are smooth.

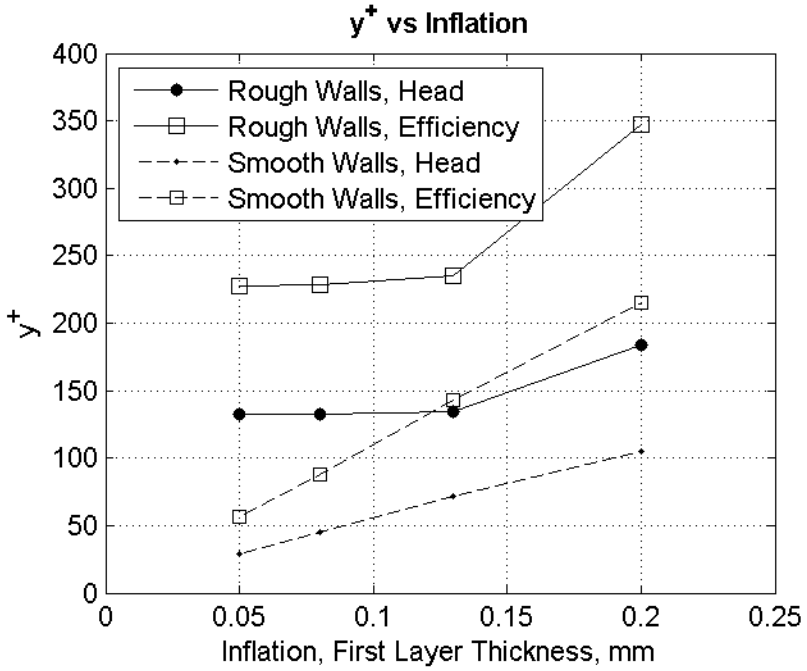

Figure 3.21. y^+ vs inflation plot

An assumption here is made that inflation layers yielding y^+ values that satisfy the desired range in a smooth wall simulation will also be sufficient with a rough wall condition. The initial mesh yielding a maximum of y^+ value of 110 was chosen especially to keep the simulation cost low since the average was well within the desired range.

Another simple but not conclusive way to examine the inflation layers is to simply look at a velocity plot of the results and see if the boundary layer appears to be defined.

Figure 3.22 shows velocity plots with the wall being at the top of the figure. Figure 3.22 (a) shows a coarser mesh and (b) shows a finer mesh (the one used in all simulations). It is clear that in the finer mesh, the velocity boundary layer curve can be seen near the wall. This provides additional confirmation that the inflation is at least minimally enough.

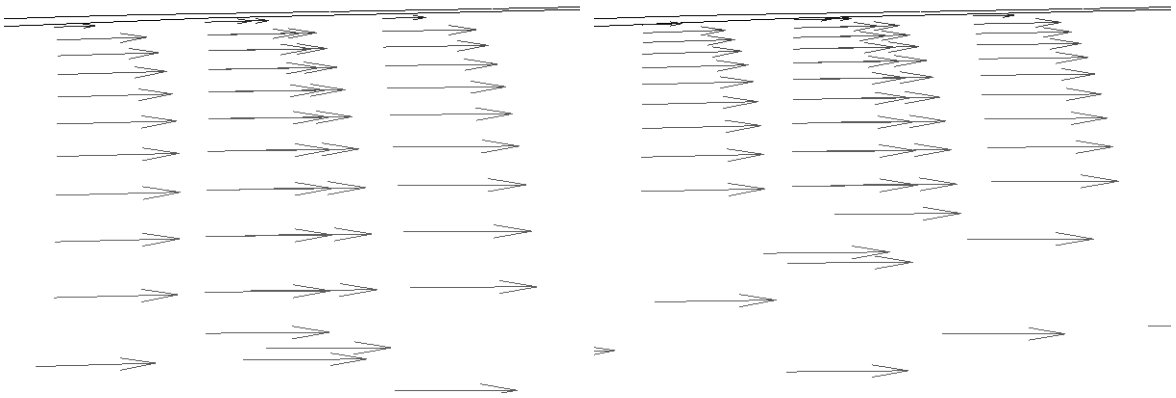

(a) (b)

Figure 3.22. Velocity plots near the wall with (a) a coarse mesh and (b) a finer mesh

Meshing Summary

Using all the above mesh settings, the final mesh count for each part of the pump is shown in Table 3.4. Note that the total mesh count includes three impeller sections and five lower sidewall sections. Figure 3.23 shows the impeller mesh. Figures of the mesh for other parts can be found in the Appendix.

Table 3.4. Mesh count

Part	Node Count	Element Count
Impeller	426,518	1,168,681
Volute	403,237	1,151,729
Lower Sidewall	90,515	234,735
Total	2,135,366	5,831,447

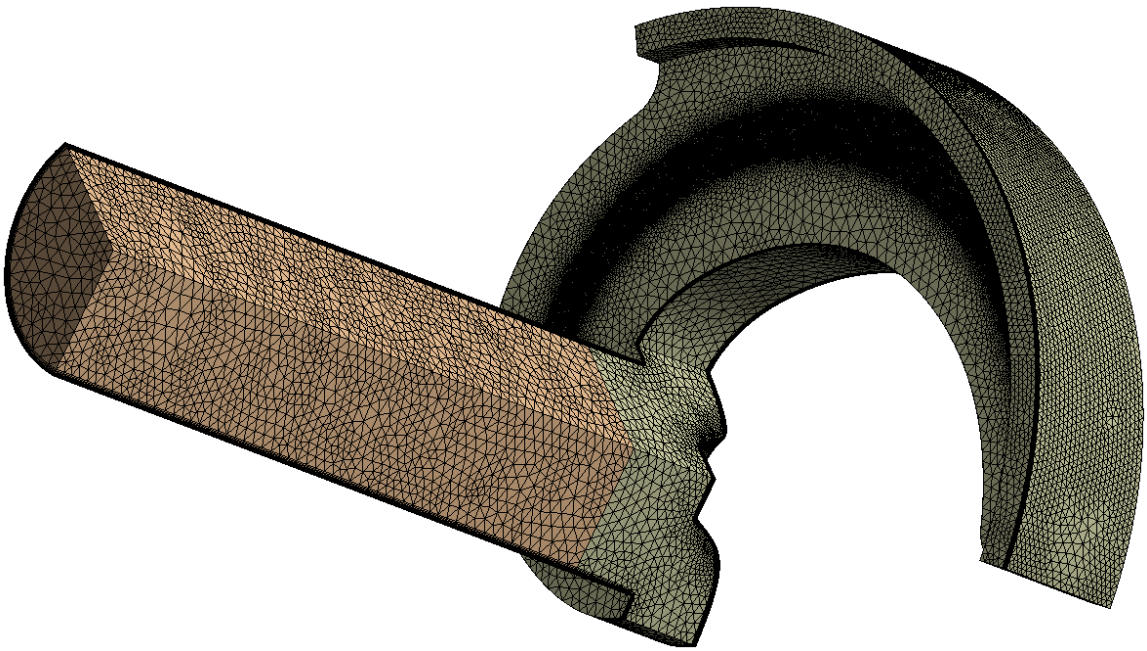

Figure 3.23. Impeller mesh

The single vane mesh is very similar to the impeller mesh shown in Figure 3.23, it just has the geometry changes mentioned in Section 3.2.3: Geometry. The mesh count for it is slightly lower, since the volute sections were simply trimmed. The node and element count is 389,478 and 1,050,095, respectively.

3.2.5. CFD Setup

The CFD setup step is where all remaining preparation occurs before running a simulation. While not necessarily the most difficult and time-consuming part of the CFD methodology, the CFD setup is the most complicated part since there are many things to consider and many settings that the user can define. Additionally, many of the settings need to be tuned which involves some degree of trial and error. CFD setup is completed in ANSYS CFX-Pre. As previously mentioned, for a full model simulation, the impeller and lower sidewall gap fluid geometries are first multiplied in CFX-Pre to once again form the full geometry. The model is shown in Figure 3.24 with the arrows representing the boundary conditions which are described later.

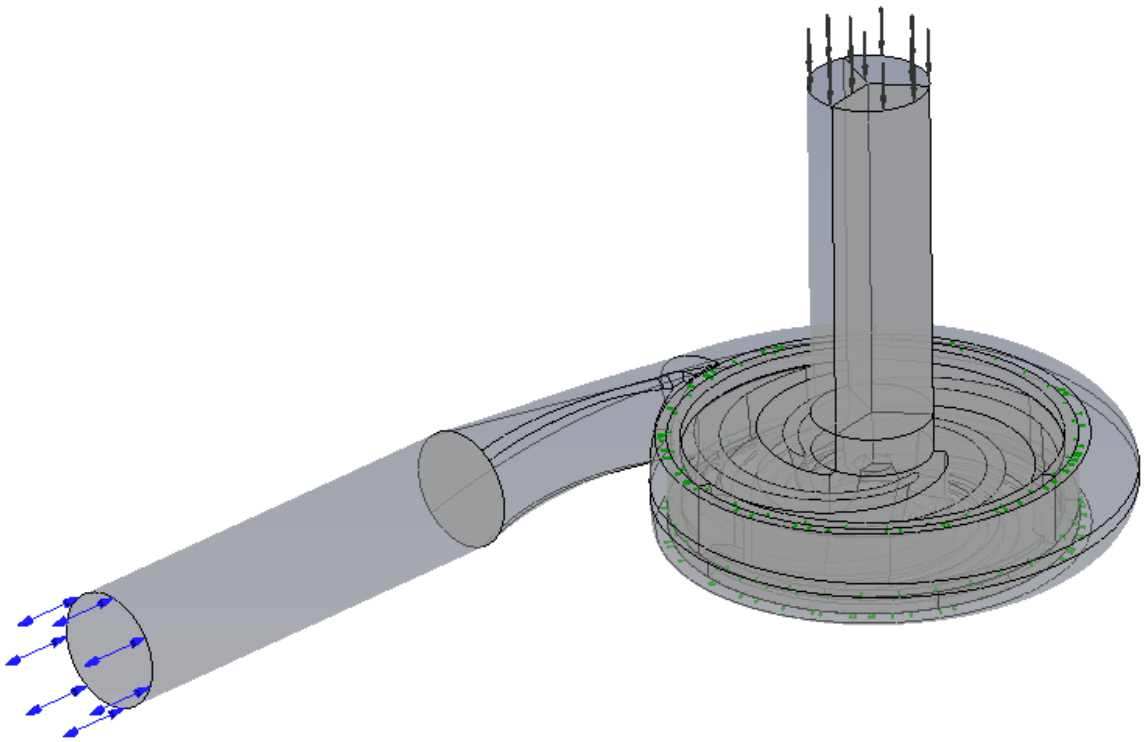

Figure 3.24. Full simulation geometry in ANSYS CFX-Pre

Table 3.5 provides a summary of all the CFD parameter settings which will be described in detail in the following sections. Some settings are different for the single vane and full model analyses since the simulations are steady state and transient, respectively.

Fluid

The fluid specified for all tests considered for research is water. While the pumps being tested are designed to handle slurry, they are tested in-house at Toyo Pumps in a water tank according to published standard and thus all available data for validation is generated from water tests. No data has been measured when pumping slurry. Furthermore, if a new impeller based on the recommendations in this thesis were to be constructed, it would also be tested in water. It is possible to simulate slurry, however it can be a difficult task and not very accurate. Slurry composition can be very random since it may have a wide variety of shapes and sizes of solid materials and the properties of the carrying fluid itself can vary. Therefore, a simulation would be a fairly ideal situation and only specific to a certain application. Nevertheless, it would still have

the benefit of giving a prediction of what might occur in a slurry flow. Based on previous studies, it is known that head and efficiency will both decrease with slurry compared to water. The magnitude of performance reduction depends on a number of factors including the solid concentration and physical properties of the solids, most notably their size, density and size distribution [11,43].

Table 3.5. Summary of CFD parameters

Parameter		Setting/Value
Fluid		Water
Fluid Properties		• Standard water properties at 25°C • Incompressible
Analysis Type	Single vane	Frozen rotor (steady state)
	Full model	Transient
Boundary Conditions	Inlet	• Mass flow rate • User-defined variable
	Outlet	• Total relative pressure = 0 • Direction = normal to the boundary
	Walls	Rotating or stationary with roughness
Wall sand-grain roughness		0.26 mm
Turbulence model		Shear Stress Transport
Convergence residual target	Single vane	10^{-5}
	Full model	10^{-4}
Timescale (single vane)		$10/\omega$
Timestep (full model)		3° of impeller rotation / timestep
Simulation time (full model)		3 rotations minimum

The properties of the water used are the standard properties at 25°C. The fluid is considered incompressible, therefore the density is constant throughout. Additionally, since this is not a thermodynamic study, the temperature of the water is constant.

Analysis Type

There are two major analysis types for CFD, based on the time dependency of the flow characteristics. Steady state is a common analysis type which is meant for flows that will achieve a steady state solution after a certain point in time [54]. Pipe flows are a

common example of a steady state simulation. When considering a rotating reference frame such as in turbomachinery, if a steady state simulation is performed, it will obviously not show the rotation but will rather give a snapshot of the flow at a certain position. A snapshot can be useful when the overall characteristics of the flow are important and the focus is not on interaction between stationary and rotating parts. Steady state analysis is often useful in symmetrical applications such as many compressors, turbines or air pumps. In one study of a multistage centrifugal pump which was much different from the one presented in this thesis, the flow was studied through two stages in the middle of the pump which were radially symmetrical as it can be seen in Figure 3.25. A steady state analysis was performed and the results compared well to physical tests performed on the same pump [19].

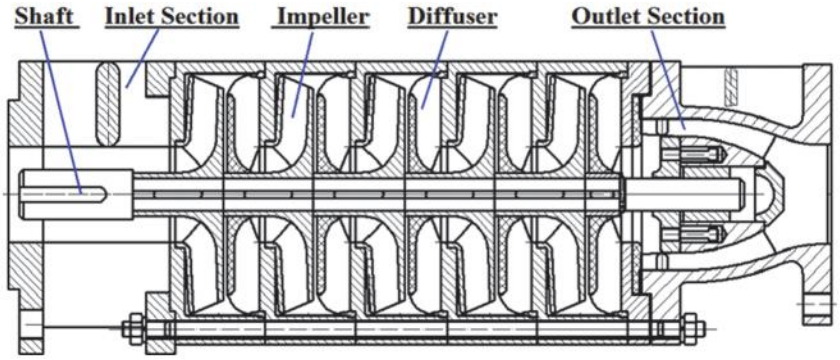

Figure 3.25. Cross-section of multistage pump [19]

Transient simulations are meant for flows that exhibit time-dependent behavior. That is, they do not reach a steady state solution. Examples of situations where a transient simulation would be appropriate would be a study of the start-up of a turbomachine or a study of a flow that has periodic properties. Transient simulations are much more complex and computationally expensive since they require real time information. A time range must be specified over which many sub-simulations will be performed at discrete points of time, referred to as timesteps. Each sub-simulation is similar to a steady state simulation and there will be several iterations to reach the solution at that timestep [54]. A transient analysis is useful for simulations such as the one presented in this thesis where the simulation domain is not symmetrical which causes periodic behaviour in the results. As it is stated in one study of a centrifugal pump during start-up, the main advantage of transient analyses are “that the computations are fully dynamic, closer to reality, and capable of capturing the

instantaneous impeller-volute interactions" [24]. With a transient simulation, every sub-simulation must converge, but the overall transient results must also converge. In a situation like with a centrifugal slurry pump, periodic oscillations in results such as the efficiency will occur with the period being based on the number of blades. That is, if there are three blades, one period will be one-third of an impeller revolution. These periodic oscillations will show a global trend as multiple periods occur and it is important that these converge.

For the study of Toyo's centrifugal slurry pump, the analysis type used depends on whether the full model or single vane model is being simulated. Part of what makes the single vane model so much easier and cheaper to simulate is that it can be analysed in steady state since it only consists of one domain - the rotating impeller. Transient will provide no advantage in this situation. When considering the full model, transient is required to obtain accurate results because of the interaction of the impeller and volute. Initially, steady state analyses were investigated in hopes that steady state would be sufficient for predicting pump performance. However, it was quickly found that results either did not converge at all or, if they did, they were not accurate when compared to physical tests. Running a transient simulation solved these problems and thus is required for a high-fidelity analysis. However, while steady state simulations require a few hours at the most on an average PC, transient analyses take much longer due to simulating over a time range, often up to around 24 hours. Therefore, it is highly recommended to begin with a steady state simulation and then use the steady state results as a starting point for the transient analysis to speed up the time to convergence [54].

Boundary Conditions

Boundary conditions are properties or conditions that must be applied to all surfaces of a domain before simulation. The main boundary conditions are: inlets, outlets, walls and symmetry planes.

Inlet and Outlet

There are many options for exactly how to define inlet and outlet boundary conditions. The ANSYS CFX Reference Guide recommends specifying a total pressure

value at the inlet and a mass flow rate (amount of fluid by mass that flows per unit time) at the outlet [54]. Total pressure includes pressure and momentum. These are common settings used in literature. However, several other sources recommended defining a mass flow rate at the inlet and then only a static pressure, not total pressure, at the outlet. With a mass flow inlet or outlet, the flow direction must be set. At an outlet, the flow direction is not necessarily known whereas at the inlet, the flow is likely simply going in at a direction normal to the boundary. Therefore, setting a pressure outlet is more accurate since the direction will not be falsely specified. Furthermore, when calculating single-phase flows, an inlet pressure is often not specified but it is recommended when calculating cavitation phenomena. Since cavitation is not considered nor expected to be present for these tests, a pressure inlet is not required [1] The mass flow rate is a value that can be set by the user depending on the flow rate desired for testing. Since generation of a pump curve requires tests at varying flow rates, this value will be changed regularly. However, the majority of tests are carried out at the pump's BEP flow rate which was determined through physical and simulated tests. The flow direction was assigned to be normal to the boundary conditions which is straight into the inlet pipe.

To set a pressure outlet, there are two options available: an outlet or an opening. An outlet is intuitively a boundary condition where the flow is mainly flowing out of the domain. An opening, on the other hand, is a boundary condition where flow may be going in or out of the domain [54]. An outlet was used initially on pump tests. However, during simulation, a message was often displayed that a wall was placed at portions of the outlet to prevent flow from re-entering the domain. This indicated that there was recirculation occurring at the inlet. Since it would be more physically accurate to not limit this recirculation and because placing the walls there slowed down the simulation, an opening boundary condition was tried.

For the opening, there are three appropriate pressure options that can be set: (1) opening pressure and direction; (2) static pressure and direction; and (3) entrainment. For the first two, a direction of the majority of the flow must be supplied. The difference between them is that opening pressure calculates the pressure based on total pressure when flow is entering the domain and static pressure when it is leaving the domain whereas static pressure calculates pressure based on static pressure for both directions.

Opening pressure is stated to be more robust and stable. The entrainment option is very similar to the previous two, having both static and opening pressure options available except that the flow direction is not set and will be fully calculated. The static pressure option will define the velocity gradient perpendicular to the opening boundary to be zero and the opening pressure option will have the solver calculate the flow direction based on the velocity field. The opening pressure entrainment option is again the more robust of the two [54]. Entrainment is the most mathematically correct which is sensible especially because of the fact that the flow direction will be calculated, which is more accurate than just setting a direction when it is not necessarily known. However, this option can be more difficult to solve. Therefore, the opening pressure and direction (not entrainment) was chosen since it is sufficient for this situation. The pressure value is simply a relative pressure and was set to zero atmospheres. The pressure value is not too important. Since the inlet is set as a mass flow input and no pressure is specified, the pressure through the domain will be calculated with respect to the outlet pressure set. Pressure would matter more if the flow was being defined by a pressure differential. In this case, important results such as efficiency and head are calculated based on the pressure difference between the inlet and outlet. Therefore, even if another value was set, the differential would still end up being the same. The flow direction was set to be normal to the boundary since the majority of the flow is expected to flow out in the direction parallel to the pipe.

For the single vane outlet, an opening is specified for the same reasoning as above. In this case, entrainment with an opening pressure is used with the relative pressure set to zero. Since the single vane analysis is much cheaper than the full model analysis, entrainment will not add much more cost and will, theoretically, produce more mathematically correct results. Additionally, the direction will definitely be more complicated since it will be flowing out radially, not in a direction normal to the boundary. Therefore, it is even more important to allow the direction to be calculated.

Walls

Other than the inlet and outlet, all other physical domain boundaries of the pump fluid model are walls or domain interfaces. Any boundaries that were cut for separating the domains or cutting out a single vane will be defined as domain interfaces, described

in the following section. Walls are simply a boundary to flow, defining a solid surface that fluid cannot flow through. Walls, by default, are stationary with respect to the domain they are in. Thus, if walls are defined in a rotating domain, they are, by default, stationary to an observer in the domain (that is, the observer is rotating with the domain), but are actually rotating walls in the global stationary domain. Walls can also be assigned a velocity if desired. There are several friction conditions that can be set for the walls, the most common one being a no slip wall. This is based on fluid flow theory and assumes that the fluid immediately adjacent to the wall has a velocity of zero with respect to the wall. If the wall is moving at a certain velocity, the fluid will move at the same velocity, still having a relative velocity of zero. As for the surface finish of the wall, the default is to assume it is perfectly smooth. A roughness can be provided which is detailed in the Wall Roughness section of this chapter.

The rotating domain consists of the rotating impeller walls and the walls of the volute on the top and bottom which are not rotating. All walls that are part of the impeller which includes the blades, hub and expeller vanes in the lower sidewall gap, are assigned as default, no slip walls. For the non-rotating walls in the rotating domain, there is a simple option to define the wall velocity as counter-rotating. In the rotating frame of reference, this simply ‘rotates’ the wall in the opposite direction of the defined rotation, making it a stationary wall in the global stationary frame. Care must be taken when using this setting since the wall must be a surface of revolution. A surface of revolution is simply a surface that can be created by rotating a two dimensional curve about an axis. This is the case on all the stationary walls of the impeller section. For the volute, it is a stationary domain and all walls are stationary, so the default no-slip wall is simply applied to those walls.

In the single vane model, the impeller walls are set to be the same except for the new walls created where the volute section was sliced off as shown in Figure 3.15. Since these new walls are not technically walls, setting them as either a rotating or stationary wall would not necessarily be correct. An option initially considered was to simply set them as an opening. A better and simpler setting recommended was to specify the boundaries as free slip walls. Free slip walls have a shear stress of zero at the walls which basically means that the wall will have no influence on the velocity [54]. It will just

constrain the flow from going through it. The velocity of the fluid at the wall will not necessarily be zero in this case.

Domain Interface

A domain interface is the connection between two separate domains or meshes. For turbomachinery simulation consisting of rotating and stationary components, a domain interface must be setup to handle this. The full and single vane models will have completely different domain interfaces since the full model involves a rotating and stationary domain whereas the single vane model only has a rotating domain, but requires symmetrical interfaces.

For the full pump model, the only domain interfacing that is required is between the three separately meshed parts. The impeller and lower sidewall sections which both rotate must be connected together and then those must be connected to the volute. Both of these interfaces use the General Connection model in ANSYS CFX. This interface is very powerful and is meant to support non-matching grids, which is the case with the pump mesh, and transient, sliding interfaces between the domains. The interface requires specification of one of three frame change or mixing models which are frozen rotor, stage or transient rotor-stator. It is also possible to set no frame change model if there is no motion between the domains [54].

For the interface between the impeller and lower sidewall, since they are both rotating, there just needs to be a simple connection defined between the two to match up the different meshes. There will be no motion between the two, so no frame change model is required. It is just a simple general connection.

The impeller and lower sidewall both need to have an interface to the volute. This interface requires a frame change model since it is the interface between the rotating and stationary domain. This is where one of the three models must be chosen which depends on the geometry, the resulting flow, and the required accuracy. The frozen rotor and stage models can both be used for steady state analyses. The frozen rotor model truly provides a snapshot of results as discussed in the Analysis Type section. Frozen rotor fixes the orientation of the domains and only changes the frame of reference

between them. For a centrifugal pump, it will simply simulate the flow through the impeller as rotating, then simulate it exiting the impeller and entering the stationary volute at the pre-defined orientation. No transient effects will be modeled. Frozen rotor is commonly used in many studies on centrifugal pumps and other turbomachines. The stage interface does not assume a fixed position of the domains but rather circumferentially averages the variables through the interface. It still does not take transient interaction effects into account. Furthermore, it is not recommended when the flow depends heavily on the orientation of the domains with respect to each other nor when testing at flow rates away from BEP. The transient rotor-stator is the only model that works for a full transient solution since it moves the rotating components at each timestep, taking into account all interaction effects. Both the stage and transient rotor-stator models recommend starting from a frozen rotor simulation. As for the computational cost, the frozen rotor model is the cheapest of the three, followed by the stage model. The transient rotor-stator model is much more expensive in terms of time, computational effort and required disk space [54].

The frozen rotor interface was initially used to test the centrifugal pumps studied since it is the easiest and results can be used as a starting point for using the other models. The frozen rotor model was able to converge and generate results near BEP. However, results did not match well with physical tests. Additionally, at flow rates away from BEP, results often did not converge. The stage model was tried next, however, it was found to be fairly difficult to setup and a number of problems were experienced including problems with results diverging instead of converging. The stage method can commonly be difficult to setup and is not very mathematically correct compared to using a transient model. Therefore, it was highly recommended to try a transient simulation since they are not hard to setup, and are just expensive. They will also almost always give the most accurate and true results. Thus, the transient rotor-stator model was used for all full model tests with the frozen rotor model only being used to generate steady state results to use as a starting point for a transient simulation.

For the single vane model, a domain interface must be specified on the sides of the geometry where the impeller fluid model was cut to form one blade. These sides are highlighted in Figure 3.26 and are not walls. The appropriate interface model for these

types of boundaries is a rotational periodicity interface. This is meant especially for cases like this where only one blade of an impeller is simulated. The interface simply assigns the boundaries to be symmetrical about the defined axis which is the axis of rotation at the centre of the impeller.

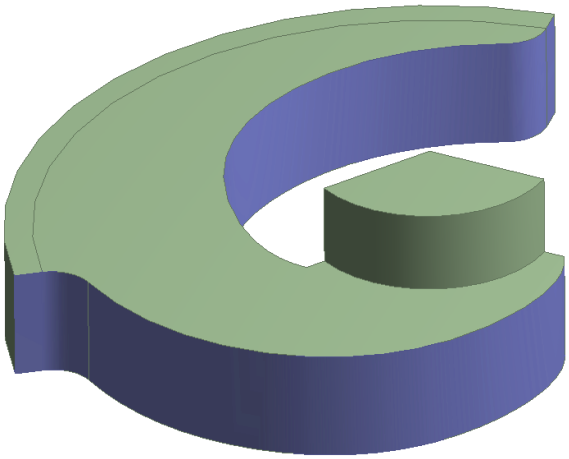

Figure 3.26. Single vane model with symmetry sides highlighted

Wall Roughness

In order to model the physical pump as accurately as possible, all walls were specified to be rough. Wall roughness increases a wall's shear stress and changes the velocity profile near the wall. Roughness is defined by the equivalent sand-grain roughness which is not the same as the measured roughness. Roughness consists of random peaks and valleys of different shapes and sizes. This would be very difficult and expensive to model. Equivalent sand-grain roughness is defined as small spheres along the wall where the numerical value defines the height of the spheres as shown in Figure 3.27 [50].

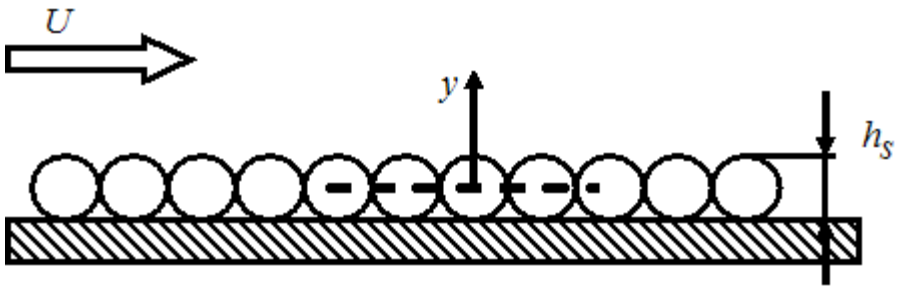

Figure 3.27. Equivalent sand-grain roughness [50]

Toyo's pump is made of cast iron and is not polished. Determining sand-grain roughness is historically performed experimentally. However, there are equations to estimate the sand-grain roughness based on the actual measured surface roughness which are outlined and discussed in works by Adams *et al*. and Elger *et al.* [56,57]. Elger *et al*. actually provide equivalent sand-grain roughness values for several different materials including cast iron which has a value of 0.26 mm [57]. In the end, the roughness will depend on the roughness of the manufactured pump which would be difficult to measure and calculate. Therefore, equivalent sand-grain roughness is often a value that cannot be predicted accurately and must sometimes be adjusted for validation if it is proven that the simulation is otherwise accurate. For this pump, the roughness value turned out to provide good correlation to physical data.

Turbulence Modelling

Turbulence models are mathematical models that are used to predict turbulence effects in a fluid flow. They are based on the Reynolds Averaged Navier-Stokes (RANS) equations and describe the distribution of Reynolds stresses throughout the fluid domain [1,54]. Turbulence models are empirical and were developed to correlate as closely as possible with specific physical tests. Out of the many models available, some are intended for very specific applications while others can be used on a variety of applications. There is no turbulence model that is necessarily the best for all applications. It is therefore very important to carefully select the turbulence model and, if at all possible, validate it by comparing CFD and physical results.

Only three turbulence models will be discussed here: k-ε, k-ω and Shear Stress Transport. They are the three most appropriate, common and recommended models for centrifugal pumps and most other turbomachines. ANSYS specifically recommends using either the k-ε or Shear Stress Transport (SST) turbulence model for liquid pumps and turbines [51]. Furthermore, these two models seem to be almost the only models used in most literature on centrifugal pump simulation. All turbulence models in ANSYS CFX use advanced wall functions to simulate the flow near walls, meaning a y^+ of one or less is not required to fully capture the boundary layer [54].

k-ε Model

The k-ε turbulence model is one of the most preferred turbulence models used in CFD and is considered the industry standard. Through extensive testing, it has been proven to be very stable and numerically robust. It can be used in a wide variety of applications as it generally has a good compromise between accuracy and robustness [54]. As the name indicates, the model is considered a two-equation model since it uses two transport equations to calculate turbulence parameters in the flow. The k represents turbulence kinetic energy which is the variance of fluctuations in the velocity. The ε represents turbulence eddy dissipation which is the rate at which velocity fluctuations dissipate [50].

The k-ε turbulence model has several drawbacks. It is unsuitable for flows with boundary layer separation, flows in rotating fluids, flows over curved surfaces and decelerated flows. All of these occur in centrifugal pumps. However, k-ε is still commonly used and recommended for use in turbomachinery because results converge better using it compared to other turbulence models. This is especially because k-ε describes the core flow away from the walls quite accurately. It was also one of the first two-equation models used in the industry, therefore it has been extensively validated [1].

k-ω Model

The k-ω turbulence model is another two-equation model which was developed especially to improve the k-ε turbulence model. The ω represents the specific dissipation which determines the scale of the turbulence or frequency of relatively large vortices [1,58]. It was developed to better simulate flows against strong pressure gradients, which can be encountered in diffusers, and to capture the flow near the walls more accurately than k-ε although k-ε is still better at capturing the core flow [1,50]. This model appears to be used much less commonly in centrifugal pumps.

SST Model

Shear Stress Transport is a more recent model developed by Florian Menter and is based on the k-ω model. It blends the core flow advantages of the k-ε model with the near-wall flow advantages of the k-ω model [1,59]. It is becoming increasingly common

in the industry and considered by some to be the new industrial standard that should be used by default in most applications [60]. It has also been validated in many studies. Being based on the k-ω model, it similarly performs well in flows against strong pressure gradients. It is also known to be very good at predicting flow separation [54].

SST still has a few weaknesses although it still remains superior to the previous two methods in most applications. One weakness is that it can sometimes produce slightly high turbulence levels in regions that experience high normal strain which may occur in stagnation regions or regions with high acceleration. This effect is much less pronounced than in the k-ε model [61]. Another weakness is that flows on curved paths are still not simulated well [1]. To address this, ANSYS CFX has a curvature correction option available for two-equation models used in such flows. It modifies the turbulence production term to make the models more sensitive to curved or rotating effects [50,54].

Selected Turbulence Model

Based on the discussion of the three turbulence models studied, it is fairly clear that SST is likely the best model to choose for this type of application. Since it basically combines the benefits of the k-ε and k-ω models, there is not much to lose in this situation. SST was thus the final chosen model used for all simulations, both on the single vane and full models. The curvature correction feature was always used.

Initially, the k-ε model was used as early research showed that it was clearly the most common turbulence model used in the past. It appeared to yield fairly good results and no major problems were encountered. However, as research was furthered, more was learned about the SST model and the decision was made to switch to it. It is also fairly common for use in turbomachinery applications although still not historically used as extensively as k-ε. A sensitivity analysis, detailed in Section 4.3: Sensitivity Analysis, was performed on the turbulence model in order to examine the difference between the results with k-ε and SST. It is good practice to check that results are not significantly different as that may show higher uncertainty in the results. In the end, results such as efficiency and head measurements were quite similar with only small, consistent differences. This illustrates a higher degree of certainty in the results and helps prove the suitability of the SST model. One study performed a comparison of numerous

different turbulence models including the three mentioned here on a centrifugal pump. It was concluded that the turbulence model did not have significant effects on results such as head and efficiency. SST was also found to be good at predicting flow separation at off-design conditions [22]. In another study, it was found that SST was the most suitable turbulence model for simulations over a large range of operating conditions, similar to the tests being performed for this thesis [62].

Solution Setup

The solution setup involves setting all other necessary parameters for the solver. These include convergence control and criteria and time information for the transient simulation.

Convergence and Residuals

First, it is important to explain how convergence is determined. As a solution iterates, results will change at each iteration when the solver first begins solving. Over time, the solution should, theoretically, change less with more iterations until a point has been reached where the solution changes by a small enough amount that the solution can be assumed to have reached a converged, steady state solution. The default and most important measures of convergence are the residuals or local imbalances of the Navier-Stokes equations in each control volume. The residuals directly describe whether the equations have been solved. CFX presents residuals normalized by the Root Mean Square (RMS) and the maximum residuals for judging convergence. CFX will use the RMS residuals to determine convergence by default, but the maximum residuals can also be used. Most simulations should require about 50 to 100 iterations to converge. While this process is what happens in a steady state simulation, it is basically the same for a transient simulation, but just occurs many times. Each timestep or sub-simulation in a transient analysis must iterate to a converged solution in the exact same way, as determined by the residuals. By choosing a correct timestep, results will not change significantly between each timestep and usually well under 10 iterations should be required. The only difference in a transient simulation is that the equations for the residuals will also include a contribution from the transient term [54].

Convergence will be determined to have been reached when the residuals reach a specified residual target as set by the user. At that point, the simulation will be terminated. The default target RMS residual value is 10^{-4}, meaning the change in all residuals must be less than 10^{-4}. The target residual should be chosen based on the required accuracy of the simulation. ANSYS CFX documentation gives recommendations as shown in Table 3.6 [54].

Table 3.6. RMS Residual Target Accuracy

RMS Residual Target	Results
$<10^{-4}$	• Not generally recommended for accurate results • May be enough to show qualitative flow field results
10^{-4}	• Relatively loose convergence • May be sufficient for engineering applications
10^{-5}	• Good convergence level • Sufficient for most engineering applications
10^{-6}	• Very tight convergence and typically not possible to reach • Sometimes required for geometrically sensitive problems

Maximum residuals are typically about 10 times larger than RMS residuals, therefore the same guidelines should be applied but the target should be 10 times larger. It is clear that 10^{-5} is generally a good target to set for the type of study presented here. It is confirmed in other sources such as [1]. If convergence is determined by the RMS residuals, it is good practice for the user to check maximum residuals. In the case where maximum residuals are much larger than 10 times the RMS residual, there is a good chance that those high residuals are only isolated to a small area of a flow where there is probably an unstable flow situation. The locations of high residuals can be plotted to confirm this. As long as this is the case where there are only a few very high residuals, it can often be assumed that the area probably does not affect the overall results prediction. However, this should be verified by checking other results such as efficiency in a pump application to ensure it seems stable and converged [54]. Additionally, an even better practice would be to refine the mesh at those points and run the simulation again. If the maximum residuals are reduced there, that shows the mesh was too coarse to generate an accurate solution there. However, if important results remain the same,

this likely proves the assumption that the results are not sensitive to the isolated high residuals. Thus, the original mesh could continue to be used to keep costs lower [1].

While convergence can be determined based on a target residual, it is extremely important for the user to carefully judge the convergence based on more than just the residual values. First of all, it is good practice to perform sensitivity analysis on the residual target. After obtaining a solution with a tighter convergence criteria, results should be compared to ensure if there is little change. Results such as head, efficiency and a visual check of the velocity profile would be good to check in a centrifugal pump. This might also reveal that a lower residual target is acceptable to use which can reduce computational and time costs. Furthermore, it is possible to define monitor points in a simulation run which will display the convergence of user defined values. CFX is not capable of automatically checking the convergence of these results, but the user should view them and calculate the residuals manually, if needed. Since head and efficiency of the pump are the most important results considered in this study, they are ideal monitor points [54].

For transient simulations, the target residual will function the same as in steady state simulations and its value should generally remain the same [54]. However, the difference will be noticed in analyzing other results and monitor points. Since a transient solution is generally used to show unsteady results, results will obviously be expected to change at every timestep. Therefore, when looking at monitors points of head and efficiency, they will not appear to converge and level off over time. Rather, they should show periodic oscillations over time. These oscillations will be what will converge. That is, the oscillations should become steady such that each period has a very similar average value and shape. Visual results such as velocity profiles should behave the same and show consistent but periodic results over time. This illustrates why it is important to run transient simulations long enough to see that they are steady over at least one rotation which would consist of several periods. Generally, for turbomachinery, the maximum number of revolutions required should be about five to eight [1].

Timescale Control

The timescale is a setting for steady state solutions which is basically a “false timestep” that is used for calculating the equations as they are iterated to a final solution. By default CFX uses automatic timescale control which calculates the timescale based on the current case. While it is robust, it is often conservative and faster convergence can be obtained through manually adjusting the timescale. The solver is very robust and can generally handle a large timescale. However, if the timescale is too large, residual convergence plots can show somewhat oscillatory behaviour rather than a more or less constant decrease. If this is observed, the timescale should be reduced by a suggested factor of four. If the timescale is too small, convergence will be very slow or, as it was observed in some centrifugal pump tests, convergence may not occur at all. For pumps as well as other turbomachines, a very common timestep recommendation is to start in the range of $0.1/\omega$ to $1/\omega$ where ω is the angular velocity of the impeller in radians/second [54]. This is derived from the recommendation that a timescale is calculated from length scale divided by a velocity scale. The outer radius of an impeller is a typical length scale and the impeller tip speed (radius multiplied by ω) is a typical length scale. Dividing them yields $1/\omega$. A timestep in the given range may not always be the most appropriate, but it is still recommended that the timescale be some factor of $1/\omega$ [1].

A maximum iteration limit can be set for the solver to automatically terminate the simulation if convergence is not achieved within that limit. The default setting is 100 iterations. When a simulation is complete, it is important to check why it stopped. If it stopped due to reaching the iteration limit, convergence may not have been reached. It may simply require further iterations although if results are oscillating, a change in the timescale may be necessary [54].

Timestep Control

Timestep control is used in transient simulations to control the time dependent behaviour of the solution by setting the physical time interval between each timestep and the total time duration or number of timesteps to run. It is possible to have changing time intervals but this is not usually practical for turbomachinery applications [54]. The total

time value should be chosen to allow for enough rotations to see steady, converged results. As for the timestep, the easiest way to define it is to define a time that allows for rotation of a certain number of degrees. That way, it is possible to easily define one rotation that starts and ends at exactly the same orientation. The timestep can depend a lot on the geometry of the pump. The smaller the timestep, the better resolution the results are. High resolution may be required with many blades since there should be a minimum number of timesteps between each blade passage of the volute. However, with fewer blades in slurry pumps, the timestep can be lower and still allow for quite a few timesteps between each blade passage. A recommended way to choose the timestep was to aim for a value that takes up to only three iterations to converge for each timestep. It is also important to ensure that plots of important results such as head and efficiency are well defined. Since they will be expected to have periodic oscillations, it is important to ensure the oscillations are clearly defined and are not 'spiky' which would be a good indication that higher resolution (smaller timesteps) may be required.

Selected Solution Setup

The selected solution setup is summarized in Table 3.7.

Table 3.7. Solution Setup Summary

Parameter	Steady State Value	Transient Value
RMS Residual Target	10^{-5}	10^{-4}
Timescale	$10/\omega$	N/A
Timestep	N/A	3°/timestep
Total Time	N/A	Depends heavily on situation Minimum: 3 rotations

For steady state solutions the RMS residual target of 10^{-5} was selected. For single vane simulations and for early attempts to simulate the full model in steady state, 10^{-4}, the default target, was initially used. It was commonly found that results were not actually converged when head and efficiency values were plotted with respect to the iteration. When the residual target was changed to 10^{-5}, it was observed that head and efficiency would almost always clearly level off. Setting an even tighter convergence criterion generally provided no added benefits. Important results including efficiency and

head were already well converged, plus the residuals would often level off before reaching 10^{-6}. Based on the literature, the maximum residuals were often used for determining convergence. Usually the maximum residual target was 10^{-4} or 10^{-3}. In [20], a maximum residual target of 10^{-4} is used and in [62], Braun used a target of 10^{-3}. Both showed good validation results. Using the assumption that maximum residuals are often 10 times the size of RMS residuals, this can show that an RMS residual target of 10^{-5} should be acceptable.

For transient analyses, an RMS residual target of 10^{-4} was selected. The reason for choosing the lower target was because it appeared to yield accurate, converged results when looking at the head and efficiency values over multiple rotations as well as examining the flow inside the pump over time. A simulation was run using 10^{-5} as the target which significantly increased the cost of simulations as expected. For the point tested, with a target of 10^{-4}, one revolution simulated in about 4.4 hours whereas with a target of 10^{-5}, one revolution simulated in about 9.4 hours. The lower target was found to be unnecessary here since there was a negligible change in results. Braun performed a transient analysis as well and used an RMS residual target of 10^{-4} which was found to be an appropriate compromise between cost and accuracy [62].

For single vane simulations, the timescale selected was $10/\omega$ based on many tests at a variety of timescales. The automatic timescale was originally used and was always observed to be at $0.1/\omega$. This timescale often yielded very slow convergence taking several hundred iterations or sometimes the residuals would not approach the target. Based on the recommendations, $1/\omega$ was tested and found to be suitable for the default geometry and most flow rates. Slow convergence was sometimes still observed. When more extensive testing was begun where geometry changes were made to the impeller, using a timescale of $1/\omega$ often did not obtain convergence. Increasing by a factor of 10 again, a timescale of $10/\omega$ was selected. It proved to be more robust and seemed to be able to achieve convergence in a wide variety of situations with varying flow rates and numerous geometry changes. It is not abnormal to use a larger timescale than recommended. For results that did converge with a timescale of $1/\omega$, when using $10/\omega$, results were very similar, further proving the suitability of using the higher value timescale. Generally, a maximum iteration limit was set to 200. Most tests converged

well within 100 iterations but 200 was used for the few tests that converged slower. For full model simulations, since the steady state simulation was only used for an initialization, the automatic timescale was used with a maximum iteration limit of 100.

The timestep used in transient analyses was selected to correspond to 3° of impeller rotation per timestep, calculated based on the rotational velocity of the impeller. One rotation consisted of 120 timesteps with 40 timesteps occurring between each blade passage. This timestep was chosen by trying several timesteps until one was found that took three or fewer iterations for each timestep to converge. With 3°/timestep, only two iterations were required for timesteps in the majority of situations. Using larger timesteps required more iterations, as expected, but also yielded less stable results. The efficiency and head plots did not look well defined, with sharp spikes appearing in the plots which made it hard to determine average head and efficiency values. A timestep corresponding to 1.5°/timestep was also tested which produced very similar results with negligible differences. In literature, there is a wide variety of timestep sizes used that are usually chosen based on the analysis of a number of trials. Most literature is based on clear liquid or air pumps that have a high number of blades, often six to ten. Therefore, the timestep is usually required to be much higher to achieve enough resolution for each blade passage. That being said, two studies concluded that a timestep allowing for 120 timesteps per revolution were sufficient for an unsteady centrifugal pump simulation [62,63].

3.2.6. Solution Strategy

Simulations were run on a single computer with the specifications shown in Table 3.8.

Table 3.8. Computer specifications

CPU	Intel Core i5-3450
# cores	4
Speed	3.10 GHz
Memory (RAM)	8 GB
System Type	64-bit

Simulations of the centrifugal slurry pump were run at a variety of flow rates ranging from zero flow (where there is still water in the pump) up to 162% of the physical BEP. Specific flow rates were chosen to correspond to flow rates that the physical pump would be tested at. Performing a transient analysis on the full model is the most important step to begin with to validate with physical results. The first simulation was a steady state test run on the model to generate a starting point for the first transient analysis. The flow rate simulated was the theoretically predicted BEP of the pump. This prediction was calculated based on the impeller design and does not necessarily correspond to the true, measured BEP. However, it is a good initial performance estimate in the design phase. Using the steady state results as a starting point, a transient analysis was run at this same flow rate. Transient results such as head and efficiency have oscillatory behaviour where each period is one-third of a rotation since there are three blades in the impeller. Plots of those values were examined for each simulation. If the oscillations appeared level, it was generally concluded that results had converged. The average was then calculated over each period to ensure the average was very similar over each of the last few converged periods. Finally, the average over the final one or two revolutions was taken.

Tests at the other flow rates were run, using the results of the next closest flow rate as the starting point. The average head and efficiency were recorded for each flow rate and then pump curves were plotted. For single vane simulations, the same method was used, but only steady state tests were run. Additionally, there was no averaging required since steady state simulations will simply converge to their final, steady value.

With the CFD methodology presented here, the full and single vane models are ready for simulations. The simulations will be used to generate results such as pump curves, pressure plots and velocity plots. Finally, the results need to be analyzed for their accuracy and, if possible, compared to physical tests for validation.

Chapter 4. Results Analysis and Validation

This chapter will present results from simulations run on both the full model and on the single vane model presented in Chapter 3: CFD Modeling. Results will be closely analyzed for their sensitivity to a number of input parameters to ensure the simulations are accurate. Validation will then be presented where simulation results will be compared to physical results to ensure the simulation is a good representation of the physical pump.

4.1. Full Model

Pump curves of head and efficiency generated by the simulation are shown in Figure 4.1. Note that this is the same plot that was shown in Section 3.1.2: Pump Performance. As explained in that section, the head, efficiency and flow rate at BEP of the physical results were used as reference values. All other measured values are displayed relative to the reference values. The simulated BEP is indicated in the graph by the circle. The theoretically predicted BEP, calculated from turbomachinery equations, was at the flow rate indicated by the square which is at 87.3% of the experimental BEP flow rate. Since this theoretical prediction is based on equations and is very ideal, the actual BEP is commonly different. However, the model should still be analyzed for sensitivity to the mesh and other settings to ensure results are accurate which will be explained in the following section.

Figure 4.2 shows monitor points for the simulation at the BEP. There are four revolutions shown in the figure with one revolution consisting of 120 timesteps. The first graph in Figure 4.2 displays the four residuals (it is not important to display which is which). Each timestep clearly converges to the target residual of 10^{-4}. The second and third graphs show the head and efficiency curves plotted with respect to the timestep, respectively. The dots joined by solid lines on the figures show the average for each

period. The straight dashed lines show the average over one revolution (three periods) which is the value plotted on the pump curve in Figure 4.1. Similar plots as these are generated for every simulation.

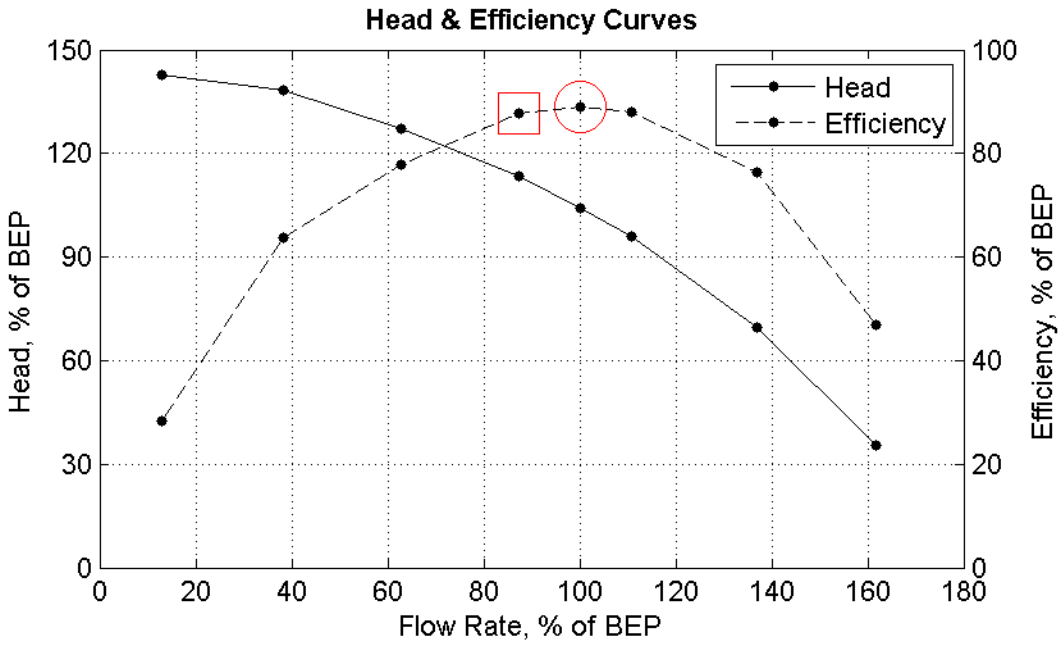

Figure 4.1. Pump performance curve data

Most of the tests required two to three revolutions for results to converge. Therefore, four revolutions were usually simulated in order to get at least one converged revolution of data. Most of the simulations only required two iterations for each timestep to converge. However, the simulations with flow rates far from BEP took more iterations since the flow is harder to predict. Figure 4.3 shows convergence details. The number of iterations per timestep is shown as well as the average time, in hours, required to simulate one revolution. If more iterations are required, the time to simulate is longer. Based on simulating four revolutions, the best total simulation time was about 21 hours on the PC used.

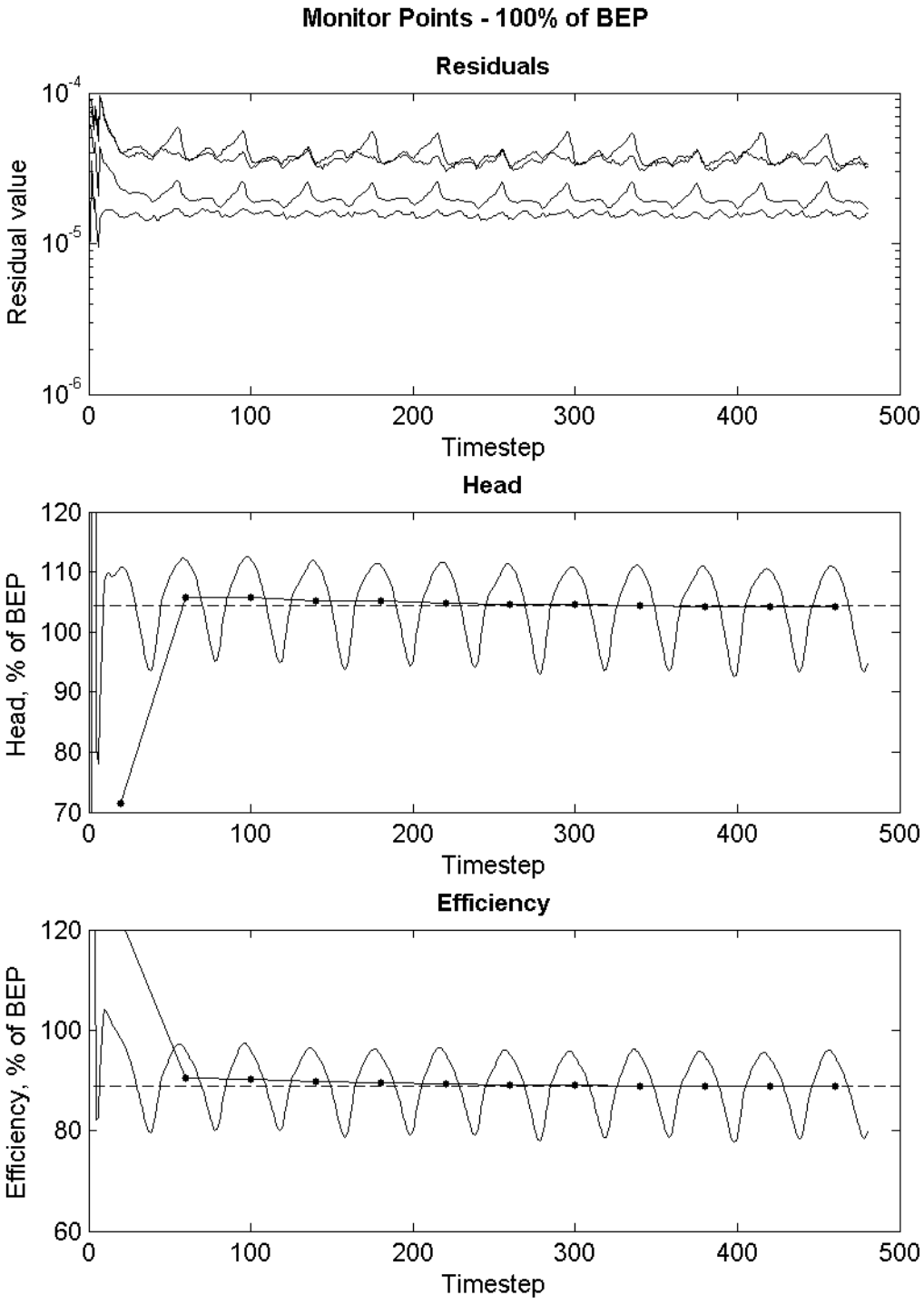

Figure 4.2. Monitors points at 100% of BEP

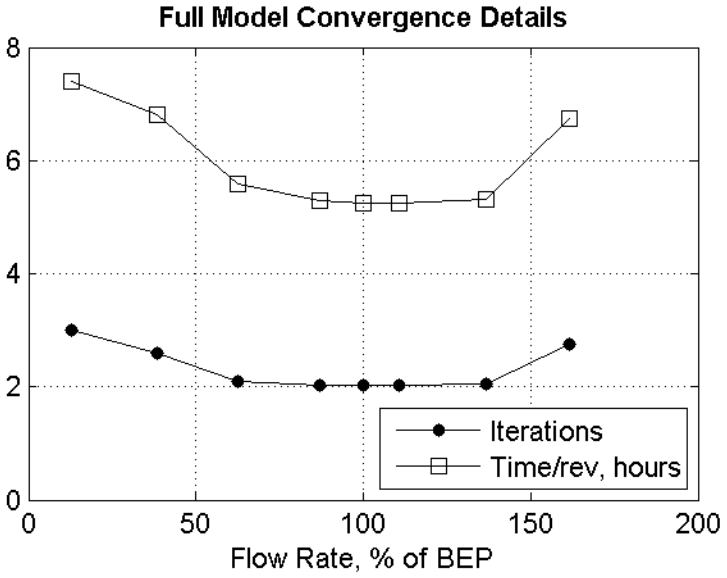

Figure 4.3. Full model convergence details

In addition to viewing numerical results, visual results were examined to observe their plausibility and validity. Pressure and velocity plots were mostly analyzed. Animations were also generated of the pressure and velocity over time as the impeller rotated. The time-dependent behaviour of the flow could then be observed to ensure the flow appeared to have converged, periodic oscillations as each blade passed the cutwater as opposed to flow that still seemed to be developing a periodic trend. Figure 4.4 shows pressure plots of the pump in a plane in the centre of the impeller at 87.3% of the experimental BEP. The plot in (b) is one half period (60°) later than the plot in (a) to show how the pressure varies over time as the impeller rotates. The main feature to look for in pressure plots is an increase in pressure from the centre of the impeller (closest to the inlet in these plots) to the outlet. The pressure clearly increases and the outlet pipe has the highest pressure as expected. Additionally, there is a clear increasing pressure gradient in the diffuser of the volute where the area increases from the volute to the outlet pipe. This pressure gradient is expected and these results prove that the diffuser functions exactly as it was designed for. Also expected is a high pressure region on the tip of the cutwater as well as along the edge of the volute to the right of the cutwater which is visible at location (i) in Figure 4.4 (a). Due to the position of the blade in (b), the pressure around the volute decreases. This shows a periodic pulsation exists inside the volute. In (b), there is a higher pressure located at location (ii) directly across from the

location of the high pressure in (a) at location (i). These two high pressure spots are expected to oscillate across from each other.

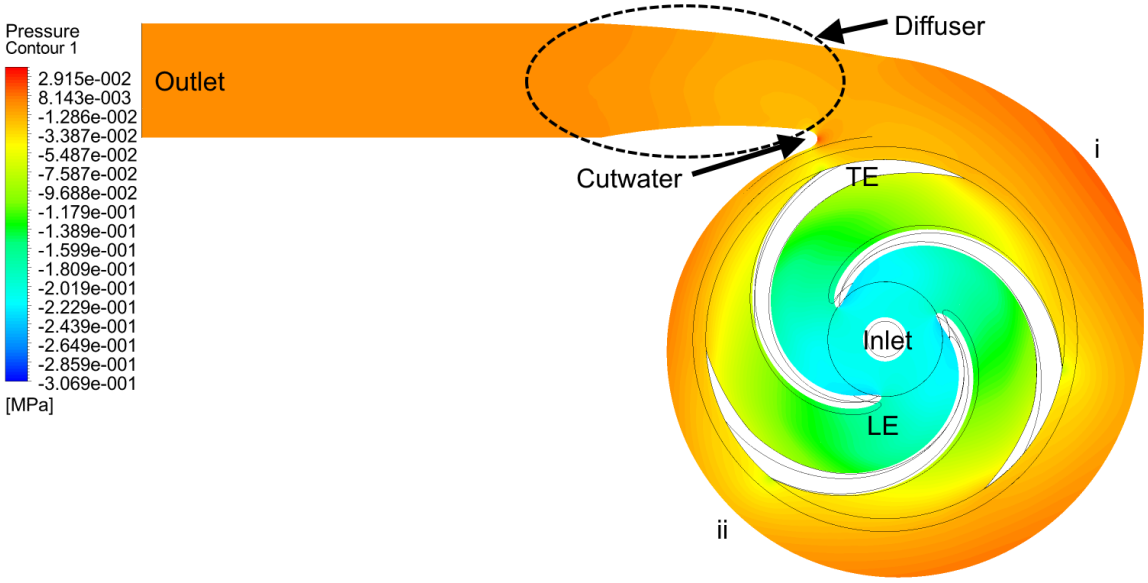

(a)

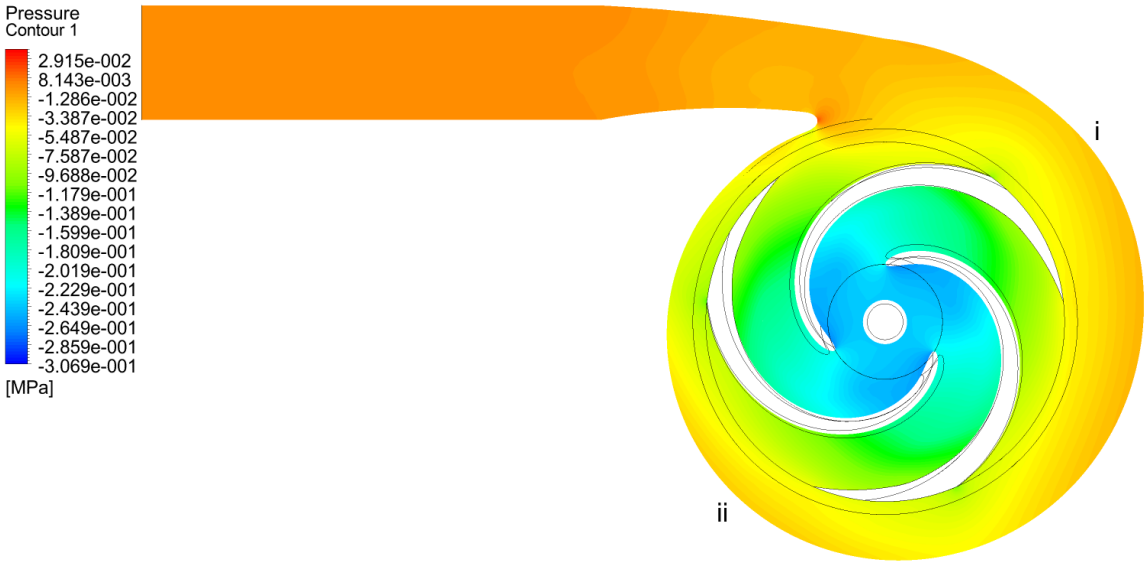

(b)

Figure 4.4. Pressure at 87.3% of BEP at two positions a half period apart

Figure 4.5 shows velocity plots at the same conditions. It is harder to display velocity since the arrows vary in size with many being quite small. It is necessary to zoom in and pan to clearly view velocity vectors. However, the figures show a general

trend and show where the maximum velocities tend to occur based on the darkness of the arrows. Inside the impeller, the vectors are shown with respect to the rotating frame. That is, they are displayed as they would be viewed from an observer rotating with the impeller. However, the frame of reference changes for the volute as the vectors are displayed in the stationary frame, therefore they appear to change direction between the reference frames but actually do not – only the reference frame changes. The highest velocities occur especially around the blade trailing edge, at a small area at the leading edges of the blades and around the cutwater. All of these are expected, especially at the cutwater since it is known to be a high wear location.

Figure 4.6 shows a zoomed in view of the velocity plot in Figure 4.5 (a). Here it is easier to see that the velocity vectors seem to be fairly closely following the contour of the vanes.

Results should also be examined at flow rates above and below the BEP to examine the changes that will occur when the pump operates away from BEP. Two simulated points were chosen to display here, one at a high flow rate of 137% and one at a low flow rate of 38.3%. Figure 4.7 and 4.8 show pressure and velocity plots, respectively, at a higher flow rate of 137% of the experimental BEP. This time, only one velocity plot is shown since it is less clear to observe much time-dependent behaviour in the velocity plots. At higher flow rates, the pressure plot changes to have relatively higher pressures inside the volute curved area, but a lower pressure in the outlet pipe. This makes sense since the head decreases as flow rate increases, thus a relatively lower pressure would be expected in the outlet. Correspondingly, the velocity is higher throughout the pump which follows Bernoulli's principle that as pressure decreases, velocity increases. The high pressure regions mentioned for the pump at BEP shift clockwise at higher flow rates, indicated by (i) and (ii). In Figure 4.7 (a), there is a very high pressure region close to the cutwater at location (ii) which corresponds to a high pressure region directly across from it that can be seen in (b) at location (i). These two locations of high pressure are expected. If pumps operate at high flow rates, the volute is known to wear extensively at those two high pressure locations, especially the one at location (ii).

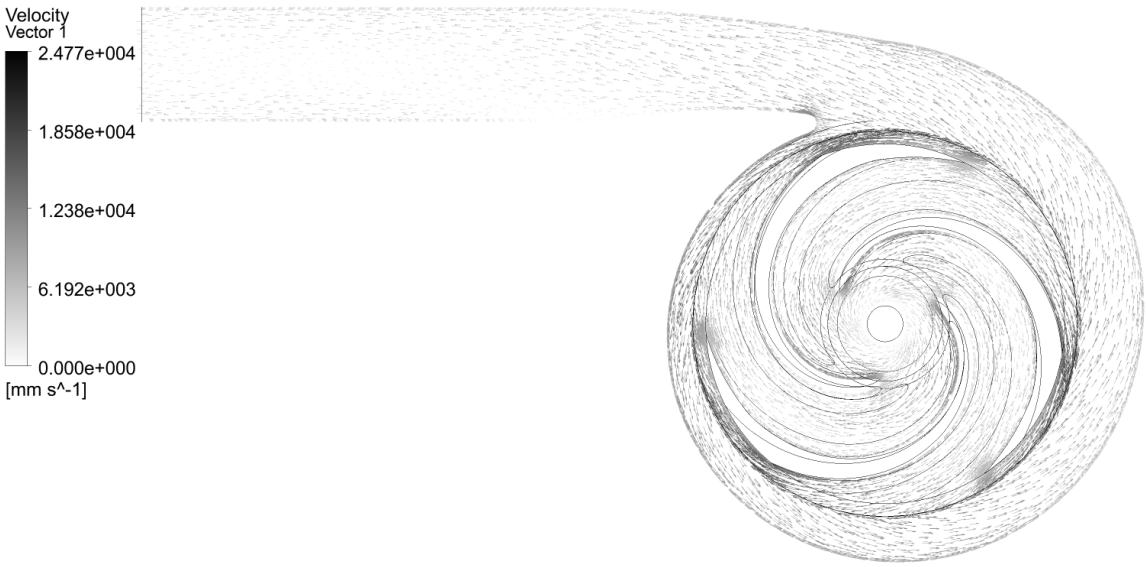

(a)

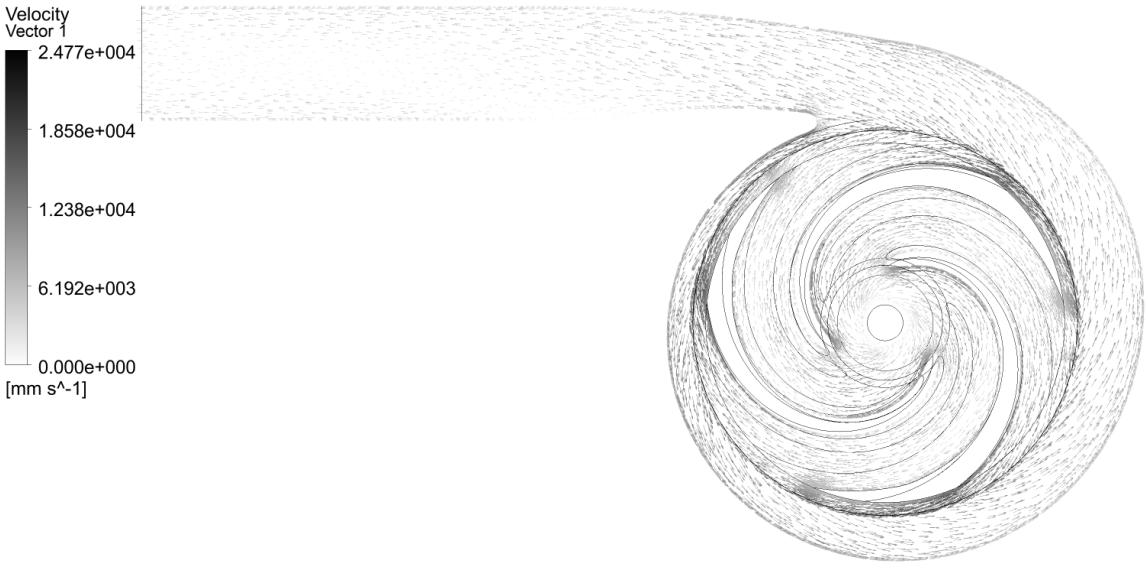

(b)

Figure 4.5. Velocity at 87.3% of BEP at two positions a half period apart

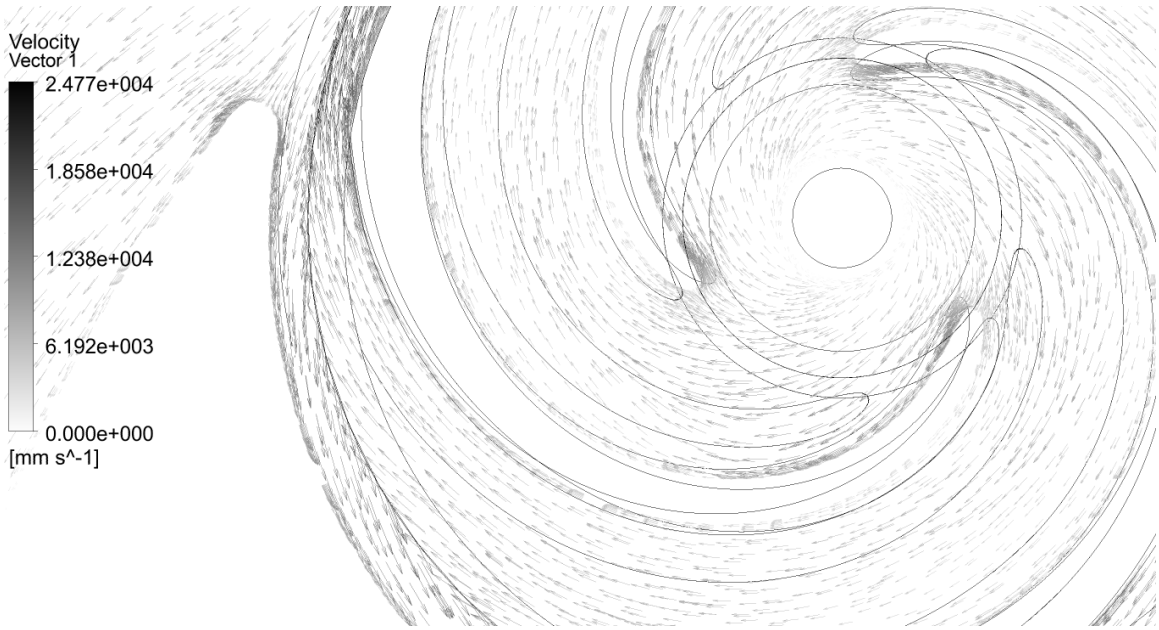

Figure 4.6. Velocity (zoomed) at 87.3% of BEP

Figure 4.9 and 4.10 show pressure and velocity plots at a low flow rate of 38.3% of the experimental BEP. At lower flow rates compared to high flow rates, the opposite characteristics are observed. The pressure is much higher in the outlet pipe, corresponding to the high head. However, the velocity is much lower. The high pressure regions are more similar to those observed in the BEP pressure plots, but they are located slightly counter-clockwise at locations (i) and (ii), as expected. Another prominent feature that is expected at lower flow rates especially is recirculation. Figure 4.11 shows a zoomed in velocity plot where recirculation can be found near the trailing edge of the blade around the left centre of the figure. Recirculation contributes to losses in the efficiency and increased wear. Note that the velocity scale is different in Figure 4.10 and Figure 4.11 because Figure 4.11 is showing velocity in the impeller only and thus the scale is based on the velocity extremes in the impeller.

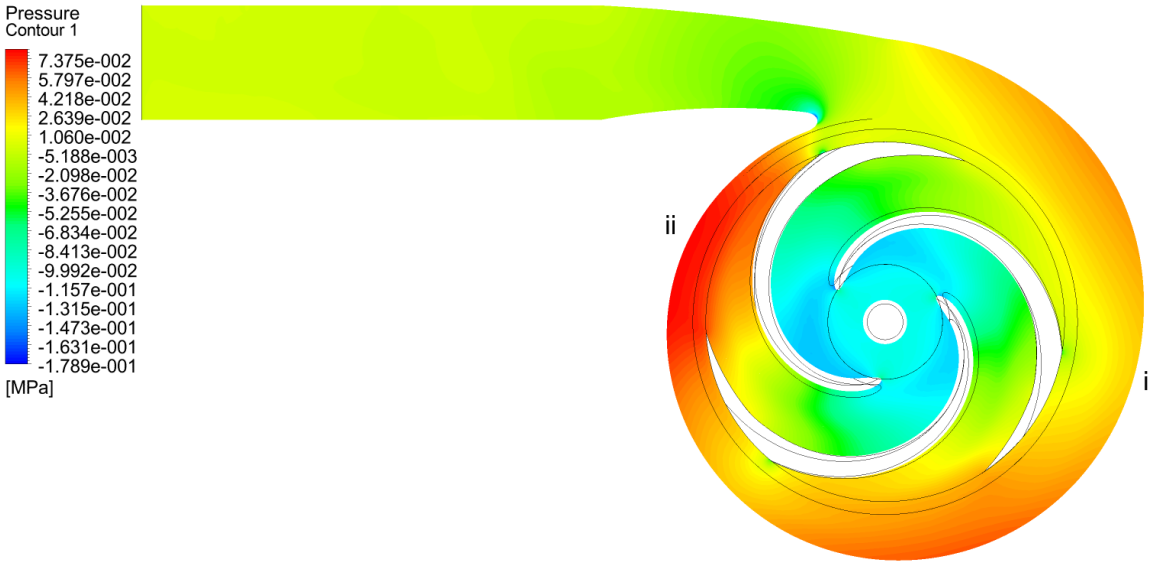

(a)

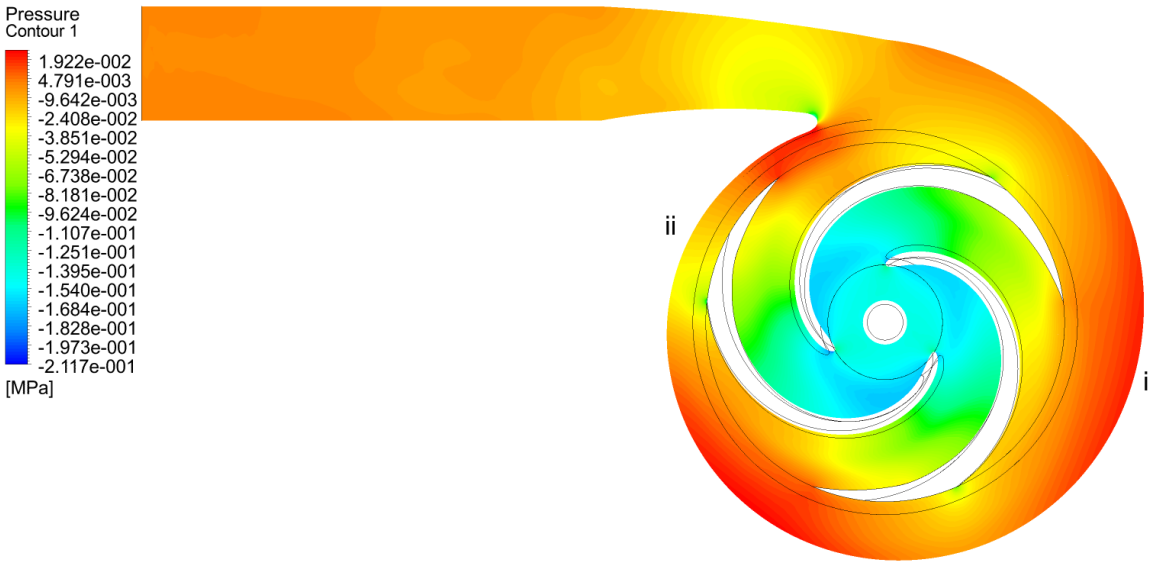

(b)

Figure 4.7. Pressure at 137% of BEP at two positions a half period apart

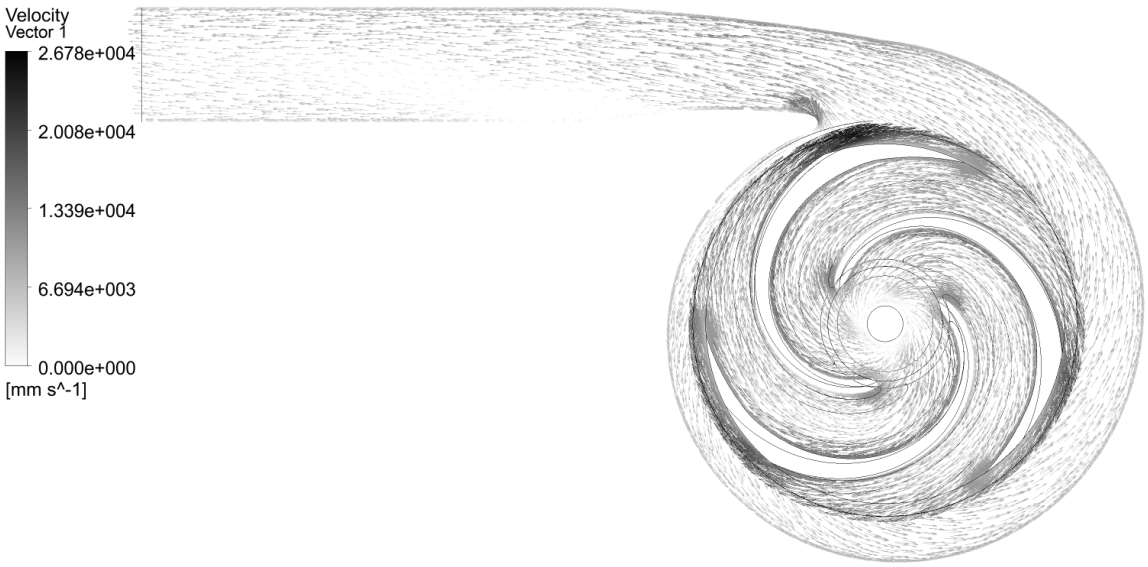

Figure 4.8. Velocity at 137% of BEP

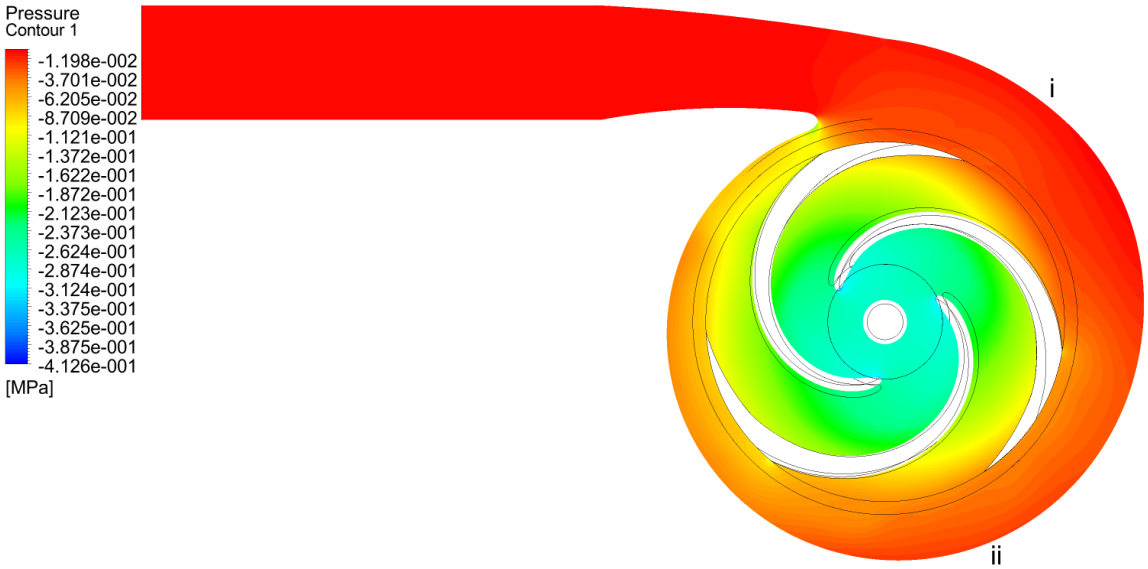

(a)

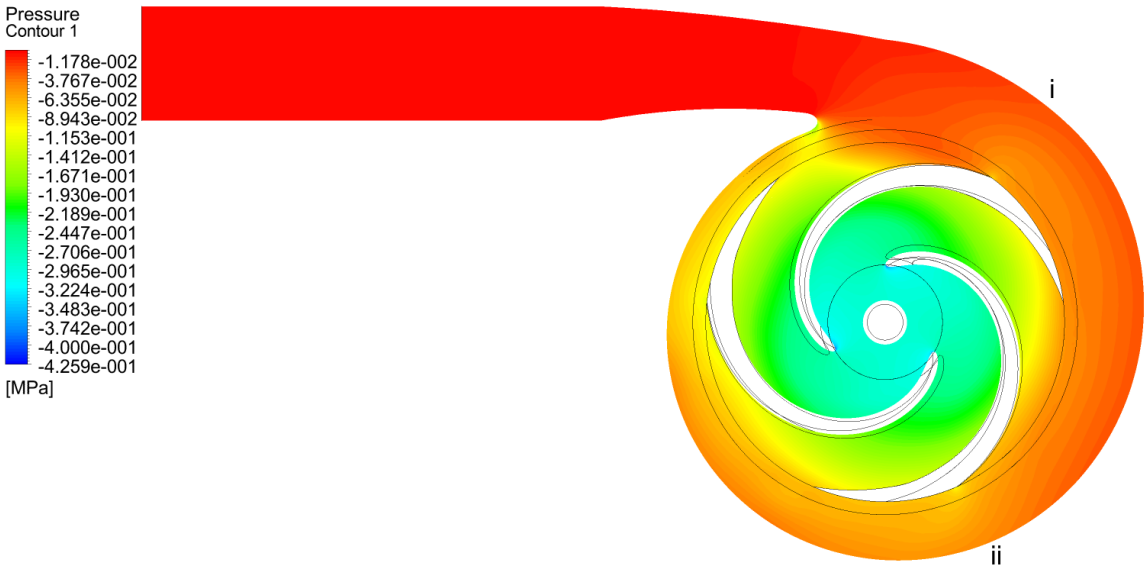

(b)

Figure 4.9. Pressure at 38.3% of BEP at two positions a half period apart

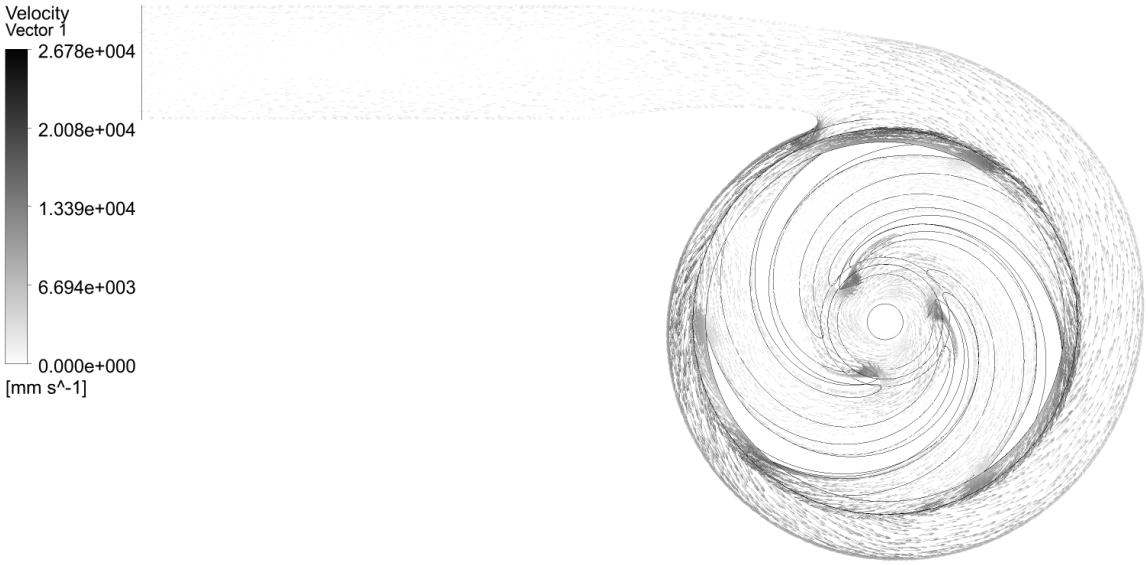

Figure 4.10. Velocity at 38.3% of BEP

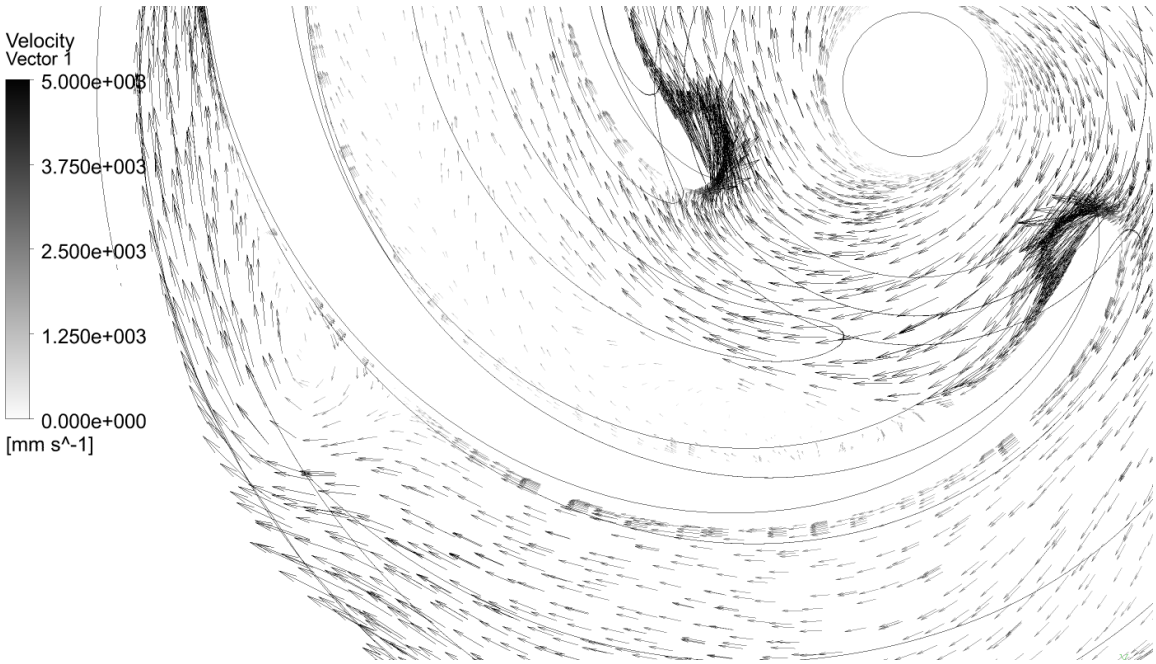

Figure 4.11. Zoomed in velocity plot at 38.3% of BEP

4.2. Single Vane Model

Simulations were run on the single vane model similarly to how they were run on the full model. Figure 4.12 shows the head and efficiency results from the single vane tests.

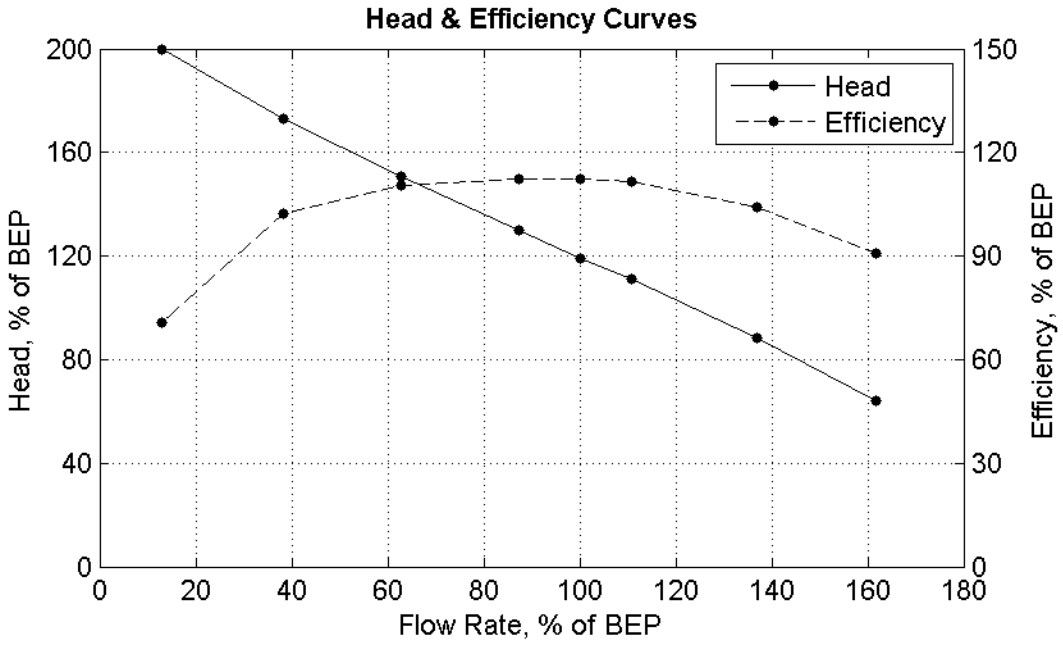

Figure 4.12. Single vane pump model performance curve data

Since the single vane model is simulated via a steady state simulation, there is no periodic oscillation of the results and results will simply approach their final converged value. Figure 4.13 shows the convergence plot of the residuals, head and efficiency at 87.3% of the experimental BEP. The residuals converged to their target of 10^{-5} within only 58 iterations. Head and efficiency constantly become flatter. While they both appear to be slightly increasing, the rate of increase is very small and any change from running the simulation longer will yield a negligible difference as was proven through several tests. Notice that when residuals reach 10^{-4}, the head and efficiency are still fairly far from their converged values, showing why it is necessary to use 10^{-5} as the target value for single vane steady state simulations.

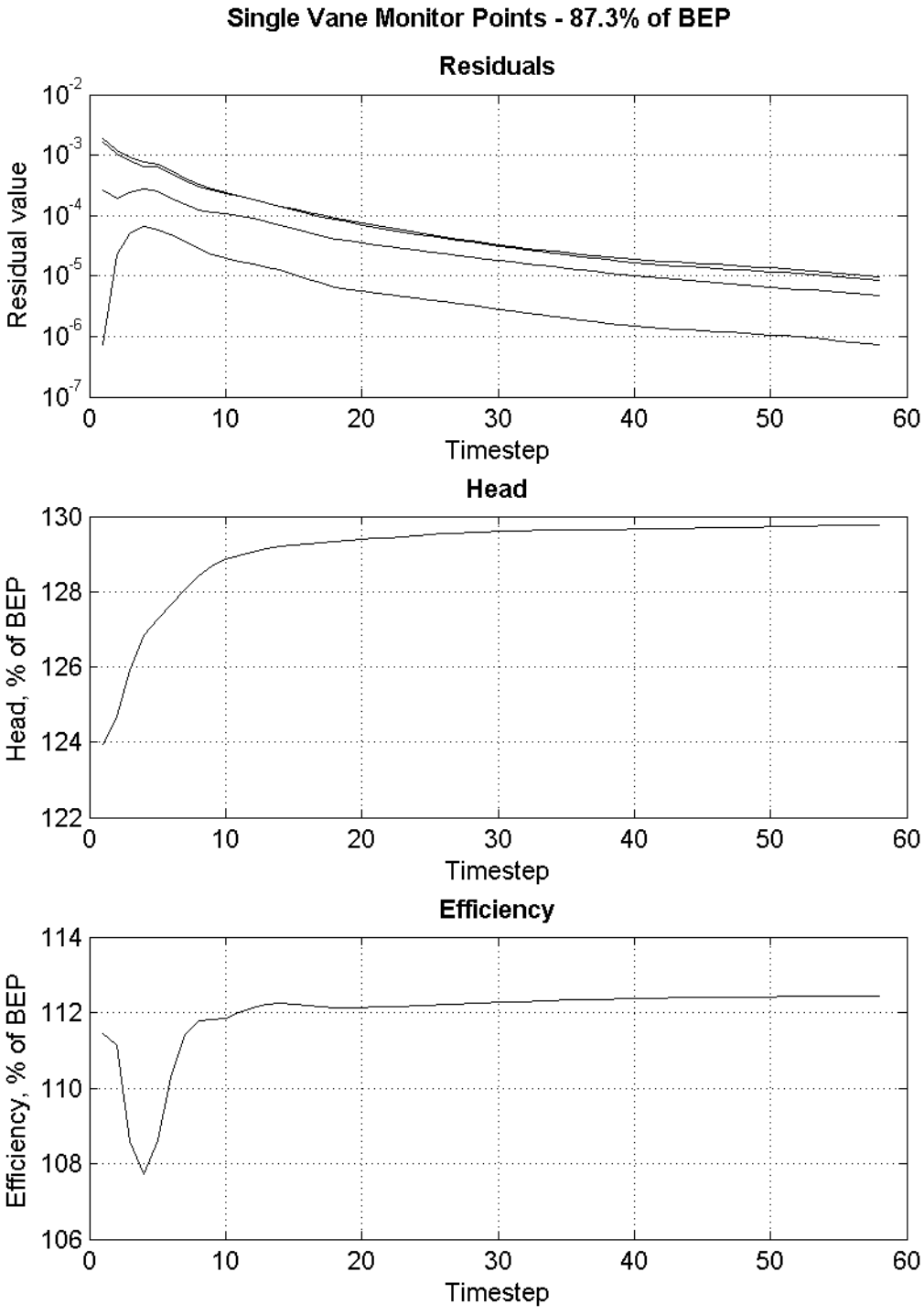

Figure 4.13. Single vane monitor points at 87.3% of BEP

Most simulations other than the extreme flow rates converged in an average of 56.6 iterations taking only 15.4 minutes on average. The extreme flow rates took longer to simulate since, similar to the full model, the flow is harder to predict and simulate.

The purpose of the single vane model was to analyse its similarity to the full model simulation to investigate if it could be used to predict the pump performance and be used for optimization through very fast, cheap tests. Figure 4.14 shows the performance curves of both the single vane and full models for comparison.

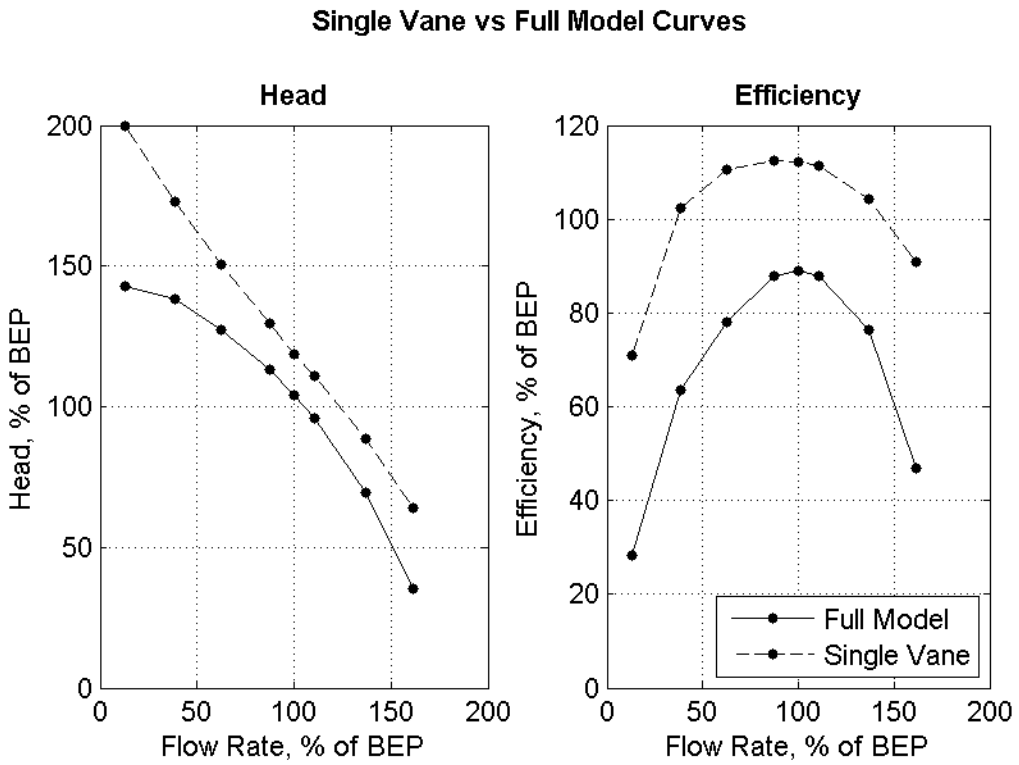

Figure 4.14. Comparison of full and single vane models

For both head and efficiency, the full model results are lower in value than the single vane model. This makes sense since, in the single vane model, there is no volute for further losses to occur. While the volute is necessary to direct the flow into a pipe, it will cause the head and efficiency to decrease compared to having no volute. The shape of the head curves definitely has some differences. The full model head curve decreases increasingly more as flow rate increases. However, on the single vane model, the head curve appears to have a fairly constant rate of decrease. This is likely due to the lack of a volute again. As for the efficiency, the curve shapes are actually quite similar. The BEP

is predicted in a different location, however. The single vane model predicted the BEP at 87.3% of the BEP predicted by the full model simulation, which is actually the theoretical BEP as discussed before. The BEP is a very important number for pump performance and, thus, the single vane model may not be accurate at predicting at what flow rate BEP will occur. However, it may still be useful for predicting general trends which will be further discussed in Section 5.2.1: Parameterization.

It is also good to compare the visual results of the single vane model to the full model. Figure 4.15 (a) shows the pressure in the single vane impeller at 87.3% of the experimental BEP. For easier visualisation, the vane was simply multiplied and rotated to display a full impeller. Figure 4.15 (b) shows the pressure in just the impeller of the full model for comparison. The numerical values of the pressure are different, however since the pressure is relative, the values are not what should be compared. The relative pressure is set to zero at the outlet. Therefore, the pressure is, by default, set to zero at the outlet of the impeller in the single vane model but at the outlet of the volute in the full model. Here, the range of the pressures is about the same, thus, the comparison is more or less visual. It is clear that the pressure contour plots are very similar, which helps to verify the use of the single vane model. The main difference in the pressure is around the outer section. Near the trailing edge of the pressure side of the blade, the pressure is lower along the outside in the full model.

Figure 4.16 shows the velocity plots of the single vane model in (a) and the full model in (b). The velocities also look quite similar. The main difference is also in the outer section here. In the single vain model, the velocity vectors at the outer edge of the impeller appear to be travelling in close to a tangential direction. However, in the full model, the vectors appear to be travelling in a less tangential direction. This is due to the effect of the volute. In the single vane model, the flow would technically keep flowing in the same tangential direction after exiting the impeller. In the full model, the volute changes this flow since there are nearby walls that force the flow in a specific direction.

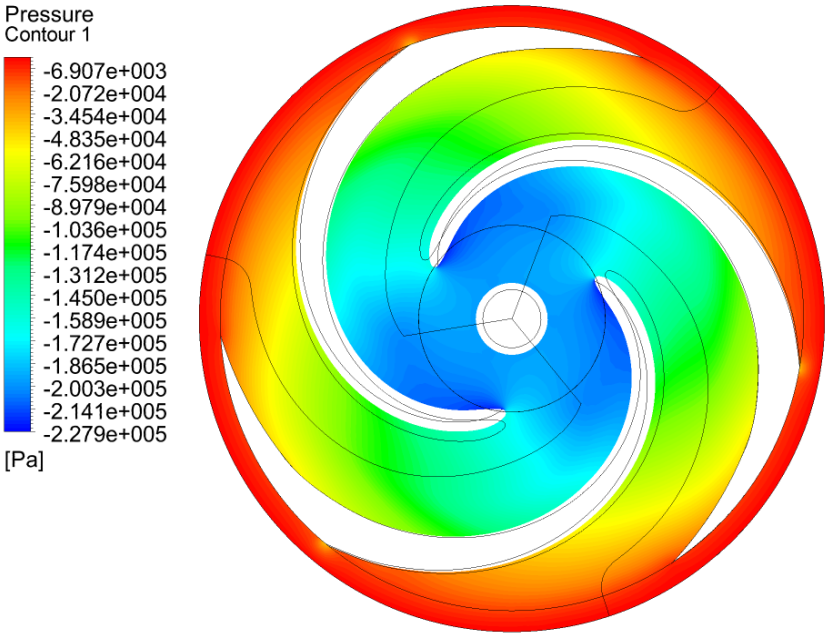

(a)

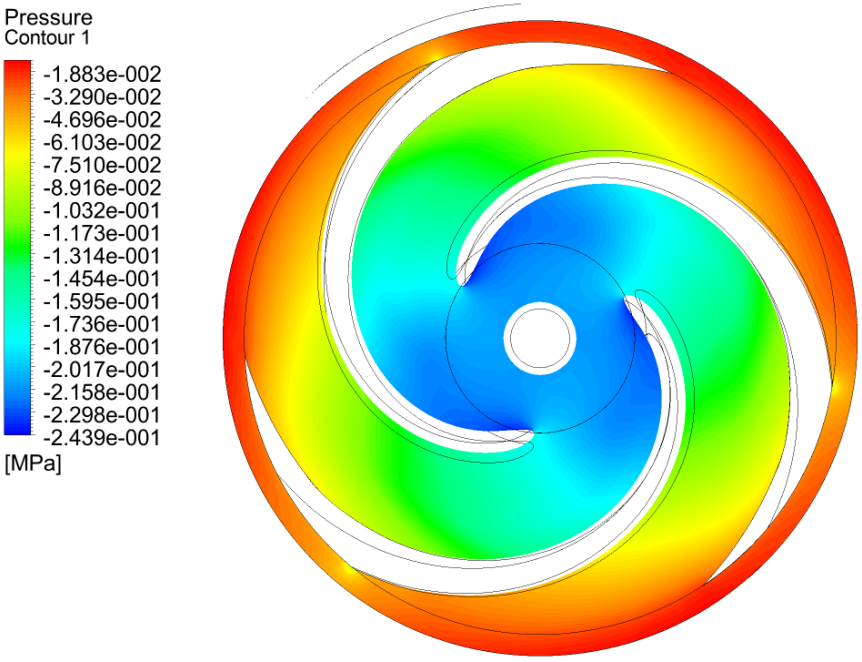

(b)

Figure 4.15. Pressure at 87.3% of BEP in (a) the single vane model and (b) the full model

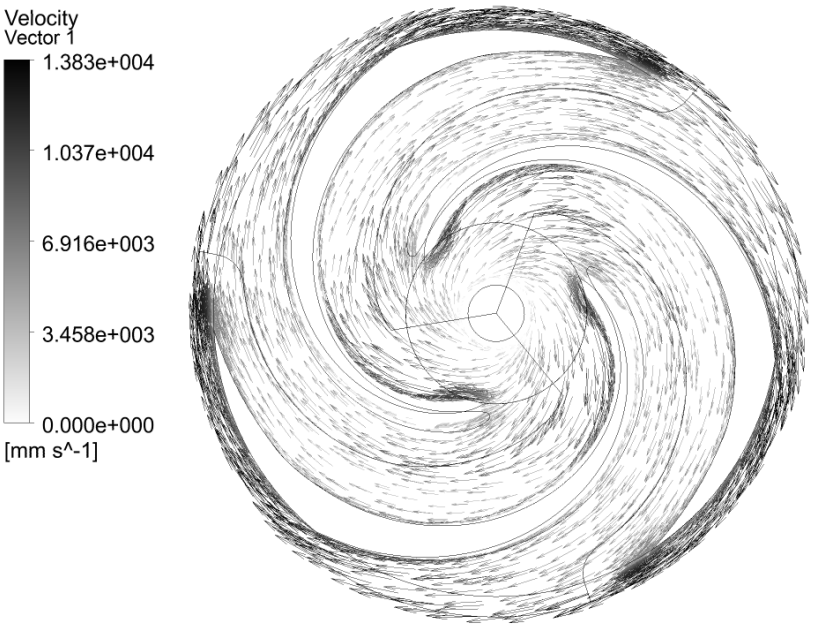

(a)

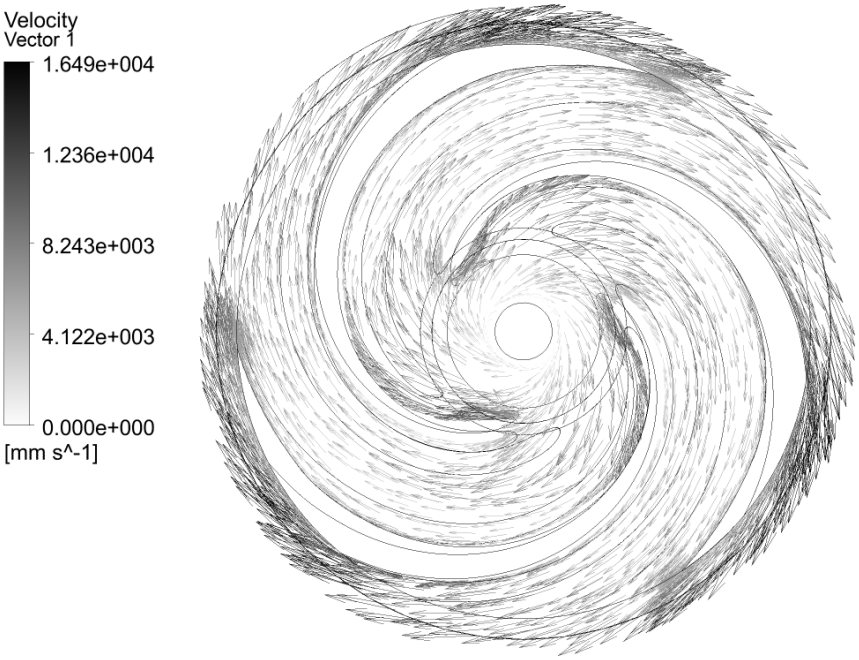

(b)

Figure 4.16. Velocity at 87.3% of BEP in (a) the single vane model and (b) the full model

Based on the results and analysis it appears that the single vane model could be used as a lower fidelity model to less accurately predict pump performance. While BEP may be incorrectly predicted, the overall curve shape seems to be fairly well predicted. The pressure and velocity profiles also seem sufficiently similar that they could be analyzed on the single vane model if design changes are being tested more cheaply. To better analyze how the two models will match for predicting performance when making design changes, it is important to analyze how results change when the same modification is made on both models. This will be discussed in Chapter 5: Optimization.

4.3. Sensitivity Analysis

The most important part of any CFD study is the sensitivity analysis. It is performed to test the sensitivity of CFD results to input parameters including geometry simplifications, the mesh and CFD settings such as the turbulence model. The mesh is the most important part of the sensitivity analysis since it defines the simulation domain and can be the sole source of error if it is not of good quality. Testing the sensitivity to the mesh is often referred to as a mesh independence study. The process of performing a sensitivity analysis is fairly straightforward. Changes are made to a parameter and the simulation is run again. If results are the same or quite similar, within reason, then it can be concluded that the results are not sensitive to that parameter and the certainty of the results is high. If results change significantly, then further testing must be undertaken to ascertain the necessary inputs required to yield accurate results.

4.3.1. Mesh Independence

Mesh independence requires testing to determine that the CFD results are independent of the generated mesh. The theory is that results should converge to a consistent value as the mesh is successively refined. That is, the elements will be made smaller and the total element count will increase. If the results remain consistent as the mesh is refined, the results are said to be mesh independent [64].

The initial goal for mesh independence was to generate a mesh that consisted of approximately 25% more elements, requiring the element size to reduce. The target of

25% was chosen since it would: (i) keep the simulation time from considerably increasing; (ii) keep the element count low enough to simulate with only eight GB of RAM; and (3) still be a large enough refinement to notice differences in results. Due to the long simulation time, small changes are preferable to avoid spending too long simulating a mesh that is already more than refined enough. In creating the larger mesh, the overall size should be reduced slightly in all areas and the first inflation layer thickness should be decreased slightly. A few additional inflation layers can then be added as well. A good recommendation for changing the inflation is to attempt to keep the total thickness of the inflation layers consistent. Generating a mesh that was 25% larger was not a simple task. Since it is easy for a small change to drastically change the mesh size, fine tuning is required. Additionally, it can be difficult to measure whether or not the mesh element size is actually smaller in the majority of the model. One of the major methods of checking the mesh after a change was by simply comparing it visually. However, important sections such as the blade faces were also selected for measurement and the average element size was calculated to clearly indicate a change in the mesh size. The mesh was changed numerous times until an appropriate mesh was found in each section (impeller, volute, lower sidewall). The most consistent change made to all parts was in the inflation. The first layer height was reduced from 0.08 mm to 0.06 mm. In the impeller and volute, 11 layers were used instead of 10. This maintained a similar thickness. In the lower sidewall, the number of layers was increased from five to six. The inflation changes and all other changes are summarized in Table 4.1. For changing the minimum size, often it was just set to a default value assigned by ANSYS, therefore this value was instead manually set to reduce the size.

After making all the changes discussed, the final mesh count was as outlined in Table 4.2 where the column displaying ‘% Larger’ is calculated based on the element count. The lower sidewall ended up having a size that was much more than 25% larger. This was considered acceptable since it has a relatively low mesh count and thus contributes less to the entire mesh count. The final mesh size was 30.34% larger than the original which is close enough to the target to allow for enough change in the mesh size.

Table 4.1. Mesh independence changes

		Impeller		Volute		Lower Sidewall	
		Original	**Refined**	**Original**	**Refined**	**Original**	**Refined**
Inflation	**First layer thickness**	0.08 mm	0.06 mm	0.08 mm	0.06 mm	0.08 mm	0.06 mm
	Number of layers	10	11	10	11	5	6
Sizing	**Min size**	Default	0.4 mm	Default	0.35 mm		
	Max size			6	5		
	Number of cells across gap					3	4
Other				• Face sizing added to cutwater: 1 mm		• Face sizing changed on outer surface: 2 mm → 1.9 mm • Face sizing added to expeller vane face: 0.7 mm	

Table 4.2. Mesh independence mesh count

	Original Mesh		Refined Mesh		
Part	**Node Count**	**Element Count**	**Node Count**	**Element Count**	**% Larger**
Impeller	426,518	1,168,681	554,784	1,483,390	26.93%
Volute	403,237	1,151,729	522,313	1,491,797	29.53%
Lower Sidewall	90,515	234,735	131,701	331,782	41.34%
Total	2,135,366	5,831,447	2,845,170	7,600,877	30.34%

The simulation was run at 100% of the BEP. The simulation time was increased with the new mesh. The average number of iterations required at each timestep remained at two, but the time per revolution increased to 6.74 hours whereas it was 5.25 hours at the same flow rate with the original mesh. Head and efficiency plots, when examined visually, looked exactly the same. To further test mesh independence, a simulation was run on the same mesh at an extreme flow rate of 162% of the BEP. Results appeared very similar at this flow rate as well. Table 4.3 shows the change in the numerical head and efficiency results for the two flow rates. It also shows the change in the maximum velocity on the blade which will be used later as an objective for optimization. This value is thus the most important value to check for mesh

independence. A negative value indicates the value from the new, refined mesh is lower. At 100% of BEP, the changes in all values are very small. The values are definitely within an acceptable range and already appear to prove that the results are mesh independent. At 162% of BEP, there is a larger head change, however the velocity and efficiency change is still quite low. Since velocity is the more important output in this study, this second simulation at another flow rate further shows that results appear to be mesh independent.

Table 4.3. Mesh independence results

Flow Rate	Efficiency % Change	Head % Change	Max Blade Velocity % Change
100% BEP	-0.193%	-0.276%	0.213%
162% BEP	0.792%	2.033%	-1.161%

A mesh independence study should consist of further test simulations. However, due to computational limits and the significant increase in time that would occur with more elements, this was not possible. The required memory in a computer is directly related to the number of mesh elements. With the resources available at the time, the mesh was at about the maximum size possible for the computer to handle. Therefore, it is concluded from the two simulations with the 25% larger mesh that the results are mesh independent and that the original mesh is sufficient for generating accurate results. Furthermore, as will be explained in Section 4.4: Validation, the results matched well with physical tests which, along with the mesh independence study presented, helps to prove that the results can be considered conclusive.

A mesh independence study was performed on the single vane model since it is much cheaper to run and it allows for a focus on just the impeller. Due to the lower cost, further refinement was specified on the single vane impeller mesh. The refinement made on the single vane is compared to that made on the full model in Table 4.4. Table 4.5 shows the original and refined mesh sizes.

Table 4.6 displays the results from the mesh independence. The initial test was performed at 100% of BEP as with the full model. The changes in results were again very small, this time both less than or equal to about 0.2%. This time, a low flow rate of

38.3% of BEP was also tested as a second mesh independence test. The reason for this was that a low flow rate test was also required for some testing to investigate the y^+ values with roughness. The changes in head and efficiency were about the same magnitude here. Therefore, this test also confirms that results are independent of the mesh.

Table 4.4. Mesh independence changes – single vane model

		Original	Full Model Refinement	Single Vane Refinement
Inflation	**First layer thickness**	0.08 mm	0.06 mm	0.05 mm
	Number of layers	10	11	12
Sizing	**Min size**	Default	0.4 mm	0.4 mm
	Max size	6	6	4.5

Table 4.5. Mesh independence mesh count – single vane model

Part	Node Count	Element Count	% Larger
Original	389,478	1,050,095	
Refined	567,754	1,500,384	42.88%

Table 4.6. Mesh independence results

Flow Rate	Efficiency % Change	Head % Change
38.3% BEP	0.132%	-0.022%
100% BEP	0.138%	-0.242%

4.3.2. Geometry Simplification

The main geometry simplification that was made that should be tested is removal of the fillets in the impeller which was explained in Section 3.2.3: Geometry, and shown in Figure 3.13. A simple test was performed on the single vane impeller model with the fillets at three different flow rates. The mesh count of the impeller with the fillets was 590,595 nodes and 1,592,644 elements. This much higher mesh count is definitely a good reason to try to avoid using the fillets. In the full model, with all three vanes there would be almost five million elements just for the impeller which would put the final

element count well above seven million whereas without fillets it is under six million. Table 4.7 summarizes the results of the tests performed with the fillets and compares them to those without fillets. It is clear that the fillets had a negligible effect on results, especially on the efficiency. Therefore, it is concluded that the fillets are not needed and should be removed from the geometry for the purpose of simplification.

Table 4.7. Comparison of results with and without fillets

Flow Rate	Head % diff	Efficiency % diff
38.3% BEP	-0.350%	-0.033%
100% BEP	0.481%	0.134%
137% BEP	1.40%	0.121%

4.3.3. Other CFD Settings

Several of the other CFD settings were changed to analyze the sensitivity of results to the settings and to further confirm that results were likely to be certain or not.

Turbulence Model

The turbulence model used was SST. While SST is superior to k-ε in theory, it was desired to test at a few points with the k-ε model to ensure no serious discrepancies between the two since the k-ε model has also been commonly used in similar tests. On the original model, a single test was performed at 100% of BEP. Later, using a different impeller model based on the original one, two comparison tests were run at 100% and 62.7% of BEP. This different model was used for optimization and will be discussed later. The results for the different turbulence models are shown in Table 4.8 where the percentage values are the values from k-ε with respect to SST. That is, for the test on the original impeller at 100% BEP, the head value using k-ε as the turbulence model was 0.138% higher with compared to using SST.

It is clear that results with the k-ε turbulence model are higher than with the SST model. There are no serious discrepancies here and the difference appears to be fairly consistent. Therefore, there is no reason for concern regarding the SST results and it is concluded that it is the correct model to use.

Table 4.8. Turbulence Model Sensitivity Analysis

	Head	Efficiency
Original, 100% BEP	0.138%	1.48%
New, 100% BEP	0.927%	2.137%
New, 62.7% BEP	1.180%	2.115%

Inlet and Outlet Settings

On the full model, the inlet and outlet were setup to have a mass flow and an opening pressure and direction specified, respectively. Since the ANSYS Reference Guide suggested instead using a mass flow outlet, the boundary conditions were switched to check for any change in results. As per the recommendations, the inlet was set to have a total pressure with the relative pressure set to zero. A simulation was run at 100% of BEP and the results turned out to be almost exactly the same as results with the inlet and outlet at their original settings. The change was negligible enough that the head and efficiency values need not be presented here.

As outlined in Section 3.2.5: CFD Setup, the entrainment option for an opening is likely more mathematically correct but was not used for the outlet since it may be more difficult to solve. Another simulation was run at 100% of BEP yielding no change in results at all. Therefore, it can be concluded that the full model results are definitely independent of the inlet and outlet settings used. This also indicates that the inlet and outlet are extended far enough away from the region of interest such that the flow has become more predictable.

The single vane model, on the other hand, yielded significant changes in results when inlet and outlet settings were changed as shown in Figure 4.17.

The curve shape and values for efficiency are significantly differently. The head values are more similar but the values using the opening pressure and direction setting do not form as straight line and then at the lowest flow rate, the head increased to a much higher value. For a single vane model, the entrainment opening setting is preferred since it does not define a direction for the flow at the outlet and rather fully calculates the flow direction. Using the opening pressure and direction setting, a

direction is specified. Since direction is not normal to the boundary and is in the radial direction, this setting generally is not the best to use for this type of situation. Looking at the head curves, the entrainment one looks much better. A massive jump in head is not expected as flow rate becomes very low, which shows that entrainment predicts a more expected curve. Additionally, the efficiency using the entrainment setting, which was used for all other tests, matched the full model results better with regard to its shape. Therefore, these results show that the single vane model results depend heavily on the correct input and output settings and that the entrainment option is a better choice for modelling the outlet boundary condition.

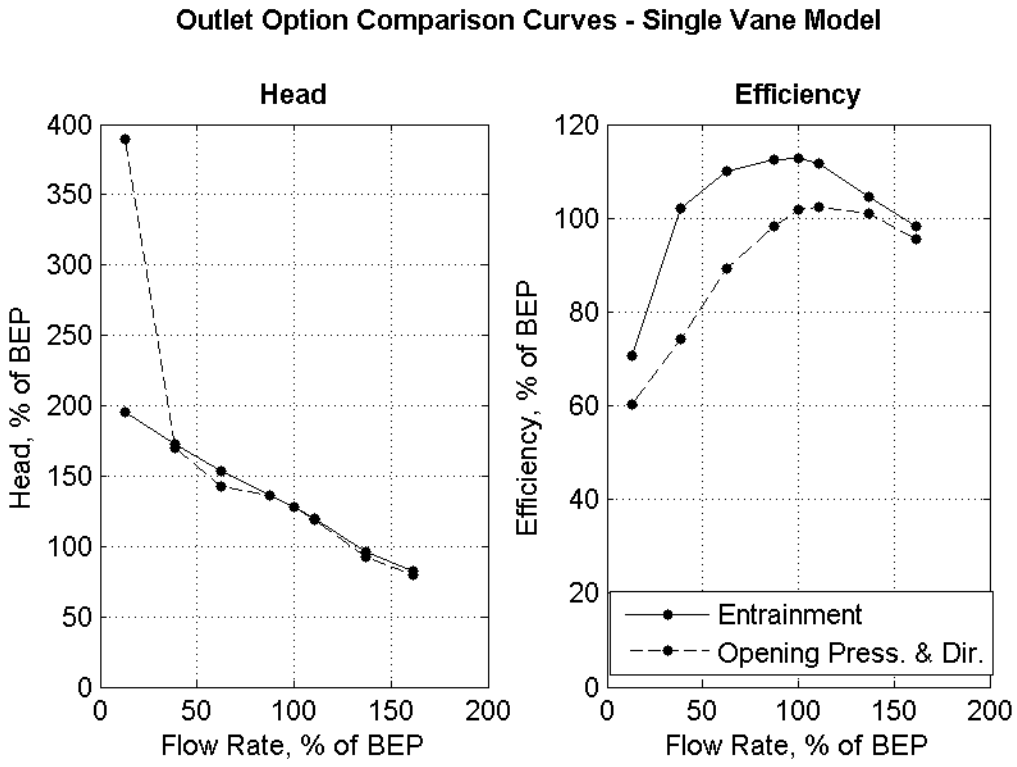

Figure 4.17. Outlet options comparison

4.4. Validation

Validation is the process of proving that CFD results are valid by comparing to results from physical tests. To ensure accuracy in any CFD results, validation is a mandatory step. Without validation, even with an extensive mesh independence study, there is no way to guarantee that results are accurate. The pump that has been

discussed throughout this thesis was a design by Toyo Pumps designed for production that was manufactured to be tested and sold. Any design changes recommended will be implemented in future revisions of the pump.

4.4.1. Physical Tests

Physical tests were performed in Toyo's own in-house designed test tank. All tests are performed to closely follow the widely-accepted Hydraulic Institute (HI) Test Standards published in the American National Standards Institute (ANSI)/HI Pump Standards. The tank was also designed to these standards. While Toyo manufactures slurry pumps, they are still tested in water and is the recommended method in the ANSI/HI standards for slurry pumps [65]. Figure 4.18 shows a diagram from the HI standard of a test tank for reference.

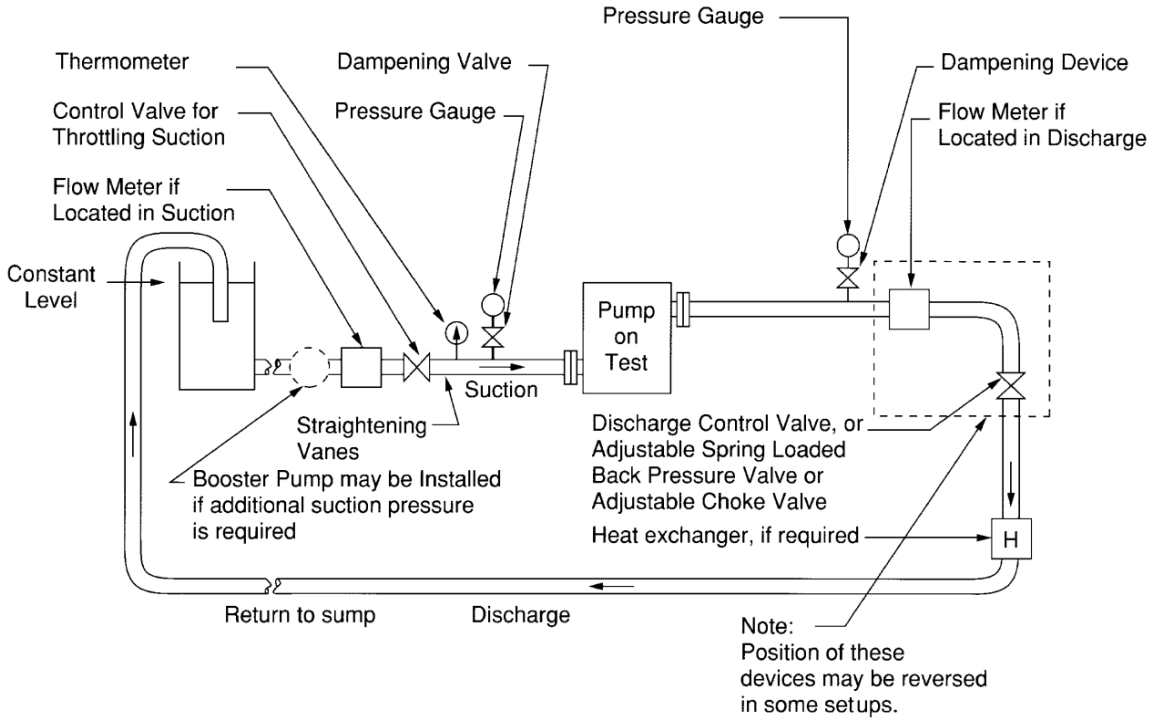

Figure 4.18. Test Tank Diagram courtesy of Hydraulic Institute, Parsippany, NJ USA, www.Pumps.org [46]

The pumps are tested manually in the tank. They will generally be tested at a variety of rotational speeds. At each rotational speed, the flow rate is varied by turning a control valve in the discharge pipe as shown in the diagram in Figure 4.18. The flow rate

is changed incrementally and measured at each increment. At each increment, two other readings are taken. One is the pressure gage reading which is measured only in the discharge pipe at a distance from the pump equal to two pump outlet pipe diameters. The other measurement is the power meter reading, which is the power that is drawn by the motor. From those measurements, the head and efficiency can be calculated to generate a pump curve at that specific rotational speed. The values are calculated according to the method outlined in Section 3.1.2: Pump Performance. The pump is tested all the way down to shutoff at which point there is no flow going through the pump. There is still water inside the pump and pipes, though, which is why a head value is still measured.

The accuracy of the measurements must be within limits as prescribed by HI specifically for slurry pumps. Table 4.9 displays these limits and they are taken to be the actual accuracy of all physical test results. Flow rate and total head can be within a certain range whereas power and efficiency can only have inaccuracies on one side of the actual value. Efficiency, for example, can only vary between the actual efficiency and 7% below the actual efficiency. These accuracy limits are fairly loose because there can be quite a variance in performance on every model of the same pump mainly because components are not machined. It is acceptable to have CFD predict results within the accuracy range of physical tests since physical test results are only taken from one pump. Therefore, it is quite possible that a different pump will yield different results, which may be closer to or farther from the CFD results than the ones presented here.

Table 4.9. Required physical pump test measurement accuracy

Test Parameter	Accuracy
Flow Rate	±9%
Total Head	±7%
Power	+9%
Efficiency	-7%

Figure 4.19 displays the head and efficiency curves from the physical pump tests. The physical tests results show the BEP exists at the same flow rate as predicted by the full model simulation which is why this flow rate was chosen to refer to the 100%

of BEP. The curve appears to have quite a spike at this point. This is likely due to measurement error, meaning the curve should be smoother with a less dramatic BEP point.

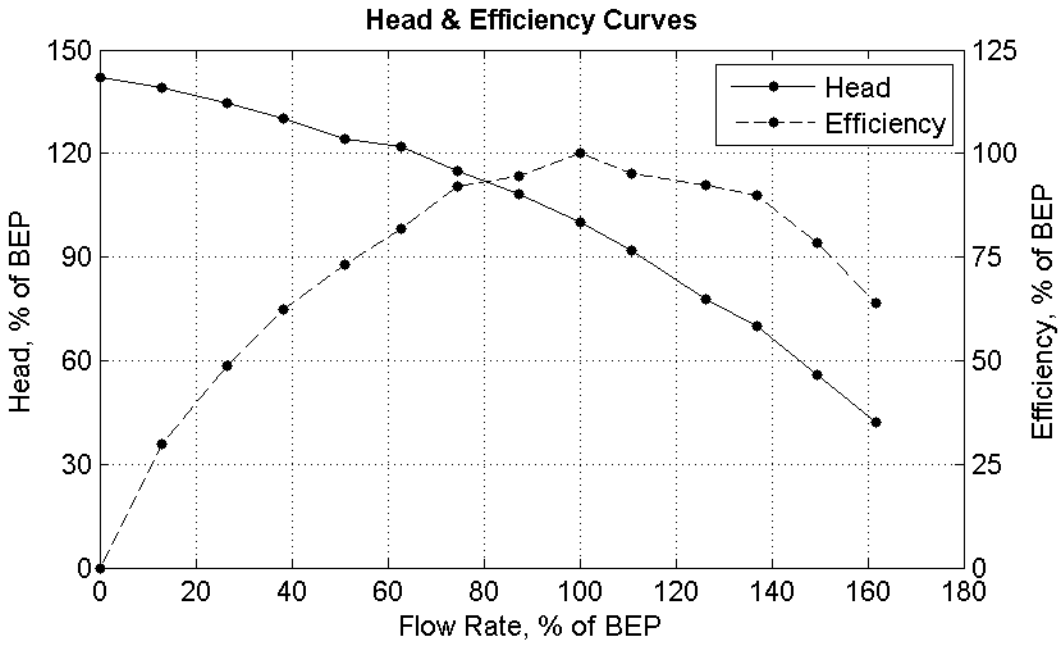

Figure 4.19. Physical pump performance curves

4.4.2. Results Comparison

Results were generated for the pump before physical test data was available for the pump. This meant it was especially important to ensure as much as possible that results were accurate based on the sensitivity analysis. Figure 4.20 graphically shows a comparison of the performance curves generated from physical tests and on the full model simulation. The simulation model data has error bars showing 7% on either side according to the HI accuracy limits. Efficiency is shown with error bars on both sides even though the accuracy should only be -7% since it is just for the purpose of comparing with simulation tests.

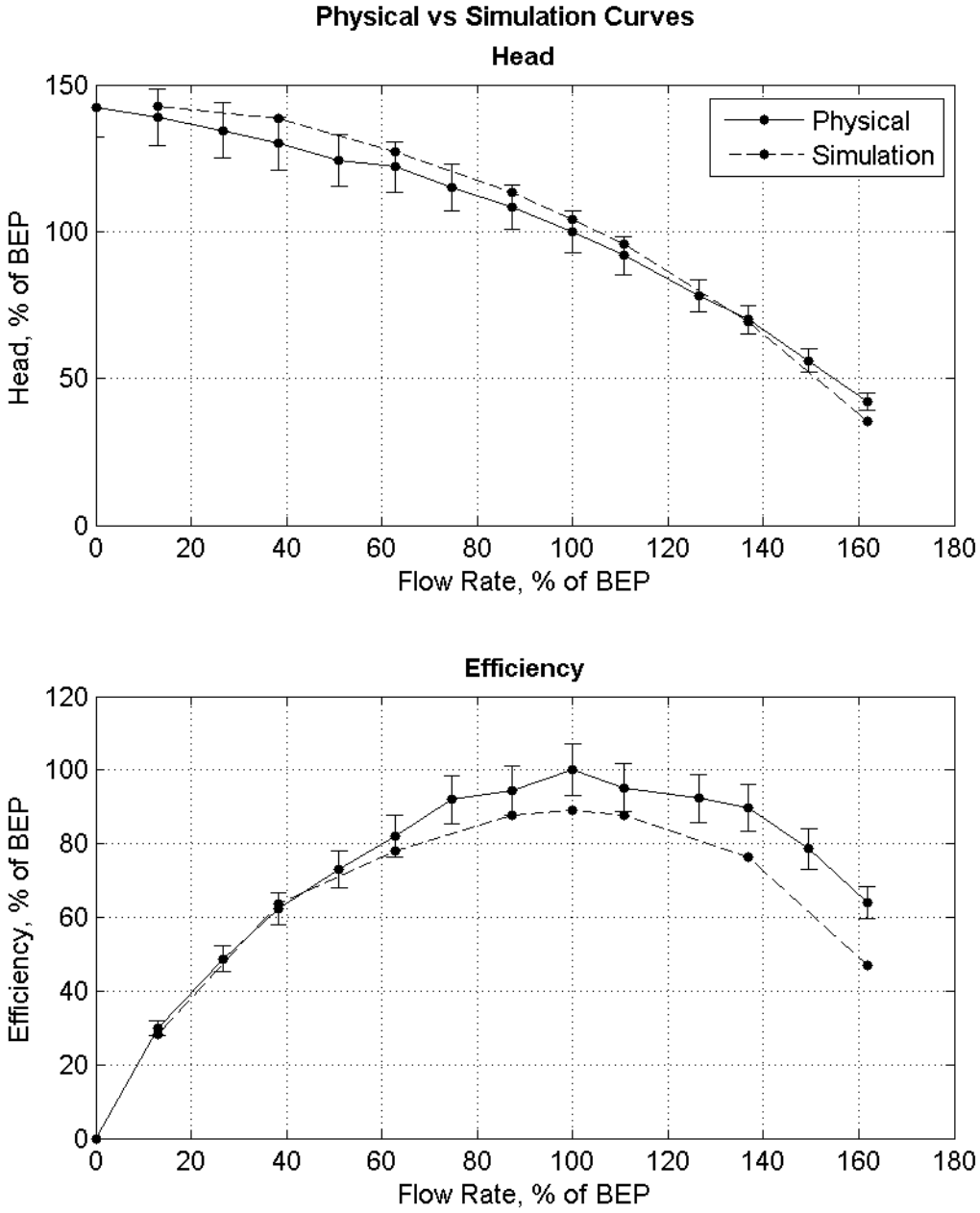

Figure 4.20. Physical versus full model simulation pump curves

The results, most importantly, show a fairly good correlation especially when it comes to the shape. The head curves are actually quite close to each other over the whole range of flow rates. The slope is slightly different, however. The simulation results begin higher than the physical results but, as flow rate increases, they slowly get closer to the physical results until they intersect and cross around 137% of the BEP. The

efficiency curves do not match as well as the head curves do. However, one of the most important and critical features to recognize is that the BEP locations match. For pump performance predictions, the BEP is a very important number and simply locating at what flow rate the BEP will occur at is extremely beneficial even if the efficiency value may not be as accurate. Additionally, the shape is quite similar between the physical and simulated efficiency curves. While the physical curve climbs higher, the overall curvature looks quite similar. Therefore, the simulation appears to give a good characteristic of how efficiency will behave with varying flow rates. That is, it shows by how much it will drop when going above or below BEP.

Table 4.10 shows the numerical pump curve data comparison for the simulated results compared to the physical results. That is, a positive value means the value is predicted higher by simulation compared to the physical results. The head results are all within 7% of each other with the exception of the very last point at the highest flow rate. Since this is a very extreme point that will likely never be reached in normal usage, it is less critical for the simulation to accurately predict results here. For the efficiency, only the first three points are within 7%. Again, the largest difference is at the very extreme highest flow rate. While the difference is larger, the results are still very useful for predicting BEP and the general shape.

Table 4.10. Physical versus full model simulation pump curve data

Flow Rate (% of BEP)	Head % diff	Efficiency % diff
12.94	2.70%	-5.23%
38.31	6.54%	2.26%
62.69	4.25%	-4.88%
87.31	4.79%	-7.06%
100.0	4.32%	-11.1%
110.7	4.40%	-7.72%
136.8	-0.82%	-14.9%
161.7	-16.04%	-26.7%

Based on the results, it is assumed that the CFD model is sufficiently accurate to predict the performance of slurry pumps. A further assumption will be made that any changes in results on the CFD model based on design changes will correspond to

similar changes in the physical model. For example, if the CFD model predicts a higher efficiency with a certain design change, it is assumed that the same design change made on the physical model will produce a similar rise in efficiency. While the values may not be the same, the trend should be similar.

In this chapter, results have been analyzed and validated. The validation showed a good correlation between simulated results and physical results. Furthermore, analysis of the simulation results by analyzing pressure and velocity plots, for example, yielded results that matched expectations based on theory. With the validated model, it is possible to now run simulations on other similar slurry pump designs to predict results. This leads to the possibility of optimizing the pump design to generate models that will theoretically provide superior performance in a physical model.

Chapter 5. Optimization

The process of optimization in the design phase is becoming increasingly common in the industry. With the tough competition that often exists in most major industries, there is always a strong push to constantly improve products to maintain an edge in the market. In the past, any sort of optimization generally consisted of simple trial-and-error. Potentially superior designs were made that would theoretically provide an improvement and then those designs were tested to evaluate whether or not any improvement was actually made. Nowadays, with the availability of advanced simulation software provided by such companies as ANSYS and the relative ease and affordability of computing power, simulation is becoming very common in the design phase to replace or significantly reduce the need for prototypes. Coupling simulation with optimization is the perfect match for truly generating the best possible designs and remaining ahead of competition. This is exactly what Toyo Pumps is intending to accomplish.

As mentioned in Chapter 1: Introduction, slurry pump design is based on science but also involves a high degree of art and experience from a designer. Without the use of CFD, accurate predictions cannot be made on the pump performance, nor can a designer visualize what is actually occurring inside the pump. With CFD, this opens up many new possibilities and can allow the designer to analyze the flow and see how the design could be optimized whether it is to improve efficiency, reduce wear or improve other flow features that may be observed inside the pump. Also as mentioned in the introduction, a major goal in slurry pump design is to reduce the wear in the pumps. The reason to focus on wear over efficiency is that, since there is such a high degree of wear in slurry pumps, the benefits of reducing wear are greater than the benefits of reducing efficiency. Since efficiency will be inherently low, improvements will likely not be significant. Additionally, when components wear, the pump needs to be shutdown to have them replaced, which is very expensive in terms of lost time and repair or

replacement costs. Therefore, reducing wear can extend the mean time between failures of the pump while decreasing the total cost of ownership.

5.1. Splitter Blades

In this study, optimization to minimize wear is performed by adding splitter blades and varying their design and location. A simple definition of splitter blades are blades on an impeller that are shorter than the main blades. The main purpose of using splitter blades in turbomachinery are to basically take advantage of the benefits of adding more blades while decreasing the negative effects since they are shorter in length. Splitter blades can be found in many centrifugal type turbomachines including pumps, turbines and compressors. In most turbomachines, increasing the blade number to a certain extent increases the performance, most notably the efficiency. However, with too many blades, the efficiency begins to decrease with the main causes being increased friction from more blades and congestion in the impeller inlet area. The congestion is caused by too many blades leaving too little space for the flow to enter the vanes. With too few blades, performance will suffer due to the flow not being guided as closely and the onset of flow separation [26]. Splitter blades provide the improved performance of adding more blades while minimizing congestion in the impeller inlet area. Splitter blades have also been found to reduce pressure fluctuations and extend the operating range [27].

There has been very limited investigation of splitter blades in slurry pumps but there are several studies on using splitter blades in clear liquid centrifugal pumps. One study investigated adding splitter blades of varying lengths to impellers consisting of five to seven blades. It was found through many physical experiments that with impellers already having six or seven blades, the splitter blades had negative effects, most prominently a decrease in efficiency. With only five blades, adding splitter blades increased the efficiency by 1.14%. Therefore, with fewer blades, it was found that adding splitter blades was beneficial [26]. This indicates that adding splitter blades to Toyo's slurry pump consisting of only three blades is likely to be beneficial. Another study used CFD to analyze the pros and cons of adding a splitter blade to a clear liquid centrifugal pump. The CFD analysis of the non-splitter model was validated with physical tests with good correlation. The findings were that splitters provide positive and negative effects.

The head was increased with splitters but it was found that efficiency did not improve. Pressure fluctuations were decreased, but radial thrust was consequently increased. Radial thrust causes vibration and decreases the life cycle of the pump since the shaft and bearings will wear out sooner [27].

For slurry pumps, one of the only studies of adding splitter vanes is outlined in a patent by Weir Minerals, one of the world leading slurry equipment providers. The benefits mentioned in the patent include reducing turbulence within the main flow of the vane and reducing recirculation. Recirculation was observed to be reduced the most when the vane was located near the pressure side of a blade. These benefits translate to reduced energy losses and thus gains in both head and efficiency over a wide flow range. It was also mentioned that wear would be reduced overall. However, Weir only considered different types of partial splitter blades such as those shown in Figure 5.1. They did not use splitter blades filling the entire width of the impeller from hub to shroud [8].

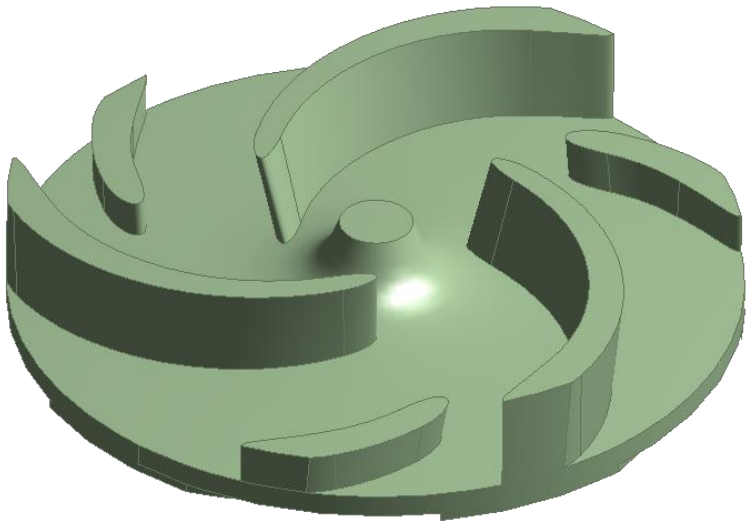

Figure 5.1. Impeller with partial splitter blades

Similar to the goals of Weir, the goals of Toyo are to use the splitter blades to reduce the wear in the pump. Toyo's splitter blade design differs from Weir's mainly in the size of the splitters blades as well as in the fact that optimization will be performed. The splitter blades to be investigated here will be the full width of the impeller from the hub to the shroud. In Weir's impeller examples, the blade length appears to always be

about the same and is quite short. For Toyo's design, the length of the blade will be allowed to vary to investigate the optimum length. The patent also shows no indication of any optimization and it appears that successful results were generated based only on numerous investigations and experiments. Toyo would like to go further and optimize for the best splitter vane possible to minimize wear.

5.1.1. Splitter Blade Impeller Model

In order to accommodate splitter blades, the impeller model needs to be changed and cannot simply have splitter blades added to it. The current impeller model has fairly narrow vane passages since the blades were designed to have a large wrap angle and thus be fairly long. The wrap angle is the angle between the leading and trailing edges of the blade with respect to the center as shown in Figure 5.2 (a), which displays the original impeller model. The vane area of the original impeller must be widened to provide space for splitters. Figure 5.2 (b) shows the new blades for the widened model with splitter vanes included. The wrap angle of the blades was reduced to 100° to create the new design. This new model will be referred to as the 100° wrap angle impeller.

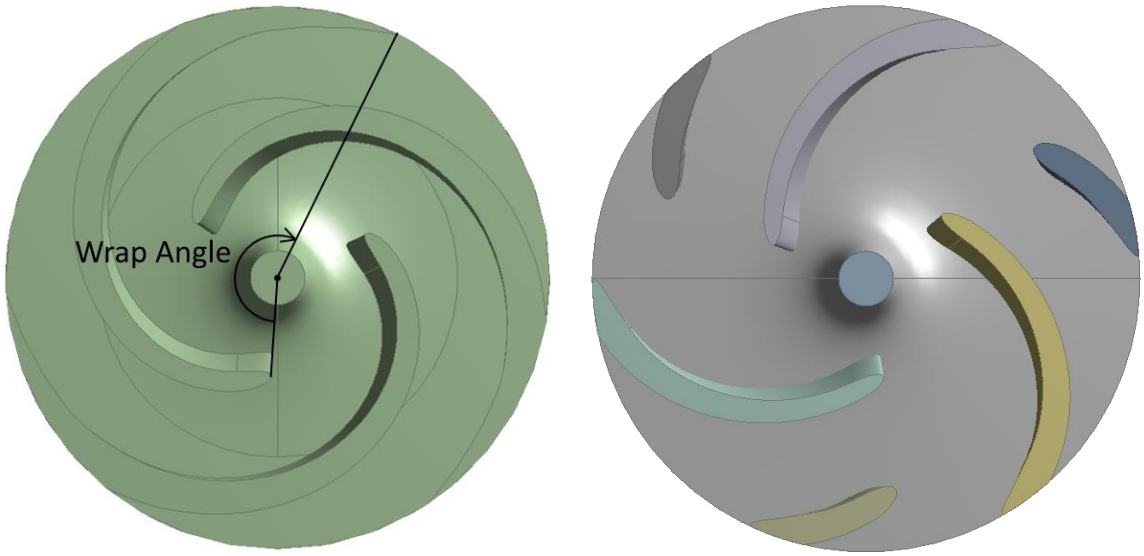

(a) (b)

Figure 5.2. Impeller models: (a) original; (b) low wrap angle

It is clear that the total blade length is shorter in the new model. It is also important to notice that the trailing edge style is different which has a very small effect on results. In the original model, the trailing edge of the blades covers a larger area along the outlet because the tip on the suction side is extended to end in a point. On the new model, there is no extension and the trailing edge area is generally much smaller along the impeller outlet. The lower sidewall and volute are exactly the same with only the impeller blades changing. Therefore, for any full model tests, the original meshes for the volute and lower sidewall sections were the same.

As for the splitter blades, they are in a nominal, fairly central location. They are much shorter than the main blades although the length can be adjusted. Their shape is based on the main blade contour. As the length is increased, the blade curvature will be the same as the main blades.

The new 100° wrap angle impeller is quite different from the original impeller. The original impeller has fairly narrow vanes that seem to guide the flow well so it may appear, at first sight, to be a better design than the more open vanes of the 100° wrap angle impeller. However, the original design was a new design created mainly to test the concept of having narrower, longer blades to better guide the flow instead of adding splitter blades. Since Toyo did not have the resources at the time to simulate and optimize a design with splitter blades, they chose the longer blades with a high wrap angle. Since splitter blades are quite a new concept to slurry pumps, it would be more risky to produce the design without having any experience with designs using splitters. Additionally, the long vanes of the original impeller means there are more walls that can cause material to clog in the passageways. There will also be more friction with the longer passageway. Most slurry pump impellers are more similar to the splitter blade model (although without splitter blades) shown in Figure 5.2 (b). Therefore, adding splitter blades is an investigation that Toyo is very interested in seriously considering that could be used on future pump designs. Older designs may also have splitter blades added to them for replacement in pumps currently in use.

5.1.2. Baseline Results

At this point in the author's research, computers with better specifications became available for use. Therefore, tests were accelerated by using several computers with the specifications shown in Table 5.1. Simulations ran faster on these computers. The mesh was very near the limits due to available memory on the previous computer used, therefore, these computers allowed a larger mesh to be used which was necessary for the splitter blade model.

Table 5.1. Computer specifications

CPU	Intel Core i7-3770
# cores	8
Speed	3.40 GHz
Memory (RAM)	16 GB
System Type	64-bit

Before beginning optimization on the new splitter vane model, it is crucial to generate a pump curve of the new impeller without splitter vanes to see how the results compare to the original model. It also gives a baseline to observe how results react to the addition of splitter blades. Figure 5.3 shows the results of a full model simulation of the pump with the new impeller design (without splitter vanes) compared to the original model results.

There are two major changes to be observed. The head curve with the new impeller is much less steep than with the original impeller. Based on pump theory, this should correspond to the BEP of the efficiency curve shifting to the right and a less steep efficiency drop, which is exactly what was predicted by the simulation. The BEP was found to have shifted fairly significantly over to 126% of the original BEP. These results show that changing the wrap angle of the blades has significant effects on the curves and even the location of the BEP. Note that all results will still use the BEP of the original full model simulation as the reference flow rate for consistency.

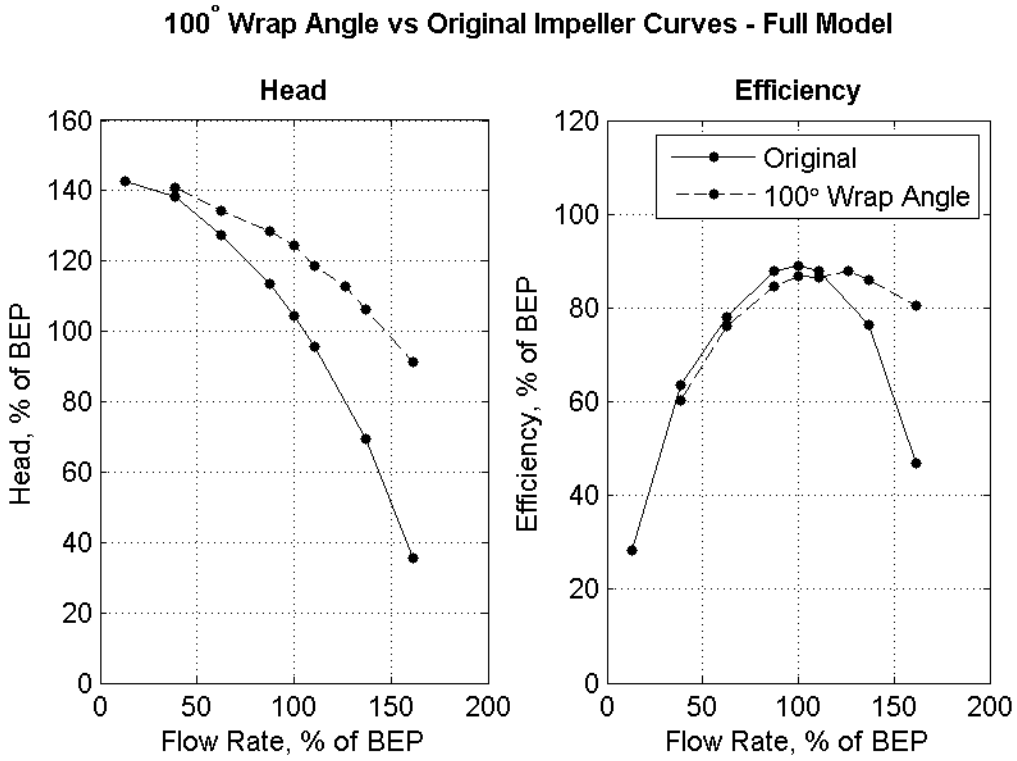

Figure 5.3. Results comparison of impeller models – full model

Single Vane Results

The same results were generated on the single vane model of the 100° wrap angle impeller since it will be used for optimization. Figure 5.4 shows the pump curves for the new and original single vane impeller models and a similar change is observed compared to the full model results. The head curve decreases less as flow rate increases in both. As for the efficiency, the BEP is shifted to the right in the single vane model and the efficiency drop at higher flow rates is less than in the original model while the values are quite similar at lower flow rates. Figure 5.5 shows a direct comparison of the full model and single vane model results calculated on the 100° wrap angle impeller (the same results shown in the previous two figures). The curve shapes are clearly similar, which helps confirm that the single vane model should still be capable of predicting results on the full model with this new impeller.

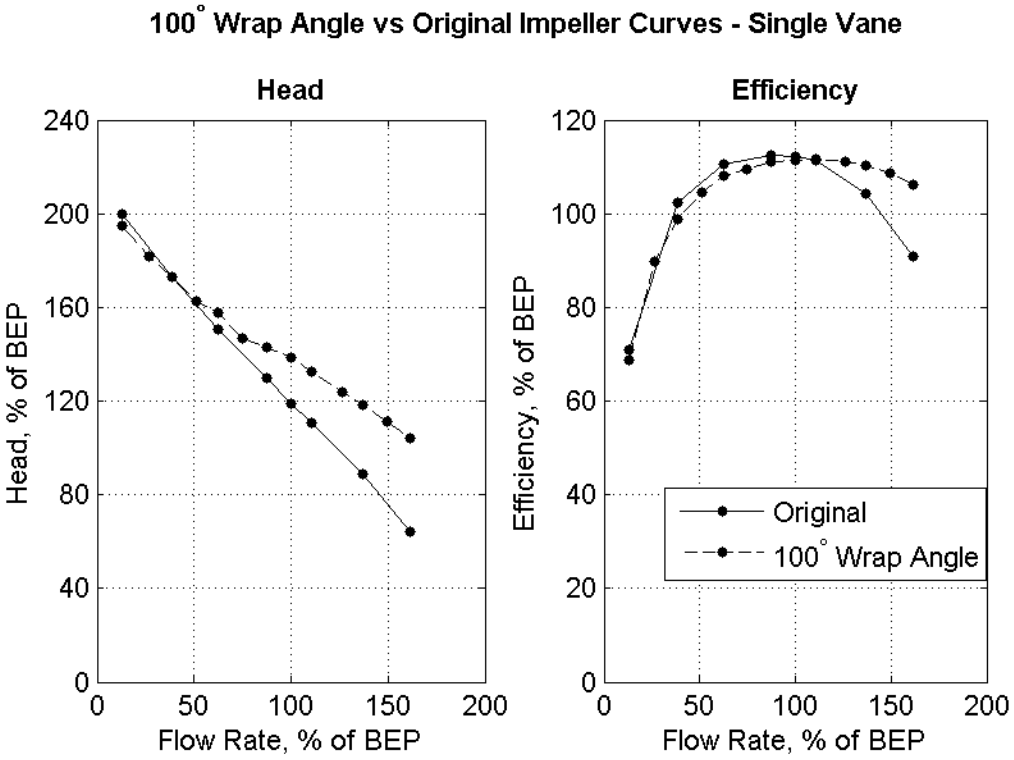

Figure 5.4. Results comparison of impeller models – single vane model

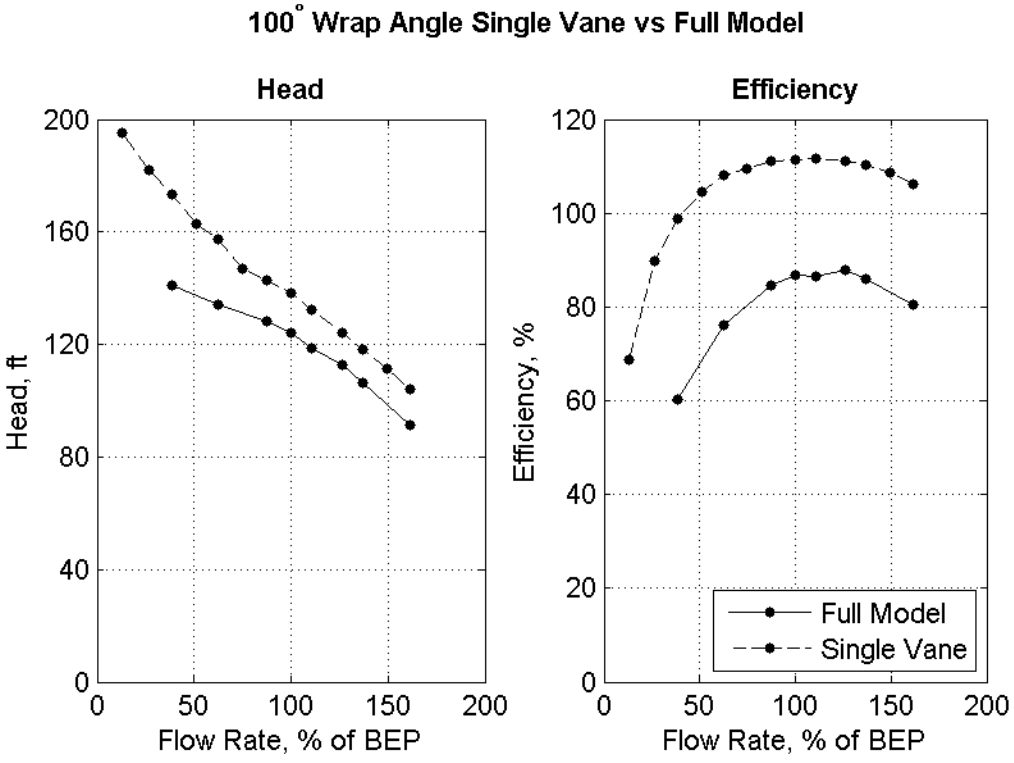

Figure 5.5. 100° wrap angle single vane vs full model results

To further assure the single vane model can be used to predict results, it is imperative to compare trends in key results to be studied such as the wear. This ensures that a response in results to a change in inputs has a similar effect on both models. While the values will likely be different, the most significant validation of using the single vane for analysis is confirming that the trends are the same. For example, if some change causes wear to decrease in the single vane model, a similar decrease in wear should be observed on the full model. A trend analysis will be presented in Section 5.2.1: Parameterization.

5.2. Splitter Blade Optimization

Since splitter blades are not very common in pumps and hardly investigated in slurry pumps, there is no guidance on the best shape and location for splitter blades. This makes splitter blades an excellent focus for optimization. The optimization goal for this study is to reduce the wear in the impeller of a slurry pump.

Wear in centrifugal pumps is caused primarily by erosion of the pump by solids suspended in the fluid. Erosion can occur in clear liquid due to small particles that are not visible to the eye. However erosion is significantly larger in slurry pumps due to the presence of solids of much larger sizes. There are two main erosion processes that occur due to the interaction between solids and the pump components. One process is friction due to particles sliding along surfaces primarily tangentially to the surface. This is most common in the impeller along the pressure and suction surfaces of the blade and along the hub and shroud. The other process is impact of the solids due to particles hitting the pump with a high velocity normal to the surface [10].

Determining wear through CFD is quite a difficult process. It involves defining a two-phase flow with solids suspended in the liquid. This is not a trivial process and is made further difficult since slurry is a very random fluid having varying sizes of solids at varying concentrations. Assumptions can be made to define an average slurry although it is still not simple. With a proper slurry simulation, erosion can be calculated based on the velocity of the solid particles and their angle with respect to the pump components. One study investigated the wear due to impact only in the volute of a centrifugal pump

using this method. The study was only in 2D and did not investigate the wear in the impeller [41].

Simulating slurry is beyond the scope of this study, mainly because a slurry flow cannot be validated. Simulating slurry would be a good choice for a future research focus. Since Toyo uses only water to test their pumps and validate simulations, water will be used for optimization as well. Other approximations must be used to determine the wear in the pump since there are no solid particles simulated to base calculations on. Recirculation near pump components can be a major cause of wear since it involves the fluid flowing repeatedly in one area, causing more contact of the particles against the wall. However, recirculation can be very random, occur at different places and would be very difficult to automatically quantify in an analysis. Another potential way to investigate wear is to look at the maximum velocity. Velocities increase due to a rise in kinetic energy with a fairly linear relationship. Higher velocities thus cause more erosion as solid particles will impact the walls harder or have increased friction [10,11]. Furthermore, impellers have been observed through experimental tests to suffer high wear due to high velocities at the blade tips [9]. One study performed an investigation of the wear in a coal pulveriser using CFD. Wear was analyzed by focusing on the velocity plots in the pulveriser where locations of high velocities were considered to correspond to high wear [66].

In this study, to reduce the wear, the goal will be to reduce the maximum velocities that occur near to the blade and splitter blade surfaces. Only the blades are analyzed since they are the most critical components for wear as observed by Toyo. The blades effectively define the flow through the entire pump and thus any wear on the blades can have significant effects on the flow, yielding large head or efficiency reductions. The maximum velocity almost always occurred near the blade trailing edge tips. However, location was not a major concern and the goal was simply to reduce the maximum velocity regardless of the location on the blade. At first, only the maximum velocity on the main blades were considered for minimizing the wear. However, it was observed that with some splitter blade configurations, the velocity on the blade was very low, but then the velocity on the splitter blade was much higher. In most cases though, the splitter blade velocity was lower. Therefore, a weighted average velocity, $V_{weighted}$,

was used as the goal. Since splitter blades are smaller and the main concern is with the main blades, the weighting should be higher on the main blades. An average using a 70% contribution of the maximum blade velocity, $V_{b_{max}}$, and a 30% contribution of the maximum splitter blade velocity, $V_{s_{max}}$, was used as shown in Equation 5.1.

$$V_{weighted} = 0.7 * V_{b_{max}} + 0.3 * V_{s_{max}} \quad \text{(Eq. 5.1)}$$

By examining the results of a number of pre-optimization tests, the weighting appeared to be very appropriate since all of the lowest weighted velocities corresponded to low velocities on both the main and splitter blades. Additionally, to help confirm the values, the ratio of the blade surface areas to the total combined surface area was calculated as shown in Table 5.2. These values were calculated with the maximum length splitter blade. With a smaller blade, the ratio will change such that the main blade has a higher percent. Therefore, 70% and 30% appear to be appropriate values considering the size of each blade.

Table 5.2. Blade surface area data

	Surface Area, mm²	**% of Total**
Main Blade	10,624	65.3%
Splitter Blade	5,639	34.7%
Total	16,263	100%

While the velocity is the goal for the purpose of reducing wear, it is also important to ensure that pump performance with respect to head and efficiency is not worsened significantly. While the objective function does not take efficiency into account, it is important to check the efficiency of the results in pre-optimization testing as well as in post-optimization results. Ideally, the efficiency should be maintained or improved as wear is improved. However, as determined with designers at Toyo, it is acceptable to improve the wear while sacrificing efficiency if it can be proven that the total cost of ownership will decrease. Since slurry pumps wear so quickly, better wear characteristics can often decrease the total cost of ownership of the pump to a greater extent compared to a pump that has worse wear characteristics but a slightly higher efficiency.

Optimization will be carried out at a single flow rate of 100% of the BEP of the original impeller. BEP is the most important point to reduce wear since that is the average flow rate at which the pump will operate. The BEP was revealed to be higher in tests of the 100° wrap angle impeller. However, it is still being tested at 100% of the BEP since the new BEP may change again when splitters are added. Additionally, the efficiency change was not significantly high between the new BEP and the original BEP.

5.2.1. Parameterization

In order to perform optimization, parameters need to be defined. Parameters are variables that are allowed to vary within specified boundaries to obtain the optimum objective. Three parameters were assigned for the splitter blades as illustrated in Figure 5.6. Figure 5.6 (a) shows the nominal position of the splitter blades as they appeared by default. That position is used as a reference point from which to measure the parameter bounds. In the other three figures, the blue splitter blade is the reference while the red blades illustrate how the parameter can vary. One parameter was used to define the blade size corresponding to the length of the splitter, shown in Figure 5.6 (b). The nominal splitter length is defined as 100%. All other lengths will be displayed as a percentage of that length to maintain confidentiality. The shape is based on the main blade, thus the shape of the splitter blade is consistent and the blade thickness and shape of the leading and trailing edge tips also do not change. For positioning, two parameters were used. One defined the position of the blade relative to the center of the impeller as shown in Figure 5.6 (c). The nominal position of the splitter is defined as zero degrees. The other parameter for position was the angle of the blade with respect to its trailing edge as shown in Figure 5.6 (d). Each parameter has minimum and maximum boundaries which are shown in Table 5.3.

Boundaries are given to all three parameters, although another very important part of optimization is to define constraints where necessary. In this situation, the maximum solid size desired to be passed through the pump is 15 mm. Therefore, a minimum distance of 15 mm must exist between the main blades and the splitter blade. Within the bounds given, the splitter blade can sometimes violate the constraint. A constraint function is used in the optimization that computes the minimum distance

between the splitter blade and the two blades on either side as illustrated in Figure 5.7. The red splitter blade is in a sample location with a length of 125%, position of -10° and an angle of 10°. The lengths $d_{suction}$ and $d_{pressure}$ are both within the constraint of 15 mm. If the constraint is violated, the set of parameter values will be considered an infeasible point. An additional constraint is to maintain a minimum distance between the splitter blade and the edge of the geometry as shown by the arrows in Figure 5.8. The minimum distance required between the blade and the geometry edge was two mm to ensure proper, successful meshing.

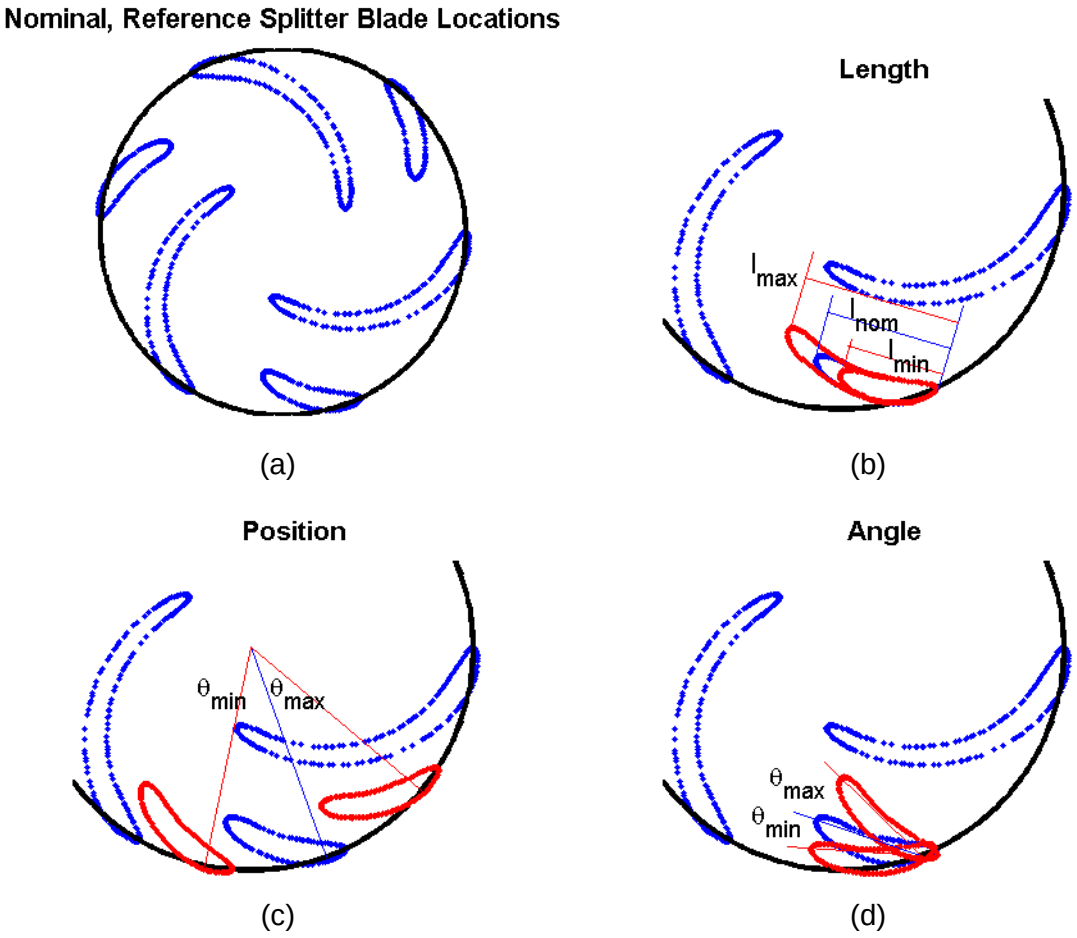

Figure 5.6. Parameters illustrated with their bounds: (a) nominal, reference splitter blade locations; (b) length parameter; (c) position parameter; (d) angle parameter

Table 5.3. Parameter bounds

Parameter	Lower Bound	Upper Bound
Length (% of nominal)	71.43%	142.9%
Position (degrees)	-32	30
Angle (degrees)	-15	25

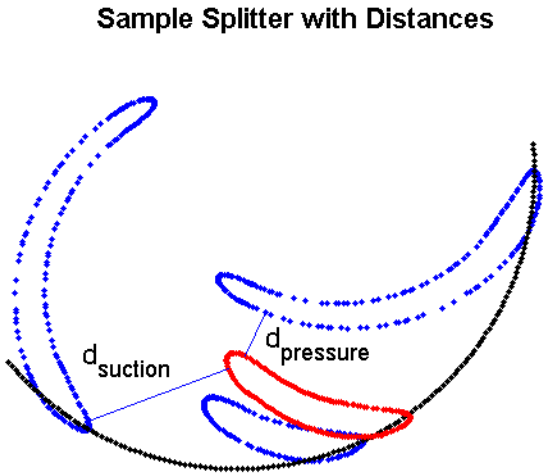

Figure 5.7. Sample splitter with blade distances shown

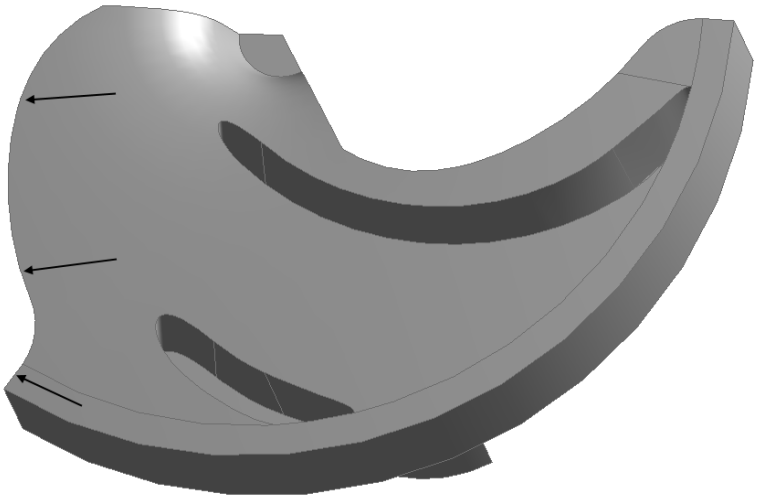

Figure 5.8. Single vane splitter blade impeller model

Enough information is now available to formulate the optimization problem. There are three constraints, indicated by $g_i(x)$ where the minimum distance between the

blades of 15 mm is represented by d_{min} and the minimum distance between the splitter blade and the geometry edge of two mm is represented by $d_{geom_{min}}$. The parameter values of length, position and angle are represented by x_1, x_2 and x_3, respectively. The optimization problem formulation is defined in Equations 5.2 to 5.6.

Minimize $f(x) = V_{weighted}$ (Eq. 5.2)

Subject to $g_1(x) = d_{min} - d_{suction} \leq 0$ (Eq. 5.3)

$g_2(x) = d_{min} - d_{suction} \leq 0$ (Eq. 5.4)

$g_3(x) = d_{geom_{min}} - d_{edge} \leq 0$ (Eq. 5.5)

$71.4\% \leq x_1 \leq 143\%,\ -32° \leq x_2 \leq 30°,\ -15° \leq x_3 \leq 25°$ (Eq. 5.6)

Parameter Sensitivity

Before running optimization, it is important to test the objective function (weighted velocity) for its sensitivity to the input parameters. If there is little to no change, the parameters likely do not affect the results or the bounds may be too small. It is also important to ensure that it will be possible for the optimization to find better results than the baseline results. The baseline results will be from simulations of the 100° wrap angle impeller model without splitter blades at 100% of the experimental BEP flow rate. Optimization will be performed on the single vane model at 100% of BEP but, once an optimum is reached, results will be confirmed by running simulations on the full model with the new optimal splitter blade. Table 5.4 shows the baseline results with head and efficiency shown in relative terms as previously seen to maintain confidentiality. The actual velocity value is shown. Since there is no splitter, a weighted velocity is obviously not possible to calculate on the baseline model, therefore just the maximum blade velocity is shown. The optimum results with the splitter blades should yield a lower velocity. Additionally, it is important to check the efficiency to ensure it is either better or only slightly worse.

Table 5.4. Baseline results

	Single Vane Value	Full Model Value
Efficiency (% BEP)	112.56	87.13
Head (% BEP)	137.05	122.63
Max Blade Velocity (m/s)	16.17	16.82

To analyze sensitivity, tests were run on the single vane model with each of the three parameters set at their maximum and minimum boundary locations as well as the midpoint, which consisted of 27 points in total. These tests were run with smaller bounds for the position and angle before the bounds were expanded to their values used for optimization, shown in Table 5.3. The smaller bounds used are shown in Table 5.5.

Table 5.5. Tighter parameter bounds

Parameter	Lower Bound	Upper Bound
Length (% of nominal)	71.43%	142.9%
Position (degrees)	-9	9
Angle (degrees)	-10	10

Based on the 27 tests, it was clear that major improvements were possible on the velocity that did not yield significantly worse efficiency results. Table 5.6 shows three samples of the results in order of the worst to best weighted velocity obtained in the 27 tests. It is clear that there is significant improvement in the maximum blade velocity between the best result and the baseline results. The splitter blade maximum velocity is also quite low. It is also important to note that in these three tests, as the weighted velocity decreased, the efficiency increased. In fact, the efficiency was about 0.7% better at the best ANOVA point compared to the baseline results.

Using the results of the weighted velocity, an ANOVA analysis was performed in MATLAB. ANOVA examines the sensitivity of the objective to each input parameter and will yield a p-value for each. The p-value reveals how sensitive the results are to that parameter where the closer the value is to 0, the more sensitive the result is. Typically in statistics, a result is considered significant if the p-value is less than 0.05 or 0.01 [67]. Table 5.7 displays the ANOVA analysis results.

Table 5.6. Select ANOVA results

Inputs			Outputs				
Length (% of nominal)	**Position (deg)**	**Angle (deg)**	**Efficiency (% BEP)**	**Head (% BEP)**	**Max Blade Velocity (m/s)**	**Max Splitter Velocity (m/s)**	**Weighted Velocity (m/s)**
142.9%	-9	10	111.8	148.8	16.21	16.74	16.37
71.43%	9	10	112.0	141.2	15.62	9.793	13.87
142.9%	9	0	113.3	144.9	12.25	8.891	11.24

Table 5.7. ANOVA results

Parameter	p-value
Length	0.0022
Position	0.0001
Angle	0.0423

The ANOVA analysis yields very small p-values for all variables, indicating that the weighted velocity is very sensitive to the splitter configuration. Both the length and position have p-values less than 0.01 showing that the velocity is very sensitive to those variables since they fit within the tighter p-value constraint. The angle has a higher p-value but it is still below 0.05 so it still has very significant effects on the results.

Four tests with different splitter blade configurations were also run on the expensive full model to analyze the trends between the single vane and full model results to ensure the single vane model is reliable. The four different splitter blade configurations are shown in Table 5.8.

Table 5.8. Splitter blade configurations for trend analysis

Test #	Length (% of nominal)	Position (degrees)	Angle (degrees)
1	71.43%	0	-9
2	71.43%	0	9
3	142.9%	0	-3.4
4	142.9%	0	0.45

Figure 5.9 shows a comparison of results at the four different configurations on both the full and single vane models. The figure shows plots of the efficiency, head and a weighted velocity value. The x-axis on the plots refers to the test number shown in Table 5.8.

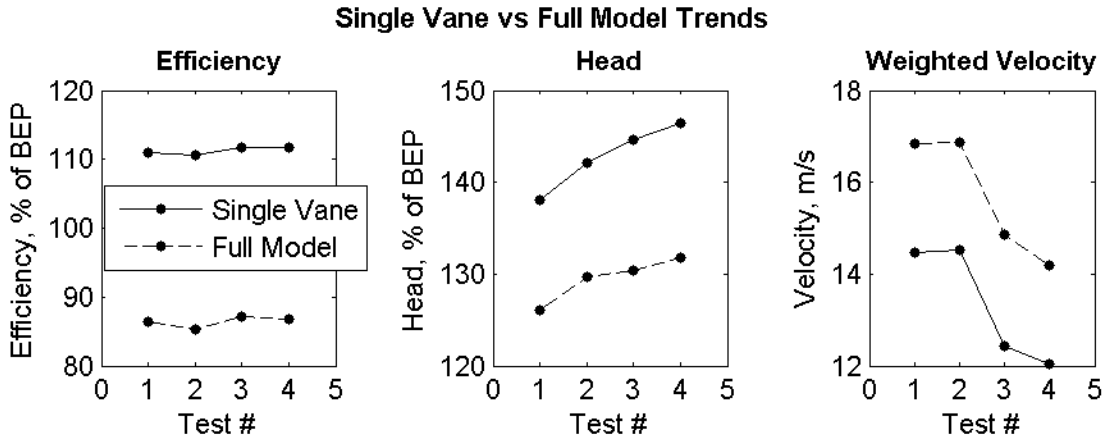

Figure 5.9. Trends in results generated on the full and single vane models

The trends plots show excellent correlation between the full and single vane models. The efficiency changes very little for each test but it is clear that the trend is the same. The head and weighted velocity change much more significantly and have very similar trends. Since the weighted velocity will be used for optimization, good correlation is required in order to justify using the low-fidelity single vane model.

5.2.2. ARSM-ISES Optimization Method

For the present study, ARSM-ISES developed by Long *et al*. was chosen as an optimization algorithm [13]. It is suitable for high-fidelity, expensive models, making it a good candidate for a CFD optimization. ARSM-ISES is based on metamodeling using the Response Surface Method (RSM). Metamodels are used instead of performing optimization purely on the expensive CFD model. ARSM-ISES uses a second order RSM with n_v design variables x to create the metamodel with coefficients β using Equation 5.7.

$$\hat{y} = \beta_0 + \sum_{i=1}^{n_v} \beta_i x_i + \sum_{i=1}^{n_v} \beta_{ii} x_i^2 + \sum_{i=1}^{n_v-1} \sum_{j=i+1}^{n_v} \beta_{ij} x_i x_j \qquad \text{(Eq. 5.7)}$$

The ARSM-ISES algorithm is summarized in a flowchart in Figure 5.10.

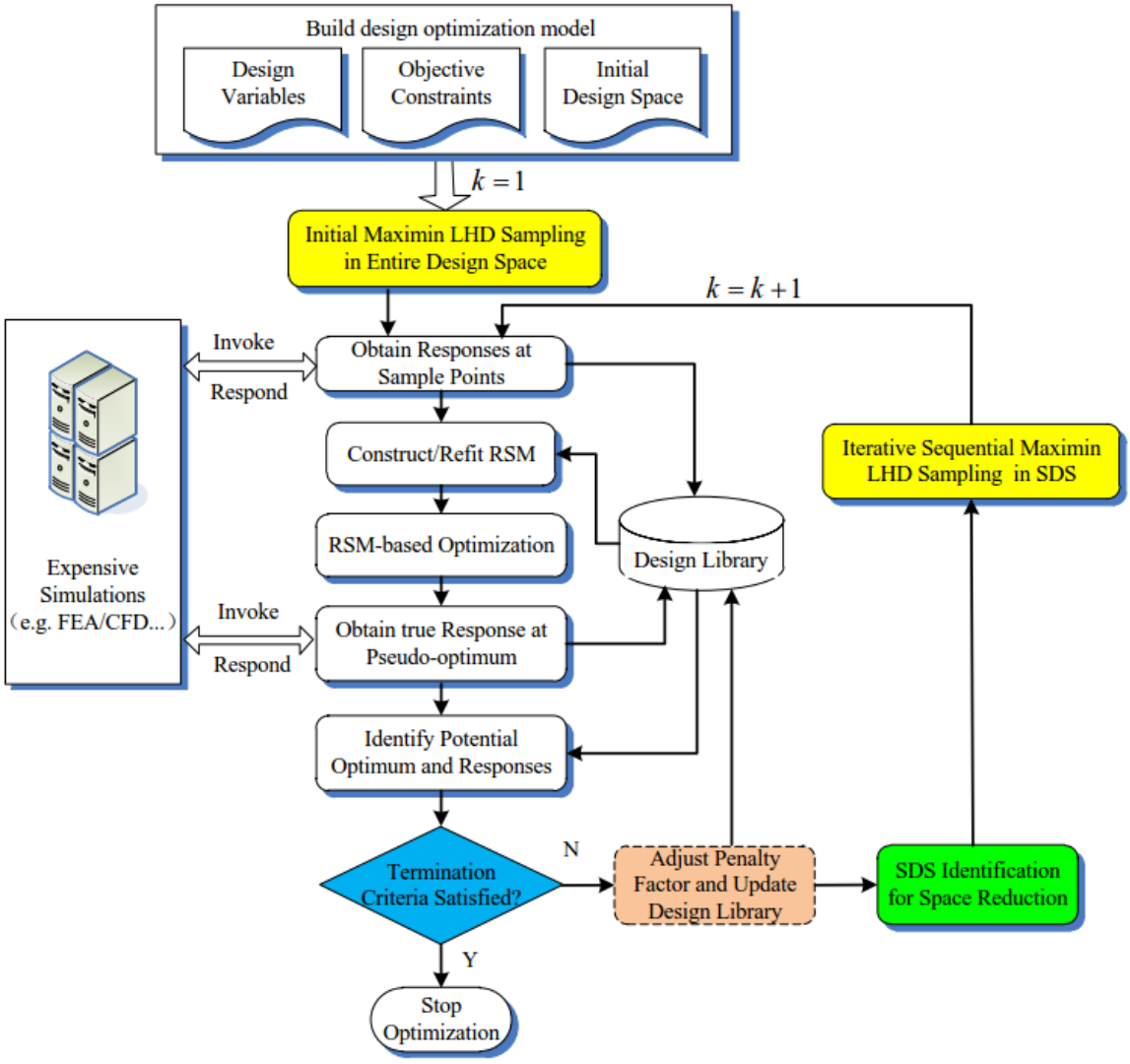

Figure 5.10. ARSM-ISES flowchart [13]

To generate points in the design space, maximin-LHD (Latin Hypercube Design) was used which randomly generates sample points while also maximizing the minimum distance between points to ensure the design space is well covered [37].

There are two major termination criteria for ARSM-ISES. One criterion is the relative difference of the current best optimum between consecutive iterations, defined as Δ in Equation 5.8

$$\Delta = \text{abs}\left(\frac{f_{po}^{*(k)} - f_{po}^{*(k-1)}}{f_{po}^{*(k)}}\right) \quad \text{(Eq. 5.8)}$$

where f_{po}^{*} refers to the current potential optimum and k refers to the current iteration number. If Δ is less than a user-specified tolerance factor, ε, or if the absolute difference, Δ_{abs}, defined in Equation 5.9, is less than 0.1ε, the tolerance criterion is met and the optimization will be considered converged.

$$\Delta_{abs} = \text{abs}\left(f_{po}^{*(k)} - f_{po}^{*(k-1)}\right) \quad \text{(Eq. 5.9)}$$

The other termination criterion is the accuracy of the RSM which refers to the fitting quality of RSM to the actual function. The RSM accuracy is calculated as the relative error at the pseudo-optimum which is the optimum of the RSM. The relative error, ξ, is defined in Equation 5.10

$$\xi = \text{abs}\left(\frac{f_{ps}^{*(k)} - \hat{f}_{ps}^{*(k)}}{f_{ps}^{*(k)}}\right) \quad \text{(Eq. 5.10)}$$

where $\hat{f}_{ps}^{*}$ refers to the objective value on the RSM model at the pseudo-optimum and f_{ps}^{*} refers to the true objective value calculated on the expensive function at the pseudo-optimum point. The RSM accuracy, ξ, must be less than a user-specified minimum accuracy of ξ_a to meet the termination criterion. There is a third termination criterion that is more of a backup criterion to terminate the optimization if both of the previous two termination criteria are not met but the objective value has not improved for a number of iterations. An iteration where there is no improvement compared to the previous iteration is called a non-improvement iteration. Each time there is no improvement, the counter N_{ni} is increased by one. If there is improvement, N_{ni} is reset to zero. When N_{ni} reaches a user-specified number of non-improvement iterations, MAX_NNI, the optimization will terminate. According to Equation 5.8, if there is no improvement in an iteration, Δ will actually be zero and the first termination criterion will be met. Therefore, the non-improvement termination criterion takes effect when the RSM accuracy does not reach an acceptable accuracy [13].

5.2.3. Optimization Results

The optimization was performed using ARSM-ISES with the following termination criteria: ε was set to 0.0001 for the objective value change; ξ_a was set to 0.001 for the acceptable RSM accuracy; and MAX_NNI was set to six for the maximum number of non-improvement iterations. The optimization was performed only on the single vane model of the impeller with splitter blades to keep the cost low. Since the time to run the full model is very long, it would likely take days or weeks to complete optimization. The single vane model usually took under 20 min to run one simulation. Therefore, optimization can be completed within days or even less than one day. However, it is important to evaluate the optimum result on the full model to ensure that the improvement actually occurs on the high-fidelity model.

The ARSM-ISES optimization yielded results after 14 iterations with 56 function evaluations, taking about 17.3 hours. Table 5.9 shows the optimum input and output results as well as the baseline results.

Table 5.9. Optimum results – single vane

Inputs			Outputs				
Length (% of nominal)	**Position (deg)**	**Angle (deg)**	**Efficiency (% BEP)**	**Head (% BEP)**	**Max Blade Velocity (m/s)**	**Max Splitter Velocity (m/s)**	**Weighted Velocity (m/s)**
136.9%	7.003	3.121	113.2	147.2	12.18	8.709	11.14
No Splitter (baseline)			112.6	137.1	16.17	N/A	N/A

Since there is no weighting possible on the model with no splitters, the maximum blade velocity will be used for a final comparison. The optimum results yielded a maximum blade velocity that is about 24% lower which is a significant reduction in velocity and thus in wear on the blades. Furthermore, the efficiency increased by about 0.6%. While it is only a small increase, any improvement is beneficial.

Figure 5.11 shows the convergence of the objective function, weighted velocity, over the 14 iterations. The plot shows that the pseudo-optimum found even in the first iteration was quite low and close to the final optimum.

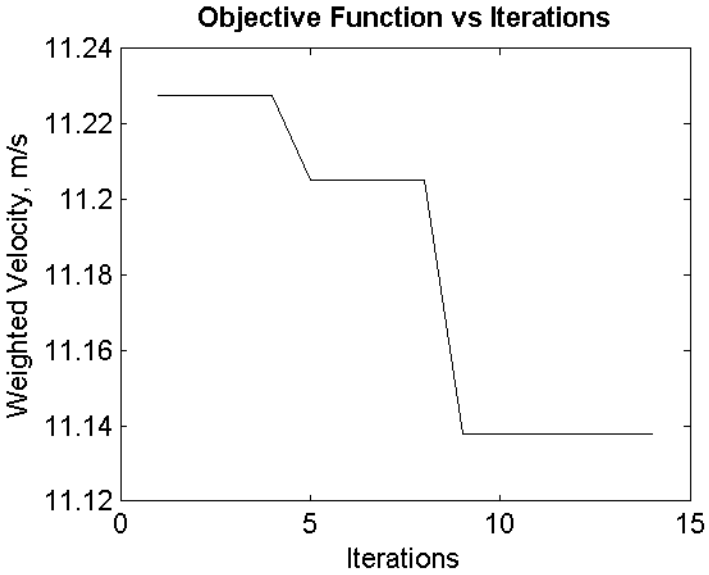

Figure 5.11. Optimization results convergence

The new splitter position is shown in Figure 5.12. It is clear that the splitter is far from the main blades and the constraint is not violated.

Head and efficiency curves were generated on the single vane model to ensure results were good at all flow rates and not just at BEP. Figure 5.13 shows these results compared to results without the splitter blades.

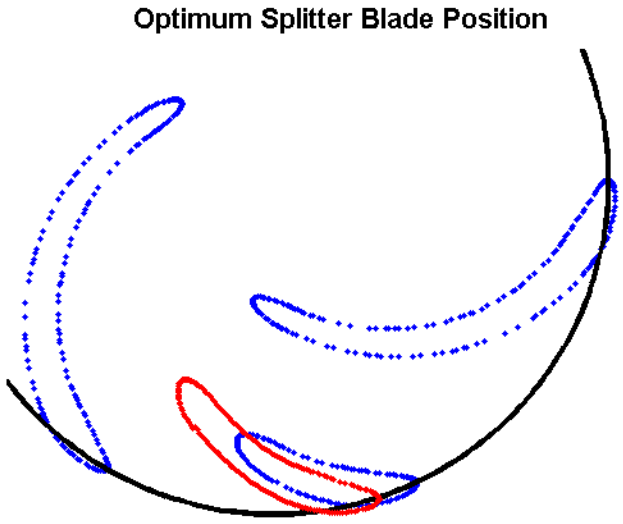

Figure 5.12. Optimum splitter blade position

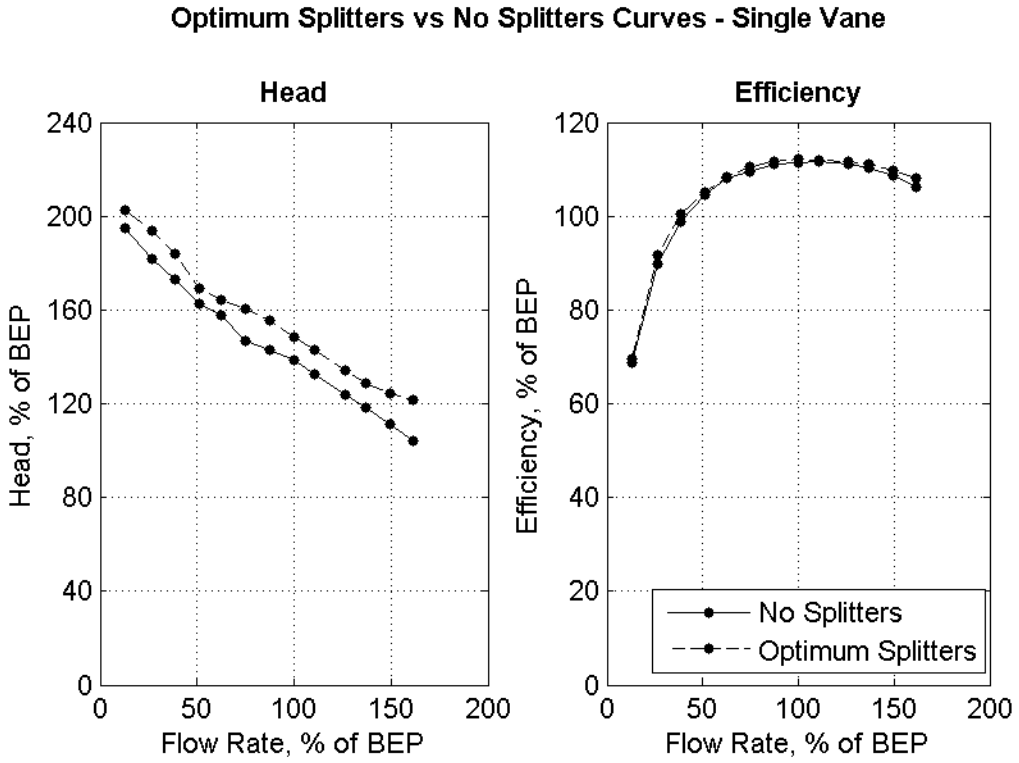

Figure 5.13. Optimum splitter blade results – single vane

Since the optimization was performed on the low-fidelity single vane model, it is imperative to generate results using the new optimum on the high-fidelity full model to confirm that results really did improve. Table 5.10 displays these results from the full model as well as the results from the single vane analysis for comparison.

Table 5.10. Optimum results – full model

	Efficiency (% BEP)	Head (% BEP)	Max Blade Velocity (m/s)	Max Splitter Velocity (m/s)	Weighted Velocity (m/s)
Full Model	87.49	130.6	13.69	13.87	13.74
	87.13	122.6	16.82	N/A	N/A
Single Vane	113.2	147.2	12.18	8.709	11.14
	112.6	137.1	16.17	N/A	N/A

The full model confirms the improvement observed on the single vane model. The maximum blade velocity reduced by almost 19% with the optimal splitter blades compared to the impeller with no splitter blades. While the improvement is less on the

full model, the change is still significantly better on both models and thus, the single vane model is still reliable. The efficiency also had a very slight increase by 0.4%. As a cost comparison, the time to run a typical single vane simulation was approximately eight minutes. To generate results on the full model at 100% BEP with the optimum splitters, three rotations were required which took about 16 hours. The full model results agree very well with the single vane results and it can be concluded that the single vane model is a good predictor of performance trends that can be used effectively for optimization to drastically reduce computational costs. Figure 5.14 shows the head and efficiency curves generated on the full model.

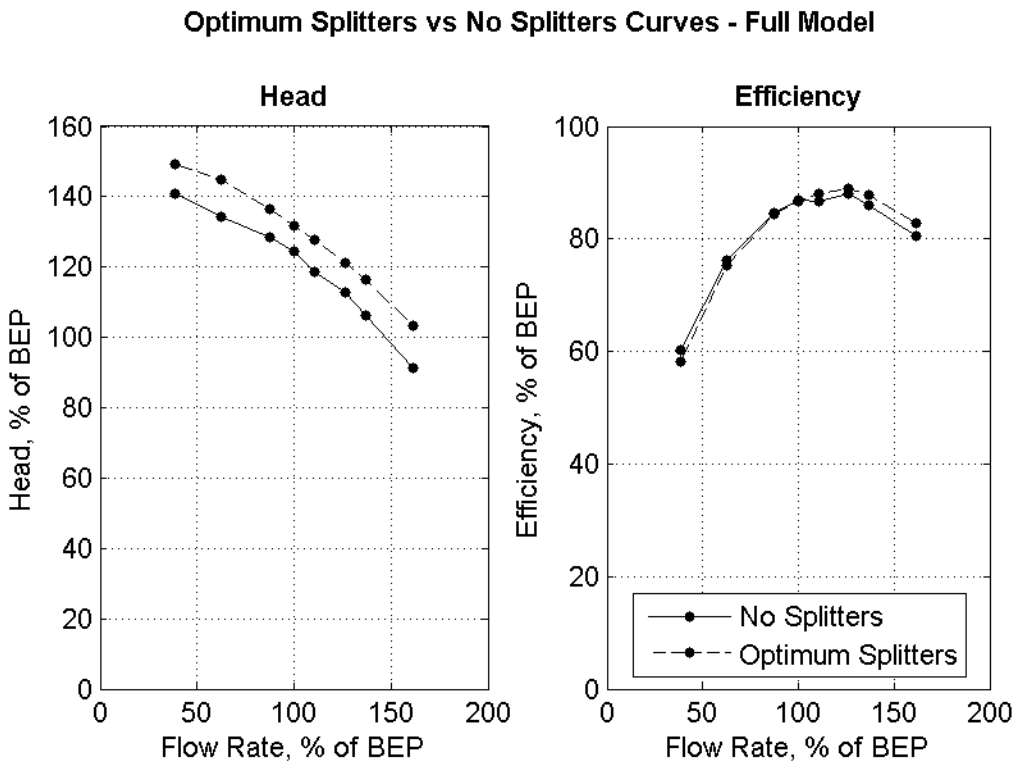

Figure 5.14. Optimum splitter blade results – full model

Figure 5.15 displays velocity plots on the full model from results generated at 100% of the BEP with the optimum splitter blades in (a), and on the same 100° impeller without splitter blades in (b). The splitters are observed to better direct the flow out of the impeller with less recirculation especially near the main blade tips. Figure 5.16 shows zoomed views of this area. Note that the colour scale has been inverted to make results clearer. In Figure 5.15, higher velocities are darker whereas in Figure 5.16, lower results

are darker. On the impeller with no splitter blades, there is recirculation that can be seen on the pressure side of the blade near the leading edge tip. There is also reverse flow along the blade in that area due to the recirculation (Figure 5.16 (b)). With splitters, the velocity all flows in the outward direction with no recirculation in that area.

The optimization using ARSM-ISES successfully yielded a superior impeller that used splitter blades to reduce the wear on the blades. Without splitter blades, the wear on the blades was fairly high. Additionally, the flow was not well guided, which caused recirculation that can worsen the wear. The optimized model using splitter blades decreased the wear as confirmed by simulating the same results on the high-fidelity model. Adding the splitter blades also brought about a slight increase in efficiency and improved the flow in the vanes, guiding the flow better and reducing recirculation.

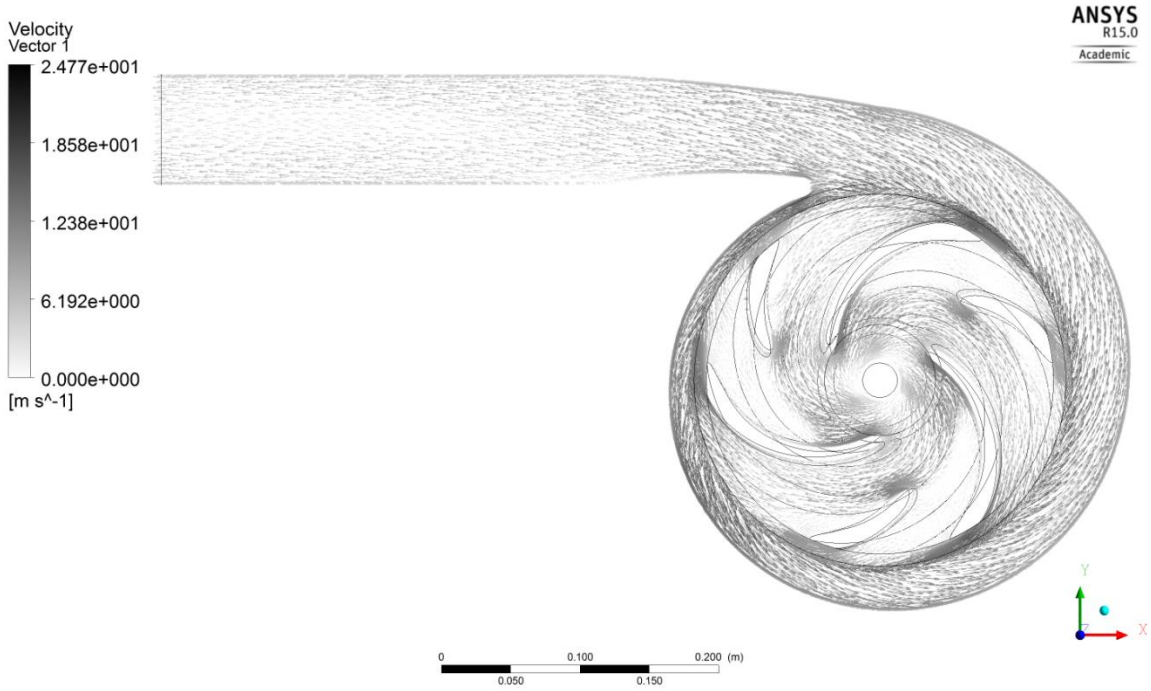

(a)

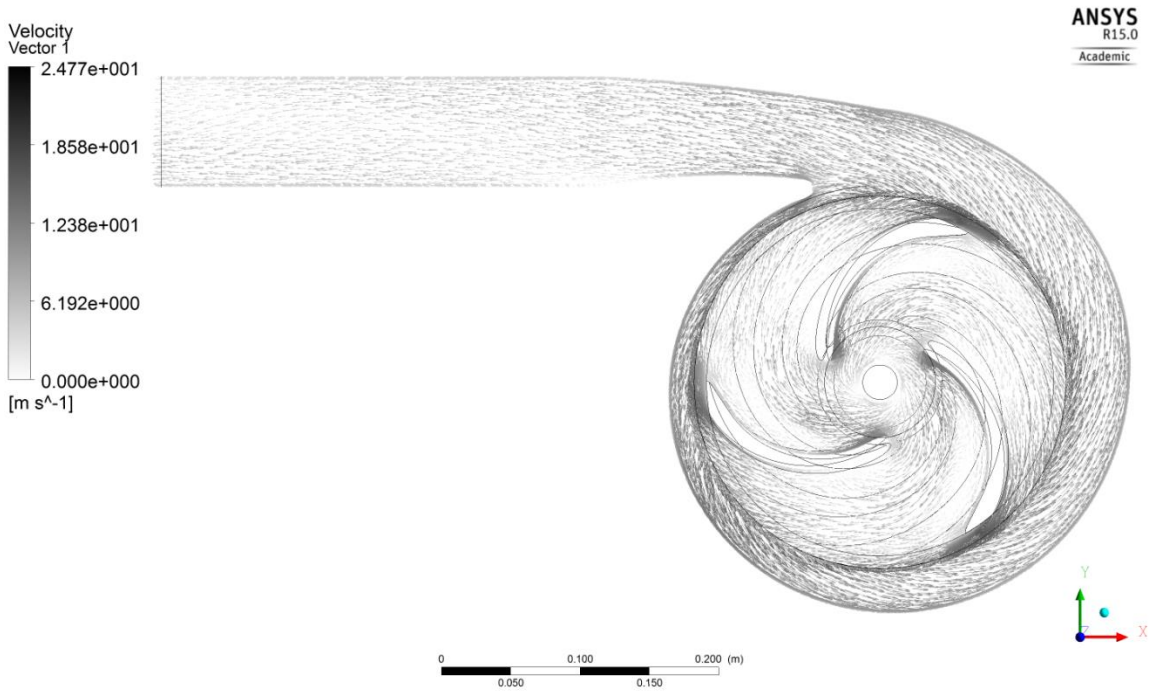

(b)

Figure 5.15. Velocity plots with (a) optimum splitter blades and (b) no splitters

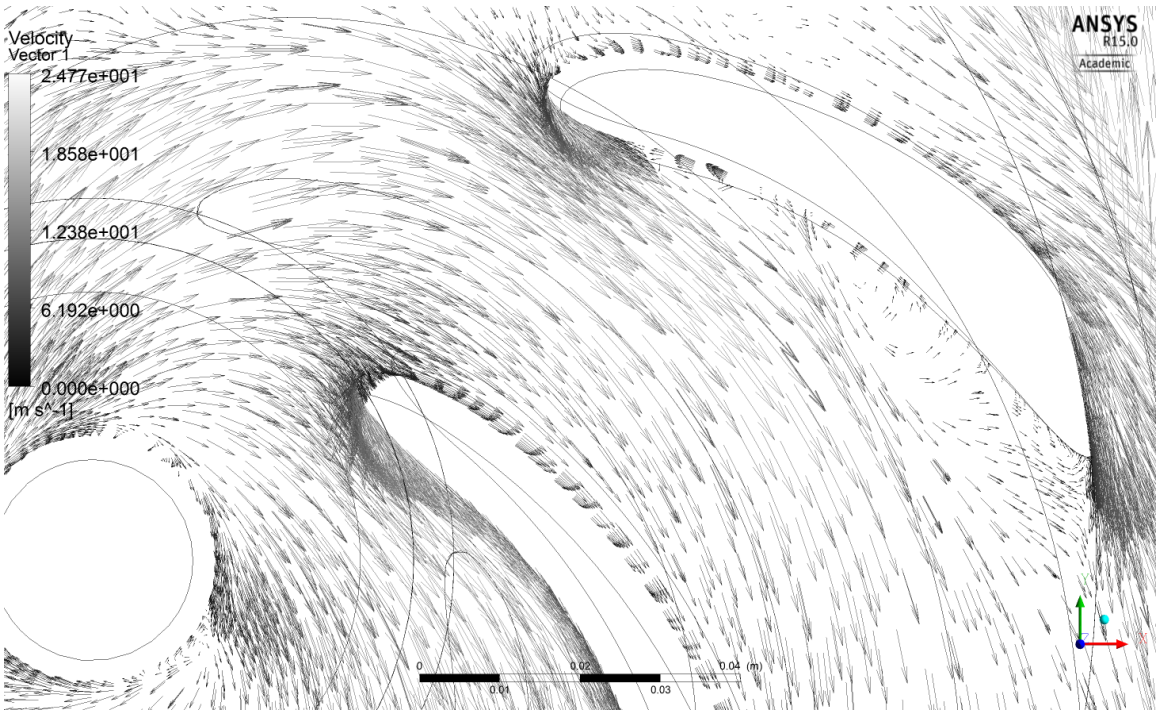

(a)

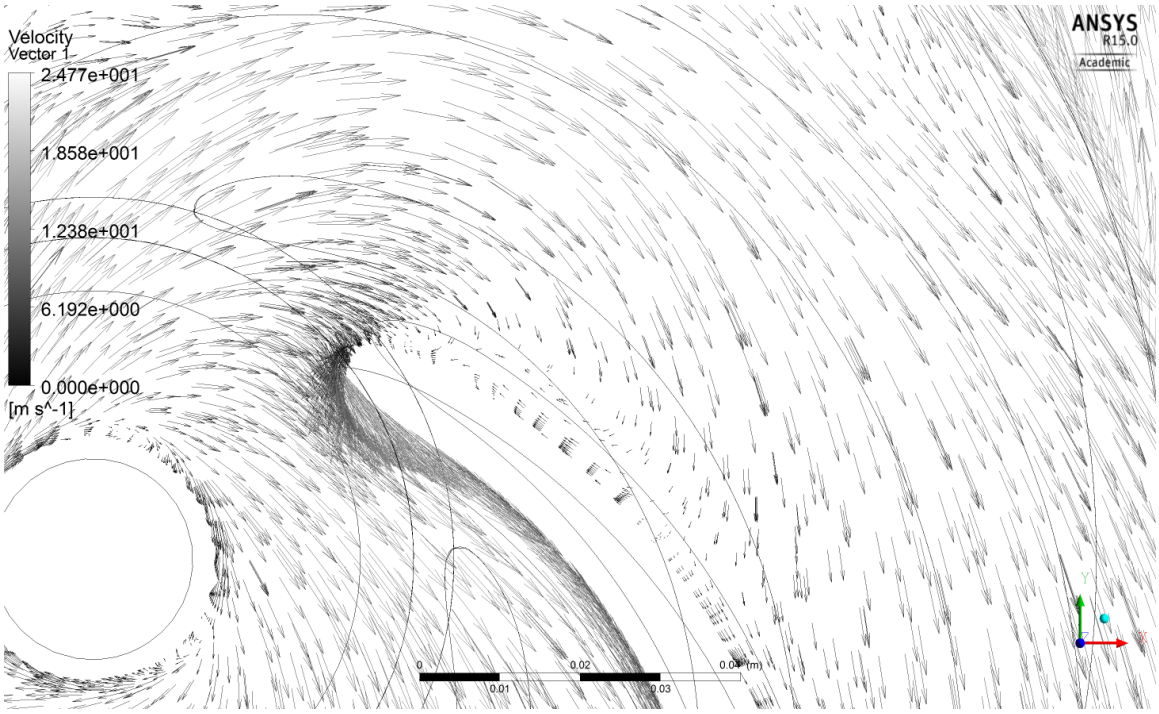

(b)

Figure 5.16. Zoomed plots with (a) optimum splitter blades and (b) no splitters

Chapter 6. Conclusion

Centrifugal slurry pumps are used widely in the industry and have been around for many years. However, due to the complexity and uniqueness of slurry pumps, very little work has been completed on optimizing their design or even using CFD to analyze designs and predict performance. This thesis presented the first extensive and accurately validated study on a slurry pump. Following successful validation, a new design incorporating splitter blades was proposed to reduce the wear in a slurry pump. That new design was optimized to yield a notable reduction in the wear.

The slurry pump studied for validation was a medium size pump designed by Toyo Pumps. CFD was used to yield detailed results of the pump performance including pump curves showing the head and efficiency versus the flow rate through the pump. Results were available to show details of the flow inside the pump as well. The CFD results were carefully investigated and tested to ensure they were accurate and, most importantly, were independent of the mesh used. The generated results were compared to physical test results of the exact same pump model to validate the CFD model. Validation yielded a good correlation between the results. Most importantly, the location of the BEP was predicted correctly by the simulation. While the efficiency values of the simulation were lower at higher flow rates, the shape was similar and is still very useful in predicting performance. Head values were very close and also had a very similar shape.

In order to significantly reduce the cost of simulations, an investigation was performed on using only a single impeller vane for analysis, not considering the volute. Simulations were run on a single vane model to compare to the full model. Results were quite different as expected with the major difference being that the efficiency values were much higher on the single vane model. However, the head and efficiency curve shapes, as well as the pressure and velocity plots inside the impeller, were observed to be very similar to the experimental data. Changes in results with varying splitter blade

configurations were compared between the single vane and full models. Trends were extremely similar between the two, which greatly helps to justify the use of the single vane model for optimization instead of the expensive, high-fidelity full model.

After validating the model, it was assumed that accurate results could be generated on other similar slurry pumps by using the same geometry, meshing and CFD setup procedure. This allowed the simulation model to be changed to allow for optimization. The main goal of this study was to minimize the wear in slurry pumps using impellers with wide open vanes. The proposed method to reduce the wear was to add in splitter blades to an impeller. The splitter blade length was assigned as a parameter for optimization in addition to two parameters defining the radial position and angle of the splitter for placement in the impeller. Due to the difficulty in calculating wear in a CFD analysis, a wear approximation was used based on the observation that high velocities corresponded to high wear [9,10]. The blades are the most critical components in an impeller for wear. Therefore, the optimization objective was to minimize the maximum velocity on the blades and splitter blades. The main blades are much larger than the splitter blades and they are more important for focusing on reducing velocities. Therefore, a weighted velocity was used as an objective function that averaged the maximum velocity on the main blades and splitter blades with weights of 70% and 30%, respectively.

Optimization was performed on the single vane model using the ARSM-ISES algorithm which is based on iterative metamodeling and optimization. The optimization yielded a result with a velocity reduction of 24% on the main blades compared to the same impeller without splitter blades. Additionally, the efficiency increased by about 0.5%. These results were confirmed by running simulations with the optimum splitter blades on the full model. The full model yielded similar results, showing a velocity reduction of 19% and an efficiency increase of 0.4%. Therefore, splitter blades can definitely improve the wear characteristics in a slurry pump significantly. Furthermore, they do not negatively affect the performance of the pump with respect to efficiency. The recommendation is that splitter blades are beneficial to slurry pump impeller designs especially when the vanes are very wide. Using optimization, one can determine an

optimal location for the splitter blades to reduce the wear without sacrificing performance.

6.1. Future Work

The most important future work recommended would be to manufacture a physical model of the optimum pump impeller with splitter blades and then test it to compare results with the simulation and confirm that the splitter blades are actually beneficial. Regarding physical tests, it is also recommended to perform tests in slurry. This would involve using a test tank built to contain slurry instead of water. Therefore, it is a more long term goal. Since wear occurs over the long term, it would also be necessary to run the pump likely for months. Therefore, another way to test the design would be to simply analyze the impeller after being used in the industry for a long period of time to observe the actual wear.

For simulations, it is highly recommended to perform slurry simulations. Going this route would allow the performance of slurry pumps to be tested in their intended environment via simulation, rather than just a prediction in water which is still necessary for validation. It would also allow for much more accurate wear prediction and would provide a platform for a much better optimization to minimize the wear.

The methodology presented in this thesis can also be used for other similar applications. Using the CFD methodology, any centrifugal pump could be simulated to validate results. The optimization methodology can easily be used on different designs and for different purposes. As an example, with very little extra work, an optimization could be setup to modify the main blade shape to maximize the efficiency. Therefore, the CFD and optimization procedures are robust and provide a framework for other similar studies.

References

[1] Gülich, J. F., 2010, Centrifugal Pumps, Springer, Berlin Heidelberg.

[2] Parrondo, J. L., Velarde, S., and Santolaria, C., 1998, “Development of a predictive maintenance system for a centrifugal pump,” J. Qual. Maint. Eng., **4**(3), pp. 198–211.

[3] Warman International Ltd., 2002, “Slurry Pumping Manual.”

[4] Japikse, D., Marscher, W. D., and Furst, R. B., 2006, Centrifugal Pump Design and Performance, Concepts NREC.

[5] González, J., Fernández, J., Blanco, E., and Santolaria, C., 2002, “Numerical Simulation of the Dynamic Effects Due to Impeller-Volute Interaction in a Centrifugal Pump,” J. Fluids Eng., **124**(2), pp. 348–355.

[6] Derakhshan, S., Pourmahdavi, M., Abdolahnejad, E., Reihani, A., and Ojaghi, A., 2013, “Numerical shape optimization of a centrifugal pump impeller using artificial bee colony algorithm,” Comput. Fluids, **81**, pp. 145–151.

[7] Grapsas, V. A., Anagnostopoulos, J. S., and Papantonis, D. E., 2005, “Hydrodynamic Design of Radial Flow Pump Impeller by Surface Parameterization,” 1st International Conference on Experiments/Process/System Modelling/Simulation/Optimization, Athens.

[8] Burgess, K. E., Liu, W.-J., Lavagna, M., and Glaves, G. B., 2011, “Slurry Pump Impeller.”

[9] LaBour Pump Company, 2005, “Pump Wear.”

[10] Krüger, S., Martin, N., and Dupont, P., 2010, “Assessment of Wear Erosion in Pump Impellers,” Proceedings of the Twenty-Sixth International Pump Users Symposium, pp. 51–56.

[11] Engin, T. and Kurt, A., 2003, “Prediction of Centrifugal Slurry Pump Head Reduction: An Artificial Neural Networks Approach,” J. Fluids Eng., **125**, pp. 199–202.

[12] Jang, C.-M. and Choi, K.-R., 2012, “Optimal design of splitters attached to turbo blower impeller by RSM,” J. Therm. Sci., **21**(3), pp. 215–222.

[13] Long, T., Wu, D., Guo, X., Wang, G. G., and Liu, L., 2014, “Efficient Adaptive Response Surface Method Using Intelligent Space Exploration Strategy,” Submitt. to Struct. Multidiscip. Optim.

[14] Wang, H. and Tsukamoto, H., 2001, “Fundamental Analysis on Rotor-Stator Interaction in a Diffuser Pump by Vortex Method,” J. Fluids Eng., **123**(4), pp. 737–747.

[15] Mentzos, M. D., Filios, A. E., Margaris, D. P., and Papanikas, D. G., 2005, “CFD Predictions of Flow Through a Centrifugal Pump Impeller,” 1st International Conference on Experiments/Process/System Modelling/Simulation/Optimization, Athens.

[16] Grapsas, V., Stamatelos, F., Anagnostopoulos, J., and Papantonis, D., 2008, “Numerical Study and Optimal Blade Design of a Centrifugal Pump by Evolutionary Algorithms,” 12th International Conference on Knowledge-Based Intellligent Information and Engineering Systems, Part II, Zagreb, Croatia, pp. 26–33.

[17] Byskov, R. K., Jacobsen, C. B., and Pedersen, N., 2003, “Flow in a Centrifugal Pump Impeller at Design and Off-Design Conditions—Part II: Large Eddy Simulations,” J. Fluids Eng., **125**(1), p. 73.

[18] Shojaeefard, M. H., Tahani, M., Ehghaghi, M. B., Fallahian, M. a., and Beglari, M., 2012, “Numerical study of the effects of some geometric characteristics of a centrifugal pump impeller that pumps a viscous fluid,” Comput. Fluids, **60**, pp. 61–70.

[19] Zhou, L., Shi, W., Li, W., and Agarwal, R., 2013, “Numerical and Experimental Study of Axial Force and Hydraulic Performance in a Deep-Well Centrifugal Pump With Different Impeller Rear Shroud Radius,” J. Fluids Eng., **135**(10).

[20] Asuaje, M., Bakir, F., Kergourlay, G., Noguera, R., and Rey, R., 2006, “Three-dimensional quasi-unsteady flow simulation in a centrifugal pump: comparison with experimental results,” Proc. Inst. Mech. Eng. Part A J. Power Energy, **220**(3), pp. 239–256.

[21] Cheah, K. W., Lee, T. S., Winoto, S. H., and Zhao, Z. M., 2008, “Numerical Analysis of Impeller-Volute Tongue Interaction and Unsteady Fluid Flow in a Centrifugal Pump,” The 4th International Symposium on Fluid Machinery and Fluid Engineering, Beijing, pp. 66–71.

[22] Feng, J., Benra, F.-K., and Dohmen, H. J., 2010, “Application of Different Turbulence Models in Unsteady Flow Simulations of a Radial Diffuser Pump,” Forsch. im Ingenieurwes., **74**(3), pp. 123–133.

[23] Spence, R. and Amaral-Teixeira, J., 2008, “Investigation into pressure pulsations in a centrifugal pump using numerical methods supported by industrial tests,” Comput. Fluids, **37**(6), pp. 690–704.

[24] Li, Z., Wu, D., Wang, L., and Huang, B., 2010, “Numerical Simulation of the Transient Flow in a Centrifugal Pump During Starting Period,” J. Fluids Eng., **132**(8).

[25] Lucius, A. and Brenner, G., 2011, “Numerical Simulation and Evaluation of Velocity Fluctuations During Rotating Stall of a Centrifugal Pump,” J. Fluids Eng., **133**(8).

[26] Gölcü, M., Pancar, Y., and Sekmen, Y., 2006, “Energy saving in a deep well pump with splitter blade,” Energy Convers. Manag., **47**(5), pp. 638–651.

[27] Kergourlay, G., Younsi, M., Bakir, F., and Rey, R., 2007, “Influence of Splitter Blades on the Flow Field of a Centrifugal Pump: Test-Analysis Comparison,” Int. J. Rotating Mach., pp. 1–13.

[28] Leifsson, L. and Koziel, S., 2010, “Multi-fidelity design optimization of transonic airfoils using physics-based surrogate modeling and shape-preserving response prediction,” J. Comput. Sci., **1**(2), pp. 98–106.

[29] Westra, R. W., 2008, “Inverse-design and optimization methods for centrifugal pump impellers,” University of Twente.

[30] Khuri, A. I. and Mukhopadhyay, S., 2010, “Response surface methodology,” Wiley Interdiscip. Rev. Comput. Stat., **2**(2), pp. 128–149.

[31] Wang, L., Shan, S., and Wang, G. G., 2004, “Mode-pursuing sampling method for global optimization on expensive black-box functions,” Eng. Optim., **36**(4), pp. 419–438.

[32] Wang, G. G., Dong, Z., and Aitchison, P., 2001, “Adaptive Response Surface Method - a Global Optimization Scheme for Approximation-Based Design Problems,” Eng. Optim., **33**(6), pp. 707–733.

[33] Wang, G. G., 2003, “Adaptive Response Surface Method Using Inherited Latin Hypercube Design Points,” J. Mech. Des., **125**(2), p. 210.

[34] Mckay, M. D., Beckman, R. J., and Conover, W. J., 1979, “A Comparison of Three Methods for Selecting Values of Input Variables in the Analysis of Output from a Computer Code,” Technometrics, **21**(2), pp. 55–61.

[35] JMP, 2014, “Latin Hypercube Designs” [Online]. Available: http://www.jmp.com/support/help/Latin_Hypercube_Designs.shtml. [Accessed: 17-Jul-2014].

[36] Panayi, A. P., Diaz, A. R., and Schock, H. J., 2008, “On the optimization of piston skirt profiles using a pseudo-adaptive response surface method,” Struct. Multidiscip. Optim., **38**(3), pp. 317–330.

[37] Long, T., Liu, L., and Peng, L., 2011, “Global Optimization Method with Enhanced Adaptive Response Surface Method for Computation-Intensive Design Problems,” Adv. Sci. Lett., **4**, pp. 1–7.

[38] Chen, L., Duan, Y., Pu, W., and Zhao, C., 2010, “CFD simulation of coal-water slurry flowing in horizontal pipelines,” Korean J. Chem. Eng., **26**(4), pp. 1144–1154.

[39] Troshko, A. a. and Zdravistch, F., 2009, “CFD modeling of slurry bubble column reactors for Fisher–Tropsch synthesis,” Chem. Eng. Sci., **64**(5), pp. 892–903.

[40] Pagalthivarthi, K. V., Gupta, P. K., Tyagi, V., and Ravi, M. R., 2011, “CFD Predictions of Dense Slurry Flow in Centrifugal Pump Casings,” Int. J. Aerosp. Mech. Eng., **5**(4), pp. 254–266.

[41] Pagalthivarthi, K. V., Gupta, P. K., Tyagi, V., and Ravi, M. R., 2011, “CFD Prediction of Erosion Wear in Centrifugal Slurry Pumps for Dilute Slurry Flows,” J. Comput. Multiph. Flows, **3**(4), pp. 225–246.

[42] Joshi, R., 2010, “Computational Investigation of Flow Field in a Centrifugal Slurry Pump,” Thapar University.

[43] Singh, S., 2012, “Numerical Evaluation of Flow through a Centrifugal Slurry Pump Handling Fly Ash Using CFD,” Thapar University.

[44] Gorla, R. S. R. and Khan, A. A., 2003, Turbomachinery Design and Theory, Marcel Dekker, Inc.

[45] Chaurette, J., 2010, “What is head?,” Fundam. Pumps that is [Online]. Available: http://www.pumpfundamentals.com/what is head.htm. [Accessed: 14-Feb-2014].

[46] 2000, “American National Standard for Centrifugal Pump Tests.”

[47] 2013, “ANSYS Academic Research, Release 15.0, Help System, ANSYS CFX Introduction.”

[48] Benson, T., 2014, “Navier-Stokes Equations,” NASA Glenn Res. Cent. [Online]. Available: https://www.grc.nasa.gov/www/k-12/airplane/nseqs.html. [Accessed: 14-Jun-2014].

[49] Versteeg, H. K. and Malalasekera, W., 2007, An Introduction to Computational Fluid Dynamics: The Finite Volume Method, Pearson Education, Essex.

[50] ANSYS Inc., 2013, “ANSYS Academic Research, Release 15.0, Help System, ANSYS CFX-Solver Theory Guide,” **15317**(November).

[51] ANSYS Inc., 2013, “ANSYS Academic Research, Release 15.0, Help System, ANSYS CFX Reference Guide,” **15317**(November).

[52] ANSYS Inc., 2012, “Lecture 10: Best Practice Guidelines.”

[53] LEAP CFD Team, 2012, “Tips &Tricks: Inflation Layer Meshing in ANSYS,” LEAP Aust. CFD blog [Online]. Available: http://www.computationalfluiddynamics.com.au/tips-tricks-inflation-layer-meshing-in-ansys/. [Accessed: 25-Apr-2013].

[54] ANSYS Inc., 2013, “ANSYS Academic Research, Release 15.0, Help System, ANSYS CFX-Solver Modeling Guide.”

[55] Zhou, L., Shi, W., and Wu, S., 2013, “Performance Optimization in a Centrifugal Pump Impeller by Orthogonal Experiment and Numerical Simulation,” Adv. Mech. Eng., **2013**, pp. 1–7.

[56] Adams, T., Grant, C., and Watson, H., 2012, “A Simple Algorithm to Relate Measured Surface Roughness to Equivalent Sand-grain Roughness,” Int. J. Mech. Eng. Mechatronics, **1**(1), pp. 66–71.

[57] Elger, D. F., Williams, B. C., Crowe, C. T., and Roberson, J. A., 2012, Engineering Fluid Mechanics, Wiley.

[58] 2011, “K-omega models,” CFD Online [Online]. Available: http://www.cfd-online.com/Wiki/SST_k-omega_model. [Accessed: 19-Jun-2014].

[59] Menter, F. R., 2009, “Review of the shear-stress transport turbulence model experience from an industrial perspective,” Int. J. Comut. Fluid Dyn., **23**(4), pp. 305–316.

[60] LEAP CFD Team, 2012, “Tips & Tricks: Turbulence Part 1 – Introduction to Turbulence Modelling,” LEAP Aust. CFD blog [Online]. Available: http://www.computationalfluiddynamics.com.au/turbulence-modelling/. [Accessed: 25-Apr-2013].

[61] 2011, “SST k-omega model,” CFD Online, [Online]. Available: http://www.cfd-online.com/Wiki/SST_k-omega_model. [Accessed: 19-Jun-2014].

[62] Braun, O., 2009, “Part Load Flow in Radial Centrifugal Pumps,” École Polytechnique Fédérale de Lausanne.

[63] Wee, C. K., 2011, “Unsteady Flow in Centrifugal Pump at Design and Off-Design Conditions,” National University of Singapore.

[64] Ferziger, J. H. and Peric, M., 2002, Computational Methods for Fluid Dynamics, Springer-Verlag, Berlin Heidelberg.

[65] 2005, “American National Standard for Rotodynamic (Centrifugal) Slurry Pumps.”

[66] Vuthaluru, R., Kruger, O., Abhishek, M., Pareek, V. K., and Vuthaluru, H. B., 2006, “Investigation of wear pattern in a complex coal pulveriser using CFD modelling,” Fuel Process. Technol., **87**(8), pp. 687–694.

[67] MathWorks, 2014, “anovan,” MATLAB Doc. Cent. [Online]. Available: http://www.mathworks.com/help/stats/anovan.html. [Accessed: 11-Jul-2014].

Appendix.

Geometry and Mesh Generation

Figure A1 shows the fluid domain of the Toyo pump model. To separate the stationary and rotating domains, the rotating domain was cut from the stationary domain as shown in Figure A2. Figure A3 shows the two domains separated.

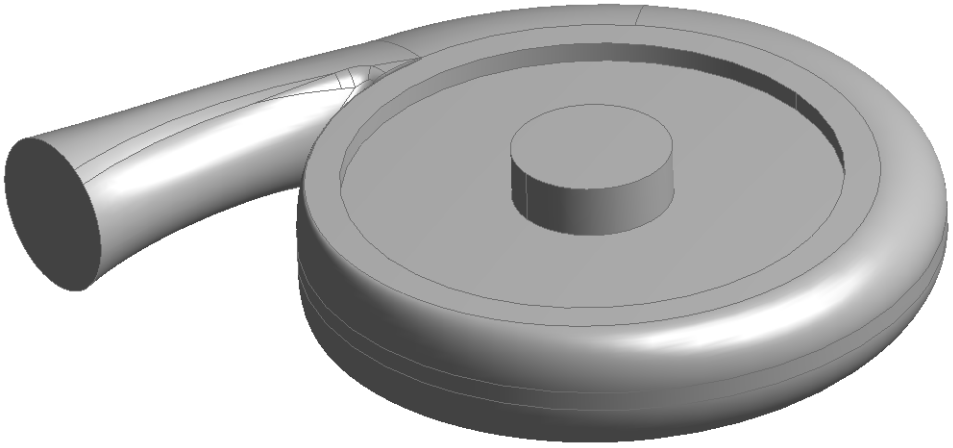

Figure A1. Fluid domain model

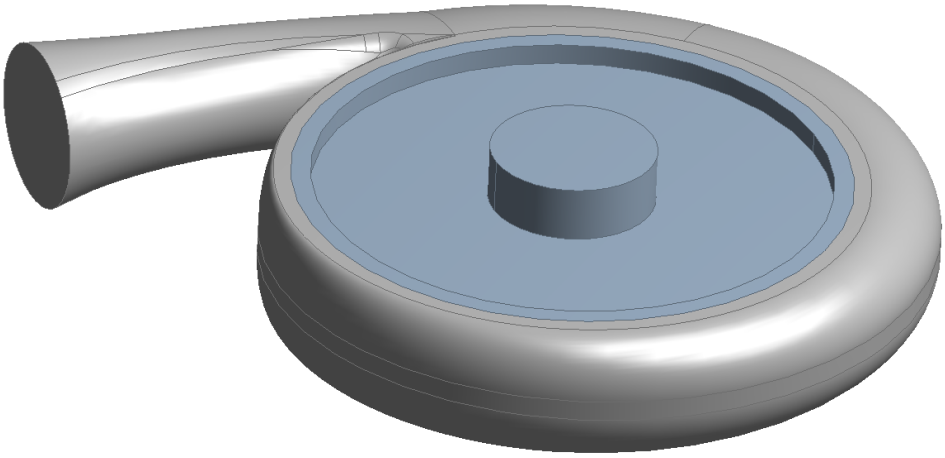

Figure A2. Cut stationary and rotating domain

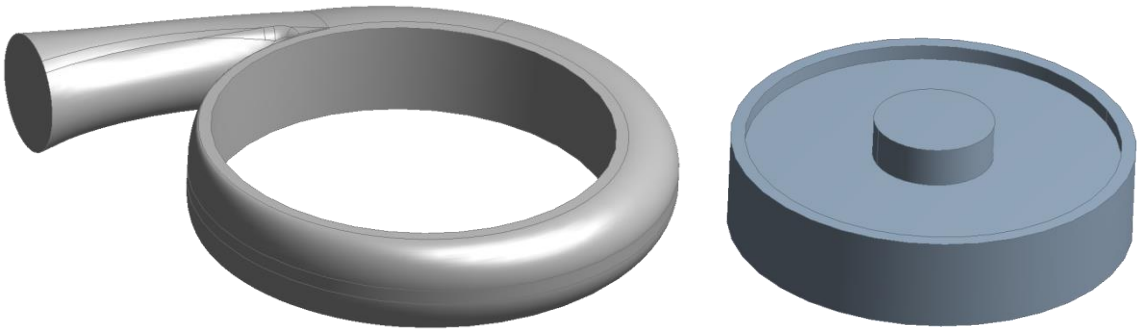

(a) (b)

Figure A3. Separated (a) stationary and (b) rotating domain

In order to separate the impeller portion of the rotating fluid domain model and the lower sidewall gap, the rotating domain model was sliced horizontally as shown in Figure A4. The top impeller portion of the rotating domain is shown from below in Figure A5.

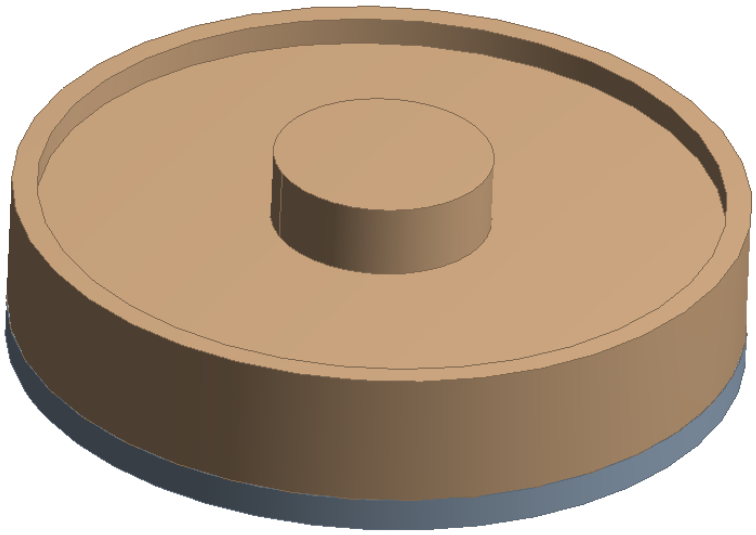

Figure A4. Cut rotating domain

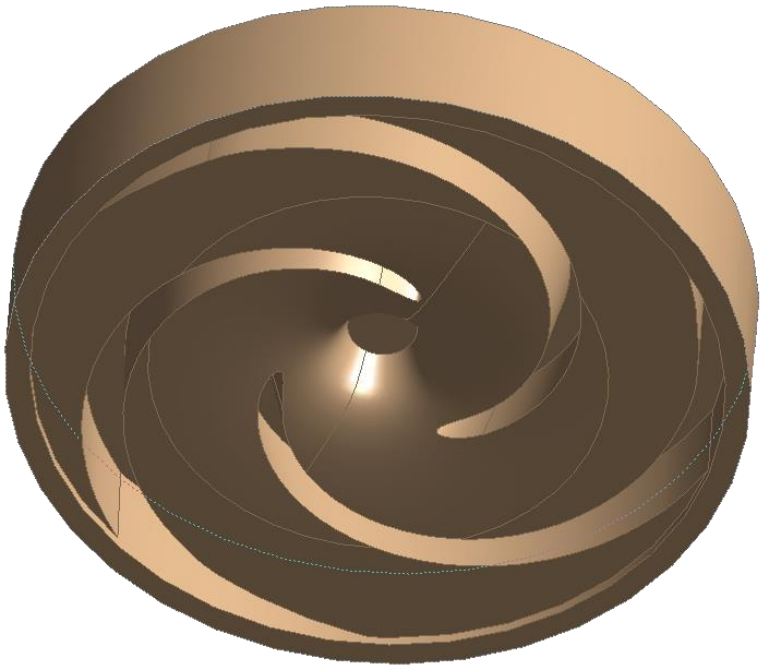

Figure A5. Cut rotating domain

The bottom of the impeller has expeller vanes as can be seen in Figure A6. Figure A7 shows the fluid domain of the lower part of the rotating domain. This models the gap between the lower part of the impeller where the expeller vanes are and the bottom of the volute.

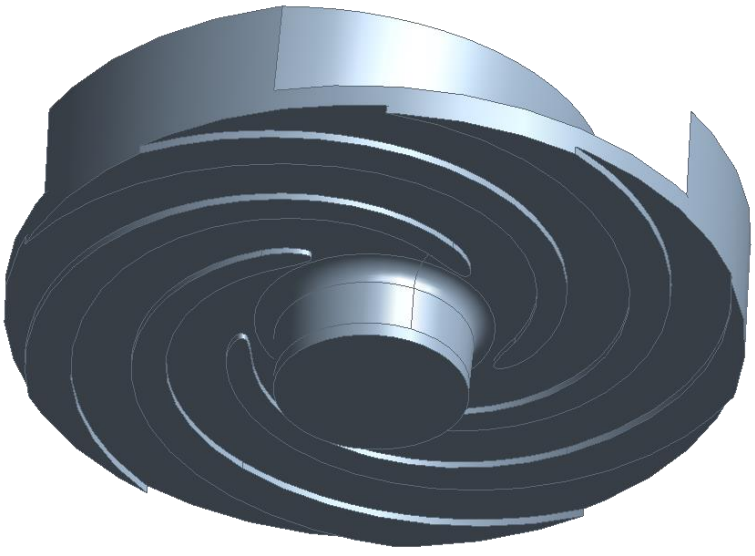

Figure A6. Bottom of impeller

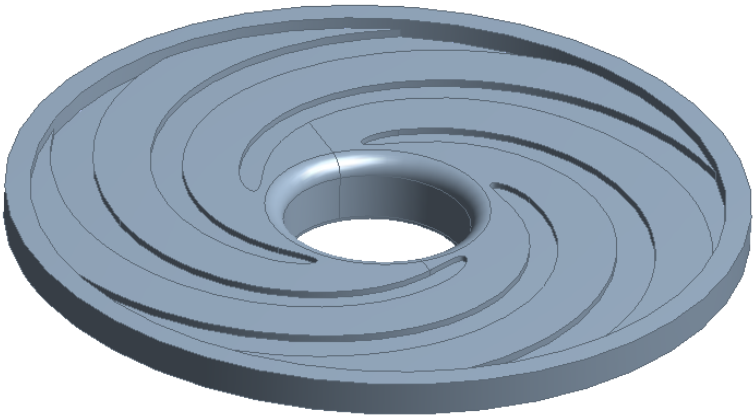

Figure A7. Lower sidewall fluid domain

Similar to how the impeller was cut to just one vane for meshing, the lower sidewall gap is also cut to one expeller vane. This fluid domain is shown in Figure A8.

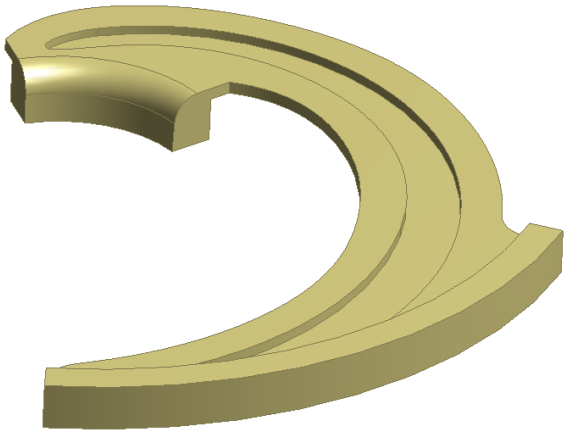

Figure A8. Single expeller vane cutout of lower sidewall gap

Figure A9 shows all the parts of the geometry to be meshed.

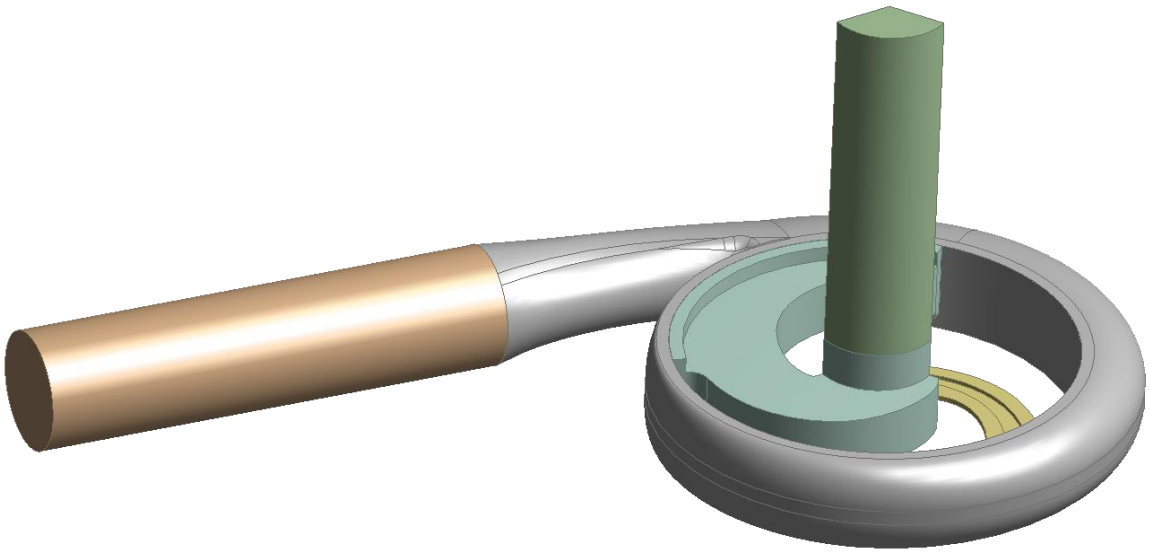

Figure A9. Full fluid domain geometry model

Figure A10 shows the volute mesh. Figure A11 shows the same mesh zoomed in near the cutwater to show how some areas automatically are refined based on the face geometry. The refinement circles are not necessary but are refined automatically due to small features on the faces. They did not signifricantly raise the mesh count and were left as such.

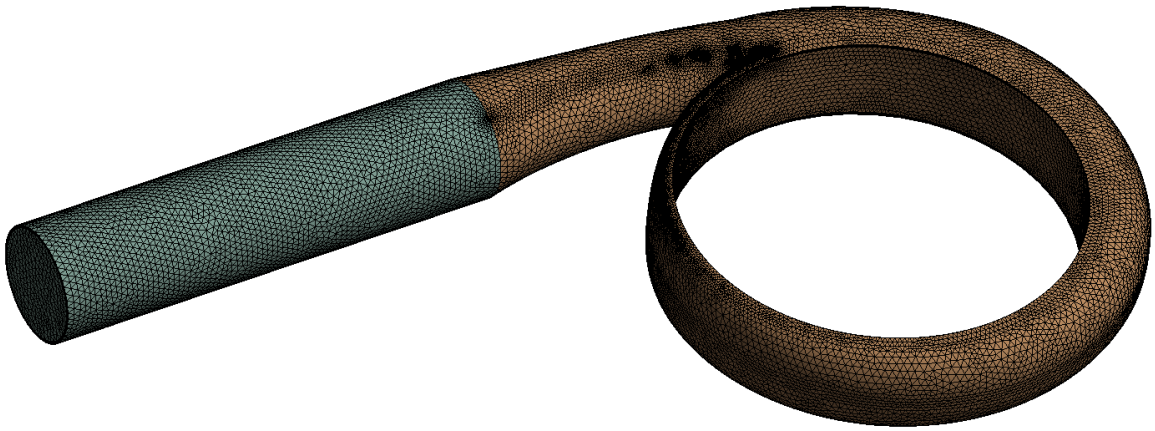

Figure A10. Volute mesh

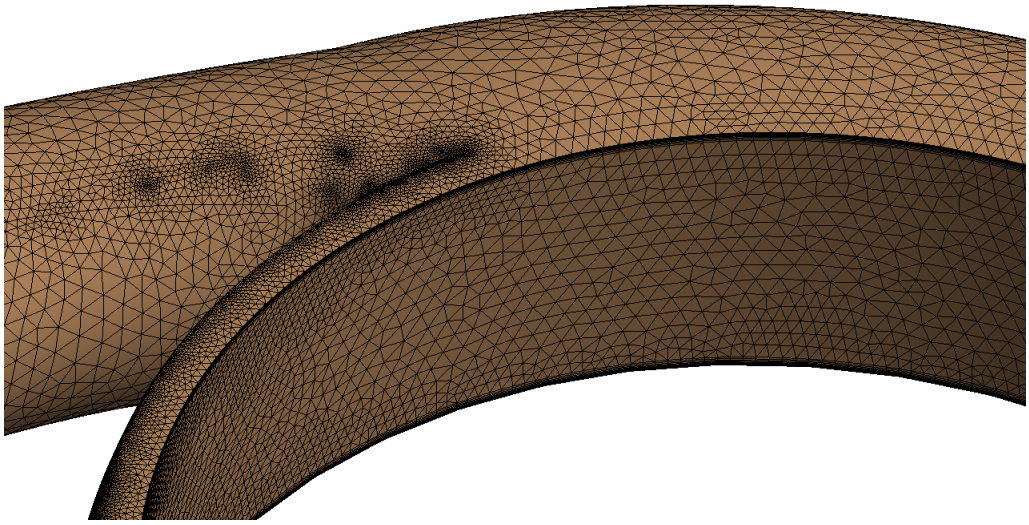

Figure A11. Volute mesh zoomed in

Figure A12 shows the mesh of the lower sidewall gap.

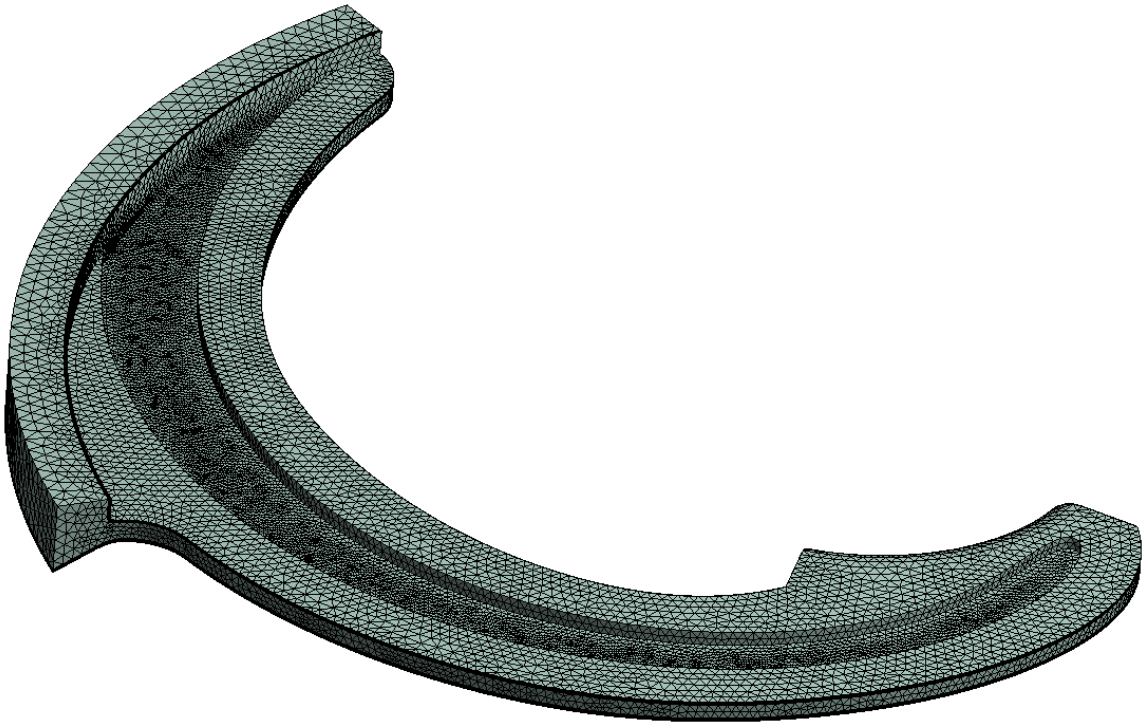

Figure A12. Lower sidewall gap mesh